DOCTOR OF PHILOSOPHY

Punching shear failure of reinforced concrete flat slabs supported on steel edge column

Ngekpe, Ebenezer Barisua

Award date:
2016

Awarding institution:
Coventry University

Punching Shear Failure of Reinforced concrete flat slabs supported on steel edge column

Barisua Ebenezer Ngekpe

A Thesis submitted in partial fulfilment of the University's requirements for the Degree of Doctor of Philosophy.

2016

ABSTRACT

This study examines punching shear failure at edge supported flat slab. Due to the significant dearth of research on punching shear at edge steel column, this study focuses on the design and performance of a novel shearhead system proposed for edge connection. By considering multi-stage processes and parameters that influence punching shear failure, both numerical and experimental studies were adopted. Firstly linear finite element analysis was employed to study the relationship between the continuous structure and the representative specimen; in order to support decisions on boundary conditions that create the similitude.

A nonlinear (NLFEA) model was proposed where various concrete material constitutive models were compared and contrasted. The Total Strain crack model was adopted on the ground that it accounts for the tensile strength of cracked concrete which was ignored in previous theoretical model that lead to poor prediction of punching shear. By considering the appropriate material constitutive model for concrete and steel, material parameters, appropriate modelling scheme capable of predicting punching shear was formulated. The adopted modelling scheme was validated using previous research work. Numerical results reveal that punching shear is influenced most significantly by concrete tensile strength, fracture energy.

The shearhead assembly was design with using ACI318-05 and Newzealand codes recommendations with some modifications. These are only codes that provide design guidance on shearhead. Experimental and numerical results show that the shearhead contributes appreciably to punching shear capacity of the edge connection.

Various design codes on punching shear were compared; Eurocode 2 provides a good prediction of punching shear at edge support; which correlate well with experimental result. Hence, it was adopted to propose an equation for punching shear for edge connection with shearheads.

Most importantly, appropriate design guidance and analytical equation have been proposed for shearhead connection. The design guidance and equation would enable practising Engineers to design shearheads without going through the rigor of experimental or numerical investigation. This study has contributed appreciably to the applicability of steel column in flat slab construction.

Acknowledgements

The author wishes to express deep gratitude to everyone who has contributed to the success of this study. First and foremost, my Director of studies: success to this doctoral thesis Dr Adegoke Olubanwo, I am very grateful to you for leading me to a successful completion. Your technical advice and support is invaluable.

In similar vein, my two experience supervisors: Dr Neil Tsang and Dr John Karadelis are gratefully acknowledged for their technical inputs and swift response to my research needs.

I am also very thankful to Niger Delta Development Commission (NDDC) Nigeria for awarding me a doctoral scholarship and members of staff Civil Engineering Department, Rivers State University of Science and Technology Port Harcourt Nigeria for their support during my academic sojourn in the United Kingdom.

I am highly indebted to my love ones who supported me emotionally and financially and fervent prayers few amongst them are listed below: Syvian Akpobari Mbaedee, Baridor Ebenezer, Lemea Ebenezer, Abolobari Ebenezer, Pastor Comfort Mbaedee, Samuel Jonah Abbey, Babatunde Famuyiwa and Bishop Vincent Mbaedee.

Above all, the Lord Almighty, the author and dispenser of Knowledge and wisdom, may your holy name be glorified for the blessing of humanity, I am forever grateful for your afflatus, exceeding grace and unfathomable love for me.

List of Abbreviations and definitions

V_c = Punching shear capacity of the connection

C = column width or diameter

b_o = Critical shear perimeter

d = effective depth

$\rho = Average\ steel\ ratio$

$f_t{}'$ = Tensile strength of concrete.

$f_c{}'$ = specified cylinder concrete (MPa)

f_{ck} = characteristic cylinder strength.

v_c = shear stress

β_c = ratio of long edge to short edge of column section

LFEA = Linear elastic finite element

$C_{AA}\gamma_v$ = distance of the centroid of the critical section

V_g = Direct shear stress developed by gravity load.

γ_v = ratio of moment transferred by eccentric shear to total unbalanced which is defined according to each design method.

K = size effect factor

d_a = maximum aggregate size.

ℓ_x = dimension of the assumed critical section in the x- direction.

ℓ_y = dimension of the assumed critical section in the y- direction.

M_{xx} = bending moment distribution in the x- direction

β = shear retention factor

G_f = fracture energy in tension

G_c = fracture energy in compression.

NLFEA = Nonlinear finite element analysis.

EC 2 = Eurocode 2

$\phi =$ Shear reduction factor

ℓ_v = shearhead minimum length

M_p = shearhead minimum length

α_v = bending stiffness ratio between the shearhead and cracked concrete.

T_s = Thickness of slab

I_{CR} = second moment of area of concrete

I_s = second moment of area of steel.

Slab 1= slab without shear reinforcement

Slab 2 = slab with shearhead

f_y = yield strength of steel

ε_x = strain in the x- direction

ε_y = strain in the y- direction

γ_{xy} = shear strain

β = shear retention factor

V_{sh}= punching shear capacity of shearhead

v_g = Direct shear stress developed by gravity load;

b_0 =perimeter of the critical section.

γ_v = ratio of moment transferred by eccentric shear to total unbalanced moment, which is differently defined according to each design method.

Table of contents

List of Figures

List of Tables

Chapter 1 Introduction

(Setting the research into framework and perspective)

1.1 A Historical Reassessment

Flat slabs are beamless reinforced concrete slabs supported directly by columns without the use of intermediary beams. They may be of uniform thickness throughout or have deeper thickness (called drop or capital) around the vicinity of the supported columns (Oyenuga 2005) .The use of column capital is no longer pleasant from Architectural point of view. Therefore, current convention ignores use of column capital in flat slab design. Flat slab structural systems have a wide range of application due to their multi-functional and economic advantages, for instance the absence of beams facilitates erection time compared to the normal frame system. It is also very useful in multi-storey residential buildings, car parks and office complex due to reduced storey height which is achieve by the absence of beams and the ease of partition location (Koppitz *et al,* 2013). The use of reinforced concrete columns is very popular in flat slab construction but the applicability of steel column will present an attractive alternative especially in regions vulnerable to seismic activity. In addition, steel columns have many practical advantages in construction of flat slabs such as quick erection time and ease of construction (Eder *et.al,* 2011).

Despite these numerous advantages, the most significant structural deficiency of flat slab system is their vulnerability to punching shear failure. This has made punching shear failure a subject of intense experimental and theoretical investigations since 1960s (Muttoni, 2008). Although flat slabs system has a simple appearance, it develops a complex behaviour in flexure and in shear. This behaviour has triggered a lot of theoretical and experimental research on the analysis of the bending moments and on the safe design for punching with and without moment transfer between slab and column. According to (CEB 1990) punching is a shear failure within the Discontinuity region (D-region) of the highly stressed slab at the column. It is a brittle type of failure where the flexural reinforcement may not yield. From structural point of view, a thin slab directly supported by a column may cause serious weakness; it is like supporting a thin plate on pin supports. In this D-region of the flat slabs very high

moments occur and the three-dimensional state of stress is extremely complicated (Fib bulletin, 2001). The problems are even aggravated if columns are placed directly at edges or corners or if openings are placed near the columns. An edge slab-column connection with an asymmetrical critical section is subjected to an unbalanced moment developed by the gravity load as well as lateral load. This makes edge supported flat slab more vulnerable to punching shear failure than interior column (Fib bulletin, 2001). By considering this effect, Eurocode 2 recommends the shear force be increased by 40 percent at the edge column and 50 percent for corner column but could lead to conservative result. For flat slabs supported at the edge and corner columns, even under gravity loads only, both concentrated loads cause shear stresses in the slab. In addition, the unbalanced moments transferred from slab to column leads to the development a complicated non-symmetrical stresses in the slab around the edges and corners (Euro code 2).

Design errors in the computation of punching shear capacity of flat slabs system have caused severe catastrophic failures resulting in great loss of life and property across the world. A portfolio of failure scenarios in various part of the world is obvious as such. For Instance, a departmental store building collapse due to punching shear in Seoul Korea 1995.The apparent catastrophic scene is depicted

Fig 1.1 before collapse (Park 2012)

Fig 1.2: After collapse (Park 2012)

Record available shows that the disaster that occurred under service condition, claimed 498 persons. The failure occurred due to erroneous computation of punching shear (Park, 2012)

Similarly, a partial collapse due to punching shear occurred in the Piper's row car park in Wolverhampton United Kingdom 1997. Though this misfortune did not claim any life because it occurred at night under gravity load only, but the closure and subsequent pulling down of the whole 400-space park caused extensive disruption in the pattern of daily life and huge waste of financial resources. It was also reported that the structural design is based on CP114, which gave a poor pessimistic estimation of punching shear capacity of the connection (Wood 2003).The scene is shown in figure1. 3. Many cases of punching shear have occurred across the World.

Fig1.3. Punching shear failure of Piper' Row Park in Wolverhampton, U.K in 1997 (Wood 2003)

1.2 Research Significance

Copious experimental, analytical and numerical works are available on punching shear failure of interior connection subject to no unbalanced moment based on these available data. Current design codes such as ACI 318-05 adopted results obtained from interior connection and calibrated it to exterior connection which underestimates punching shear significantly. Current design codes such as Eurocode 2, BS8110, and Model Code 90 adopted similar design principles in their prediction of punching shear except ACI318-05 that ignores the contribution of flexural reinforcement to punching shear. Considering the variation of punching shear in the various codes, further comparison on the one that provides best approximation for punching shear shall be reviewed in this study. According to the available results, the dominant parameters influencing punching shear strength of the slab-column connection are the tensile strength of the concrete (f_t), tension reinforcement ratio (ρ_t), edge length of the column section (c_1), and effective depth of the slab (d). The effects of these parameters have generated a lot of divergent views amongst researchers which need further investigations.

In order to provide an in-depth theoretical background for punching shear strengths of slab-column connections, numerous theoretical strength models have been

developed. For instance, Nielsen (1999) and David and Orit (1999) have proposed strength models based on the theory of plasticity. Johansen (1962) and Bazant and Cao (1987) have proposed design equations based on the yield line method and Fracture mechanics. Alexander and Simmonds (1987) have also proposed the strut-and-tie model for slab-column connections. Eder (2010) carried out experimental and numerical studies on the contribution of shearheads to punching resistance of a hybrid flat slab supported on steel interior column subjected to both gravity and cyclic loading. It was concluded that shearheads have significant influence on the punching shear capacity of the connection.

Menetrey (2002) developed an analytical model that includes the contributions of tensile strength of concrete, dowel action of reinforcement, tension in case of prestressed and shear reinforcement.

Punching shear failure becomes complicated to evaluate for edge slab- column with asymmetrical critical section subject to unbalanced moment developed by gravity load plus lateral load. Based on this, there is a significant dearth of data on edge connections. To account for unbalanced moment that aggravates punching shear at edge connection, the ACI 318-05 provisions (ACI 2005) implemented the use of eccentric shear stress model for the design of edge column. Although, ACI model was developed from experimental data of interior column and extended to edge supported column. In the ACI model, the unbalanced moment carrying capacity of the edge supported connection is defined as the summation of the flexural moment capacity and the moment induced by the eccentricity of shear stresses developing at the connection. In a similar fashion, CEB-FIP MC 90 and BS 8110 have also defined the unbalanced moment carrying capacity as the summation of the flexural moment capacity of the critical section and the moment transfer by eccentric shear. But these vary from the ACI 318-05 provisions due to a variation in the ratio of flexural moment capacity and moment transferred by eccentric shear connection. A few researchers have examined the capability of ACI model in the prediction of strength of edge connection. For instance, Moehle et al. (1988) developed an improved strength model based on the results of tests performed on edge connection. By comparison, they observed that the strength of the exterior connection was significantly underestimated for connection subject to high punching shear (Park and Choi, 2006). Moehle's model

considers only the flexural moment capacity, therefore, ignores the moment due to eccentric shear.

Bompa and Elghazouli (2016) carried out an experimental investigation on the punching shear behaviour of hybrid flat slabs system embedded with shearhead connected to a steel column. Their result revealed that the behaviour of the connection was influenced by the shearhead properties. Furthermore, they suggested that the main function of the shearhead is to shift the critical sections away from the column vicinity; in term of bending moment and punching shear therefore, delay the failure load.

Eder et al. (2011) investigated the behaviour of a partially integrated shearhead system connected to interior tubular steel column subject to cyclic loading. They reported that shearhead increases the ductility of the connection under cyclic loading. In addition, the behaviour of the connection is governed by the strength and stiffness of the shearhead.

Almeida et al. (2016) conducted an experimental investigation on RC flat slabs reinforced with shearheards supported on interior connection subject to punching shear failure. The slab was tested under both vertical and lateral loading. They observed that lateral loading leads to significant reduction of the slab-column connection stiffness.

1.3 Problem Statement

- The analytical model of Menetrey, when compared to design codes equations gives a poor prediction of punching shear which could be attributed to the assumption of a uniform tensile stress across the inclined crack profile. This was perceived as a drastic simplification of the model (Menetrey, 2002)
- The assumption of a uniform shear stress distribution across the asymmetrical critical section is seen as a limitation of ACI eccentric shear stress model (Fib bulletin, 2001)
- To improve on ACI model, Park and Choi (2007) developed a model using nonlinear finite element method based on the observation that ACI318-05 assumption of unbalanced moment transfer by both flexure

and shear using different critical sections in which the critical section for shear is located in that of flexure induces torsional moment which contradicts this assumption. In order to enhance it; a single critical section for both flexure and shear with a critical section of 0.5d from the column face was used. But their results underestimate the strength of edge connection due to low flexural capacity of the assumed critical section.

Based on this limitation, a higher critical section from the column face for both flexure and shear is suggested.

- From literature available the use of steel column connected with shearhead is still very unpopular. There is a significant dearth of experimental data for edge steel column supporting flat slab. The two dissimilar materials (concrete flat slab and steel column) would require a shear head system for their connection. Eder (2010) research work is limited to interior column without unbalanced moment.
- Another important parameter that is almost completely lacking is the boundary conditions of isolated specimen that does not represent the real continuous slab. Although many researchers have always mimic ends fixity that correspond to the real slab which is very difficult to achieve (Alender and Markonvic, 2008). If assumed, what about the effects of compressive membrane and moment redistribution. To reconcile the difference between the real slab and isolated specimen is dealt with in this research work.

Based on the inherent limitations and gap identified in available literature, the research objectives are drawn.

1.4 Aim and Objectives

This research aims at studying the punching shear failure of RC flat slabs supported on steel edge column. The study was undertaken by employing state-of –the- art computational technique and experimental investigations. The finding was used to make design recommendations that would enhance the applicability of steel columns in flat slabs construction.

This aim was achieved through the following objectives:

- Reviews of existing studies to identify research gaps.
- Apply nonlinear finite element analysis to investigate punching shear capacity of the proposed shearhead assembly subject to static loading.
- Investigate punching shear failure of edge connection without shear reinforcement and compare to design codes equations.
- Modify ACI shearhead system for its applicability to steel edge column connection and propose a design procedure.
- Apply nonlinear finite element analysis (NLFEA) to undertake parametric study of governing parameters influencing punching shear failure.
- Validate and calibrate results of NLFEA via experimental investigations.

1.5 Scope of Research

Taking cognisance of the research materials available, firstly, specific focus is given to unrestrained boundary conditions by ignoring the effects of compressive membrane and moment redistribution that increase punching shear strength in real slab. Firstly, slab column supported at the edge without shear reinforcement is tested for comparison with design codes prediction. Secondly, innovative shearheard that enhances punching shear capacity at the edge was designed and tested in punching shear. Lastly detail parametric study on all governing parameters affecting punching shear was investigated. The effects of lateral load have been studied by previous investigators, therefore, not considered in this study.

1.6 Layout of Thesis

Chapter 1 sets the research into perspectives by exploring the phenomenon of punching shear failure. Catastrophic structural failure due to punching shear was reviewed. For the research significance, copious research works on both concentric and eccentric punching shear have been examined. Various strength models on edge supported flat slabs subjected to unbalanced moment by previous investigators have been examined. Based on the gaps and limitations identified, the research aim and objectives were drawn.

Chapter 2: Provides adequate theoretical background for this study by a rigorous exploration of various theoretical and analytical models that have been developed by previous researchers and design codes. A thorough review was carried out by tracing,

commenting, criticizing and recommending the work of previous investigators. This enhanced the development of sound theoretical understanding for this research. A grand summary was provided to synthesise valuable information drawn from the review.

Chapter 3 provides a theoretical numerical review and numerical models adopted by previous investigators on punching shear. These include nonlinear finite element method and experimental method. Brief review of the use of NLFEA in modelling punching shear problem is provided; this gives further understanding the type of elements, concrete failure criterion to be adopted. Comparison of various concrete failure criteria was carried out and the most appropriate was recommended.

Chapter 4 provides the research methodology. It provides the sequence in which each method was logically implemented.

Chapter 5: Provides the validation of adopted modelling scheme for the numerical modelling. Analytical solution of plate and experimental investigation of previous research work were validated using TS-Model implemented in Midas FEA (Finite element software used)

Chapter 6 provides thorough detail of the numerical procedure use in validating all experimental specimens and exhaustive parametric study of all governing parameters influencing punching shear failure.

Chapter 7 provides a comprehensive detail of the experimental programme performed at Structural Laboratory of Coventry University. It provides the rationale for performing tests and reports all procedures, observations and measurable quantities in the testing regime.

Chapter 8 presents the analysis of Results: results obtained from experimental, numerical and analytical studies are compared and analysed in line with the research objectives.

Chapter 9 provide the conclusion and recommendations for design guidance of flat slab supported on edge steel column.

Chapter 2: Review of theoretical and experimental studies

2.0 Introduction

This chapter provides in-depth theoretical and experimental studies on punching shear. Extensive review of relevant research works of previous investigators on both concentric and eccentric punching shear failure of flat slab to column connections were carried out by reporting, tracing, criticizing, commenting and identifying gaps for further investigation.

Since 1960, Punching shear failure has been a subject of intense experimental and theoretical investigations. Until now, there are still divergent views on the various design parameters and failure mechanisms of punching shear. This is discernible in the various design principles adopted in current codes of practice. According to (CEB 1990), punching shear failure occurs within the discontinuity region (D-region) of the highly stressed areas, usually within the vicinity of the slab-column connection. Punching shear is a brittle type of failure, which may occur before flexural yielding of the steel reinforcement. This reveals that the D-region is not adequately ductile to gain capacity from redistribution of forces. It also indicates that safety level cannot be increase up to certain point by provision of additional flexural reinforcement. According to (Elsanadedy *et.al*, 2013) significant higher stresses developed at flat slabs to column connection, which causes a catastrophic and brittle punching shear failure. This failure usually occurs as a result of the transfer of vertical shearing force due to gravity loads; in addition to unbalanced bending moment due to non-uniform gravity load or lateral loads due to wind. The possibility of progressive collapse requires a higher safety class in structural design.

For flat slabs design, the flexural and punching shear capacity need to be properly addressed. The intersection between the column and the slab is critical as concentrated forces can induce a cone shaped perforation through the slab thickness as depicted in figure 2.4. The perforation is developed as the cracks on the top surface caused by hogging moments extend downwards to the perimeter of the column. A ductile flexural failure occurs by a gradual decrease in load-carrying ability with increasing displacements. While a sudden loss in strength of the connection indicates a brittle failure known as punching shear failure which is very risky.

2.1 Failure Mechanisms

According to Menetrey (2002) (Cited in FIB Bulletin 2001) identified three possible types of failure for reinforced concrete flat slabs supported on columns as thus

- Flexural failure due to the formation of a yield line mechanism.
- Punching failure with a conical plug perforating the slab above the column.
- Bond failure, which is characterized by a slip of reinforcement.

2. 2 Current design methods for punching shear resistance.

Proven experimental works on punching shear failure by (Kinnunen and Nylander 1960) and others, have led to the development of some current design codes such as ACI 318-08, Canadian code (CSA), BS8110 and Euro code 2. The design resistance to punching shear is, generally in building codes, an empirically derived formulations based on various test results. The resistance is determined along a control perimeter where the nominal shear force per unit width is compared to the shear resistance per unit width of the control section. The definition of the critical perimeter differs in the various design methods. Code comparison is carried out to understand the one that provide the best approximation for punching shear. Detail account of punching shear provided in these codes is presented as such.

Table 2.1 control perimeters defined by various codes

CODE	CRITICAL PERIMETER	NORMINAL SHEAR CAPACITY (Unit: N and mm)
ACI 318-08	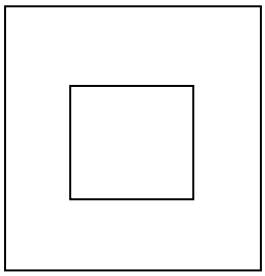 b_0 = 0.5d	$V_C = \frac{1}{3}\sqrt{f_c'}\ b_0 d$
BS8110	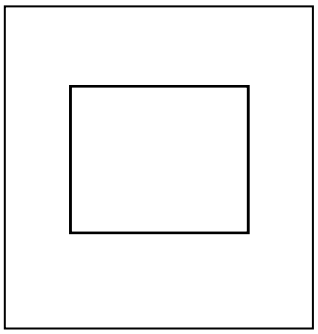 b_0 = 1.5d	$V_C = \mathbf{0.79}\left(\frac{\mathbf{400}}{\boldsymbol{d}}\right)^{1/4}(\mathbf{100}\boldsymbol{\rho})^{1/3} b_0 d$ The value of V_C shall be multiplied by $\sqrt[3]{f_{cu}/25}$ for $f_{cu} > 25\ MPa$ The value of $\sqrt[4]{\left(\frac{\mathbf{400}}{\boldsymbol{d}}\right)}$ shall not be less than 1.0 The upper limit of f_{cu} = 40 MPa has been ignored
Eurocode 2	b_0 = 2d 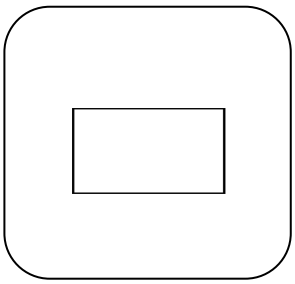	$\boldsymbol{V_c} = \frac{0.18}{\gamma}\left[1 + \sqrt{\frac{200}{d}}\right](\mathbf{100}\boldsymbol{\rho})^{1/3} b_0 d$ γ_c = partial safety factor = 1.5 (taken as 1.0)

2.2.1 ACI Code, ACI318-05

In this design principle, a simple equation for punching shear capacity of flat slabs system is proposed. The equation is based on classical shear strength equation. In ACI 318-08, the control perimeter is only 0.5d from the loaded area as depicted in table 2.1. The ACI code ignores the significant contribution of flexural steel reinforcement and the effective depth of the slab in its limiting shear stress. The code requires that the ultimate punching shear resistance for slabs without shear reinforcement, $v_{c,}$ be governed by the expression below.

$$V_{C} = 0.33\sqrt{f_c'} \quad \text{.....} \quad (2.1)$$

From these current design codes, there are significant variations in the approaches used to assess punching shear resistance of reinforced slab-column connections. Generally, all design codes adopt a simple punching shear on certain critical perimeter. The critical section for checking punching shear is usually situated a distance between 0.5 to 2.0 times the effective depth (d) from the edge of the loaded area. Another significant variation amongst codes is in the way they represent the effect of concrete compressive strength (f_c') on punching shear capacity, generally these codes expressed this effect in terms of $(f_c')^n$ where (n) varies from $(\frac{1}{2})$ to $(\frac{1}{3})$ in the European codes.

2.2.1.1 ACI318-05 recommendation for shearheads

ACI318 is the only code that provided design guidance for punching shear resistance using shearhead, but is only applicable to reinforced concrete column. The critical slab sections applicable to edge columns are depicted in fig2.1.

Fig.2 .1. Critical sections for edge columns reinforced with shearheads. (ACI318-05)

The plastic moment strength, M_p required for each arm of the shearhead shall be computed by

$$M_p = \frac{V_u}{2\phi n}\left[h_v + \alpha_v\,(\ell_v - \frac{C_1}{2})\right] \quad \text{..... (2.2)}$$

where ϕ is for tension-controlled members, n is number of shear arms. h_v = the overall depth of the slab. $\ell_v =$ the minimum length of the shear arm. α_v = the flexural stiffness ratio between structural steel section and concrete.

ACI 318-05 further recommended that the ratio α_v between the flexural stiffness of each shearhead arm and that of the surrounding composite cracked slab section of width $(C_2 + d)$ shall not be less than 0.15

Fig 2.2. Pressure distribution on shear arms (ACI 31-05 design guide)

The code also recommended that, the critical slab section for shear shall be perpendicular to the plane of the slab and shall cross each shearhead arm at three-

quarters the distance $(\ell_v - \frac{c_1}{2})$ from the column face to the end of the shear arm. But the assumed critical section need not be less than $^{d}/_{2}$ to the column.

2.2.2 EUROCODE 2 Design code

The recommendations provided in EC2 (2004) with respect to punching shear resistance are largely based on section 6.4.3 in the CEB-FIP Model- code (CEB 1990) both codes consider the following parameters

- Flexural reinforcement in the tensile zone (ρ_l)
- Concrete cylinders strength
- Size effect

Eurocode design principle assumed the conventional formulation similar to the uni-directional (one-way shear) case of a beam although a control perimeter is defined as the assumed crack periphery on the top surface of the slab. The punching shear strength is assumed constant for the entire control perimeter $(b_{0),}$ around internal columns with balanced moments. EC2 equation in table 2.1, relates punching shear strength in direct proportion to the bending reinforcement $(100\rho_l)^{\frac{1}{3}}$ where ρ_l is an average reinforcement ratio obtained from ρ_x and ρ_y EC2 limit ρ_l to a maximum value of 2% and 3% whereas no restriction is given explicitly to $(^{\rho_x}/_{\rho_y})$.

2.2.3 BS8110 code

The use of shear reinforcement other than links is not treated particularly in BS8110. The design procedure is as thus: the shear capacity of unreinforced slab is checked first (see Table 2.1 for control perimeter). If the computed shear stress does not exceed the design shear stress $v_{c,}$then shear reinforcement is no longer required.

If the shear stress exceeds $v_{c,}$then shear reinforcement should be provided on at least two perimeters according to figure 2.3.

- The first perimeter of reinforcement should be located @ approximately 0.5d from the face of the loaded area and should contain not less than 40% of the computed area of the shear reinforcement added.

- The spacing of perimeters of reinforcement should not exceed 0.75d and the spacing of the shear reinforcement around any perimeter should not exceed 1.5d.

- The shear reinforcement should be anchored around at least one layer of tension reinforcement.

The shear stress should be verified on perimeters @ 0.75d intervals until the shear strength is not less than the design concrete shear stress

.

Fig.2.3. BS 8110 guide on shear reinforcement (CEN 2002)

Table 2.2 Existing design methods for exterior columns (Park and Choi 2007)

Design codes	Shear strength (Mpa)	Unbalanced moment-carrying capacity
ACI318-05 (REF) Eccentric shear model	$v_{c,ACI} = (0.167 + \frac{0.33}{\beta_C})\sqrt{f_c'}$ .....(a) $v_{c,ACI} = (\frac{2.48d}{b_0} + 0.167)\sqrt{f_c'}$ .....(b) $v_{c,ACI} = (0.33)\sqrt{f_c'}$ ..... (c) β_C = ratio of long edge to short edge of column section. $v_{c,ACI}$ is the smallest of a, b and c	M_{ACI} is the smallest of (a) and (b) $M_{ACI} = (v_{c,ACI} - v_g)\frac{J}{C_{AA\gamma_v}}$ $M_{ACI} = (v_{c,ACI} + v_g)\frac{J}{C_{AA\gamma_v}}$ J = polar moment of inertia of the critical section. $C_{AA\gamma_v}$ is the distance of the centriod of the critical section to edge A-A.
CEB-FIP MC 90 (REF)	$\tau_{,CEB} = 0.18k(100\rho_l f_c')^{1/3} \geq 0.35k^{2/3}\sqrt{f_c'}$ $k = 1 + \sqrt{\frac{200}{d}} \leq 2.0$ where d is in mm ρ_l = reinforcement ratio for slab width $C_2 + 3d$	$M_{CEB} = (\tau_{,CEB} - v_g)\frac{W_1 d}{\gamma_{\gamma_v}}$ $W_1 = {C_1}^2/_2 + C_1C_2 + 4C_1d + 8d^2 + \pi dC_2$
BS8110	$\tau_{,CEB} = 0.18k(100\rho_l f_c')^{1/3} {f_{c\,cube}}^{1/3}$ $k = \sqrt[4]{400/d}$. $\rho_l \leq 0.03$ $f_{c\,cube}$ = compressive cube strength of concrete.	$M_{BS} = (\tau_{,BS} - 1.25v_g)\frac{b_0 d.x}{1.5}$ x = width of critical section = C_2 +3d.

2.3 Concentric Punching shear failure mode

In this section, selected models on punching shear failure of slab-column connection from available literature are presented. These models can be categorized as thus:

- Models based on Cracked slab segment (Kinnunen/Nylander approach)
- Models based on fracture mechanics
- Models based on plasticity theory
- Strut and Tie Model
- Numerical models
- Analytical models.

2.3.1 Model based on cracked segment by (Kinnunen and Nylander 1960)

Kinnunen and Nylander (1960) experimentally examined the punching shear capacity of a reinforced concrete flat slab supported on interior columns. The model was proposed based on the results of 61 tests; based on equilibrium considerations of a circular slab with radial cracked segments around a circular column. Test was conducted on specimens made up of circular slab supported on a circular reinforced concrete columns positioned centrally and loaded along the circumference. They observed the following punching failure mode.

- Firstly, tangential cracks developed on the top surface of the slab above the column. These were flexural crack due to hogging moments.
- As the load increases, radial cracks were formed after tangential crack initiation.
- After further loading, the tangential cracks departed from their original vertical direction into an inclined path towards the column face on the bottom surface of the slab.
- Bond failure of flexural reinforcement.
- Failure of the compressive cone shell.

This was the first mechanical model developed for punching shear; however, it does not yield good result when compared to test results. But the model visualized adequately the flow of forces which provides very useful hint for other researchers. The Kinnunen/Nylander approach could be characterized as a failure mechanism approach where rigid bodies separate at defined failure surfaces i.e. the radial cracks

and inclined shear crack surfaces. The basic idea was to create equilibrium of forces acting on the sector element as shown in Fig 2.4.

Fig.2.4. Mechanical model of Kinnunen/Nylander 1960 (FIB Bulletin 2001)

2.3.2 Modified mechanical model by Hallgren (1996)

The mechanical model proposed by (Kinunnen and Nylander 1960) provides a realistic description of the punching shear mechanisms. However, the failure criterion is given as a set of semi-empirical expressions which are based on strains measured in punching shear tests. But this model does not account for the size effect on the punching strength. A failure criterion was developed based on the finite element analysis of (Hallgren 1996) which revealed that the concrete between the tip of the shear crack and the slab-column root was in a triaxial state of compressive stress as shown in fig2.5. When crack appears, the confinement given to the tri-axial state of compressive stress at the slab-column root is lost and the shear crack can break through the radial compression zone, causing a sudden loss of load carrying capacity. This is believed to be the cause of punching shear failure. This formed the basis of the failure criterion adopted in the modified mechanical model. The proposed punching model, suggests that just before failure, the strain is equal to the vertical tensile strain, Based on this, and by adopting the fictitious crack model by (Hillerborg et al. 1996);the ultimate tangential strain is equated to the average strain across the compression

zone when the critical crack width W_c is reached. Based on the previous finite element analysis and on test observation, a modified mechanical model of punching of RC slabs without shear reinforcement was proposed.

But the proposed model is limited to the analysis of symmetric punching of RC slabs without shear reinforcement. Based on this limitation, there is a need to modify the model to include forces from shear reinforcement and forces from prestressing tendons.

Fig.2.5. Slab-column connection subject to triaxial stress (Hallgren 1996).

2.3.3 Fracture mechanics model by Bazant and Cao

Bazant and Cao (1987) adopted fracture mechanics approach. They developed this model based on the concept that punching failure does not occur concurrently along the failure surface; instead the failure zone propagates across the structure with the energy dissipation localized into the cracking front. On this basis, fracture mechanics should be adopted in the prediction of punching load instead of plastic limit analysis. That is, it should be based on energy and stability criteria instead of strength criteria.

They further argued that the basic difference between plastic analysis and fracture mechanics is the size effect .Fig 2.6 illustrates that the nominal shear stress at failure in equ. 2.3 of geometrically similar structure for plastic analysis is size independent, whereas for fracture mechanics it decreases as the structure size increases

$$\sigma_N = \frac{P_u}{bd} \quad \text{.....} \quad 2.3$$

Where b presents punching diameter and d is slab thickness

Fig.2.6. size effect law (Bazant and Cao 1987).

. According to their investigation, it was observed that linear fracture mechanics always overestimates the size effect of RC structures. Therefore, nonlinear fracture mechanics is deemed suitable for application because it represents a gradual transition from the failure criterion of limit analysis to the nonlinear elastic fracture mechanics as depicted in fig 2.6.

Bazant and Cao (1987) performed an experimental investigation on specimens for size effect on punching shear. The thicknesses were 25.4mm, 50.8mm and 101.6mm thick. The load-deflection curve in fig 2.7 shows that the failure was caused by brittle cracking and not by plasticity of the concrete. It was also observed that the larger the specimen size the steeper is the decline of load after the peak point. The test results confirmed that significant decrease of the nominal shear at failure $\sigma_N = \frac{P_u}{bd}$ occurred with an increase of the slab thickness.

Fig 2.7 a,b,c Load deflection curve for slab specimens (Bazant and CaO 1987)

From their findings, equation 2.4 below was proposed for the computation of punching load

$$V_c = C.(1 + \frac{d}{\lambda_0.d_s})^{0.5} \quad \text{..... (2.4)}$$

Where V_c is the nominal shear stress C = value of the nominal shear stress according to plastic limit analysis $= k_1 f_c\,(1 + k_2.\frac{d}{b})$

d = slab thickness. b = diameter of the punching cone.

$k_1 k_2$ = empirical constants.

$\lambda_0 =$ Empirical parameter characterizing the fracture energy of the material and

d_a = maximum aggregate size.

2.3.4 Model of Yankdevshy and Leibowitz

Yankelevshy and Leibowitz (1995) proposed a model for concentric punching based on a rigid-post-fractured behaviour. This model considers equilibrium and kinetic conditions, which makes it capable of also computing the load displacement behaviour. The model disregards the significant contribution of reinforcement but considers strain based on aggregate interlock mechanisms. Their model is capable of

- Computing the normal and shear stress distribution along the failure surface.
- Computing the variation of these stresses relating to the axial displacement.
- Predicting the ultimate punching force.

2.3.5 Plasticity model of Bortolotti

Bortolotti (1990) applied plasticity theory based on modified coulomb yield criterion for concrete. Bortolotti model considers strain softening in concrete. He applied the upper bound solution to determine the punching load by virtual work method. But the model underestimates punching shear strength of interior connection.

2.3.6 Truss model (Alexander and Simmonds 1986)

Alexander and Simmonds (1986) proposed a space truss model composed of steel ties and concrete compression struts as depicted in the shaded area in fig 2.8 The concrete compression strut is inclined at an angle α to the slab plane.

Some basic assumptions of the model are:

- The steel bars at the vicinity of the column behaves as tension ties and yield before failure.
- Punching shear occurs when the concrete cover spalls due to a vertical component of the compression strut at the intersection of compression struts and tension ties.
- The angle of inclination α was assumed to be a function of various variables such as: tension bar spacing, concrete strength bar area and yield strength, column size and effective depth.

Fig .2.8 Truss model (Alexander and Simmonds 1986).

Alexander and Simmonds (1992) suggested that a curve compression strut with varying α along the slab depth correlated more with test results.

2.3.7 Analytical model of Menetrey

Menetrey (2002) proposed an equation (2.5) connecting punching and flexural failure based on tests on circular slabs. In the case of pure punching, α_0 in equation 2.5 represents the inclination of the shear crack. The flexural failure load could be obtained from yield line analysis around the column where $r_s\ is$ the radius of the circular slab .The main assumption of this model is that the punching failure is significantly influenced by the tensile stress in the concrete along inclined punching crack. The novelty in this approach is the addition of all parameters contributing to the enhancement of shear resistance of the connection as depicted in equation 2.6, where F_{ct} represents the contribution of the tensile strength and can be obtained by the integration of all the vertical component of the tensile stress along the conical failure surface

$$F_{fail} = F_{pun} + (F_{flex} - F_{pun}) \left\{ \sin \left[\frac{\pi}{\pi - 2\alpha_0} - (\alpha - \alpha_0) \right] \right\} \quad \text{..... (2.5)}$$

$$F_{pun} = F_{ct} + F_{dow} + F_{sw} + F_p \quad \text{..... (2.6)}$$

Fig. 2.9 showing inclined tensile crack of concrete in the vicinity of the column (Menetrey 2002)

The fundamental idea of the model is the assumption that punching shear failure corresponds to the failure of the concrete tie, so that the tie strength is equivalent to the punching strength.

The assumption of zero tensile strength across crack resulted to a drastic simplification of the model. Because nonlinear fracture mechanics has proven that tensile stresses can still be transmitted across the inclined cracked as depicted in fig 2.9 which underestimates the punching shear strength.

2.3.8 Model of Theodorakopoulus and Swamy

Theodorakopoulus and Swamy (2002) have developed analytical punching shear model which is based on the physical behaviour of the connection under load. From their findings, it was observed that punching shear is influenced by the following parameters

- Ratio of the column size to the effective slab depth.
- Ratio of shear resistance to flexural resistance
- Concrete compressive strength
- The column shape and lateral constraints

The model presumes that punching is a form of combined shearing and splitting, occurring without concrete crushing under complex three dimensional stresses. Failure is assumed to occur in the compression zone above the inclined cracking when the limiting shear stress equals the tensile splitting strength of concrete.

2.4 .0 Eccentric punching shear

Punching shear failure becomes more significant at the edge connection, due to the presence of unbalanced moment induced by gravity and lateral loads. ACI –code provides appropriate design guidance especially when a shearhead is used in the slab-column connection. The ACI 318-05 code assumes a linear elastic shear stress distribution along the defined control perimeter around the shearhead as depicted in fig.2.11.

Adel and Ghali (1996) performed a linear finite element analysis on external and internal slab to column connection. They observed that the shear stress distribution along the control perimeter is not linear as documented in the ACI-code. They believed that code assumptions are practical and conservative. It was observed that rotational stiffness of the connection decrease continuously with increasing load.

Krueger et al. (1998) performed tests on 2.7m × 2.7m square reinforced concrete slabs with 300mm × 300mm reinforced concrete columns. A rigid frame was formed around the perimeter to support the slabs. Lateral and vertical loads were applied concurrently with three different eccentricities of e = 0, e = 160 mm and e = 320 mm. They observed a decreased in punching strength when unbalanced moments were present. The decrease could be in excess of 30% for large eccentricities of column load. It was also observed that the flexural reinforcement significantly increase the ductility of the punching mechanism, by inducing much larger rotations of the column at failure.

2.4.1 Moment Transfer

Elgabry and Ghali (1993) investigated the moment transferred by shear in slab-column connections in accordance to ACI 318-89. According to ACI provision on slab-column connection transferring unbalanced moment, it was recommended that the unbalanced moment transferred from the slab-column connection should be resisted by both flexural moment of the slab and the eccentricity of shear stress. The ACI

model assumes that shear stress varies linearly over the critical section. ACI code provides for the following equations for the proportion of moment resisted by shear.

$$\gamma_{vx} = 1 - \frac{1}{1+\left(\frac{2}{3}\right)\sqrt{\ell_x/\ell_y}} \quad \text{..... (2.7 a)}$$

$$\gamma_{vy} = 1 - \frac{1}{1+\left(\frac{2}{3}\right)\sqrt{\ell_x/\ell_y}} \quad \text{..... (2.7b)}$$

Where $\ell_x \; and \; \ell_y$side are dimensions of the assumed critical section in the x and y directions as depicted in equation Fig.2.10

This item has been removed due to 3rd Party Copyright.
The unabridged version of the thesis can be found in the
Lancester Library, Coventry University.

Fig 2.10. Critical section for edge connection (ACI318-05)

They observed that these equations were formulated by ACI based on tests on interior slab-column connections without shear reinforcement. Therefore, they developed an equation that can be applied to edge column by employing linear finite element analysis as thus.

$$\gamma_{vy} = 1 - \frac{1}{1+\left(\frac{2}{3}\right)\sqrt{\ell_x\ell_y - 0.2}} \quad \text{(when } \ell_x/\ell_y \geq 0.2\text{)} \quad \text{..... (2.8)}$$

γ_{vx} The same as equation 2.8

But this equation does not correlate well with experimental results .Their finite element was further reduced by 0.15 which shows that it over estimated the eccentric shear stress.

Moehle (1986) reviewed some selected experimental data on strength of slab-column edge connections transferring moment perpendicular to the edge. These data were

compared with ACI 318-83 eccentric shear stress model and were found not correlating. Therefore, an analytical model based on moment transferred by flexure was developed; neglecting moment transfer by eccentricity of shear stress. This negligence of the eccentric shear is based on the assumption that no significant interaction between shear and flexural moment occurred at the edge column at failure. He concluded that either the connection fails at its pure shear strength or at its pure flexural strength, whichever first occurred. He recommended that the ratio of moment due to eccentric shear of ACI eccentric shear model should be reduced in order to achieve better correlation with experimental data.

2.4.2 Combined shear and moment transfer

According to ACI 318-05 code, shear and a portion of the transfer moment computed at the centroid of the slab critical section are assumed to produce shear stresses that are distributed linearly on the slab critical section

Fig 2.11.Critical section for edge connection and eccentric shear stress (ACI318-05)

The proportion γ_v of the transfer moment assumed to be carried by eccentric shear stress is given by Equation 2.9 as thus

$$\gamma_{vx} = 1 - \frac{1}{1+\left(\frac{2}{3}\right)\sqrt{\beta_{cr}}} \quad \text{..... (2.9)}$$

Where β_{cr} = ratio of the slab critical section dimension measured parallel and transverse to the direction of moment transfer. Under combined shear and uni-axial

moment transfer, nominal shear stresses acting on the slab critical section are computed according to Equation 2.10

$$\boldsymbol{v_c} = \frac{\boldsymbol{V_u}}{\boldsymbol{A_{cs}}} \pm \gamma_v \frac{M_s c_v}{J_c} \quad \text{..... (2.10)}$$

In which $\boldsymbol{v_c}$ **=** the factored concrete shear stress, $\boldsymbol{V_u}$**=** the factored design transfer shear, M_s = The factored design transfer moment computed at the geometric centroid of the slab critical section to the point where the shear stress is computed parallel to the direction of moment transfer. J_c = polar moment of inertia of the slab critical section about its geometric centriod. According to the Eccentric shear model, a proportion of moment not transferred by eccentric shear stresses is to be resisted in flexure by slab reinforcement placed within a width extending 1.5 slab thicknesses on both sides of the column. The reinforcement should be positioned as either top or bottom reinforcement, or both as required in order to resist the tensile stresses due to moment. This flexural reinforcement is not included in the reinforcement bars already provided for non-transfer. According to the eccentric shear model, strength is reached when the computed shear stress in equation 2.10 reaches a critical value equal to $\boldsymbol{v_o}$ or when the moment transferred by flexure reaches the flexural strength of reinforcement within the effective transfer width $\boldsymbol{c_2 + 3h}$

2.4.3 Effect of connection proportions.

According to Moehle, Leon and Kreger (1988) suggested that for a typical small value of the ratio of the perimeter of the slab critical section to slab effective depth for instance ($\frac{b_0}{d} = 8$), shear failure involves a complex three-dimensional failure surface that is confined by in-plane stresses within the slab. As the ratio of $\frac{b_0}{d}$ increases, there is a likelihood of the confinement to be reduced, which may result to a decrease in shear strength.

This observation was also substantiated by the data presented by Dilger and Ghali (1981) in which the variation of shear strength as a function of the $\frac{b_0}{d}$ ratio was observed. Been satisfied with the evidence that shear strength varies with $\frac{b_0}{d}$ ratio, it is recommended that the shear strength be taken as $0.75V_0$ if $\frac{b_0}{d}$ is in the range 20 and 40 and as $0.5V_0$ if $\frac{b_0}{d}$ exceeds 40, where V_0 is defined by equation 2.11.

2.4.4 Shear Transfer

For connection having no moment transfer, the basic shear strength equation according to ACI 352-88 is given as

$$V_0 = 0.17\left(1 + {}^{2}/_{\beta_c}\right)\sqrt{f'_c}\,A_{cs} \leq 0.33\sqrt{f'_c}\,A_{cs} \quad \text{..... (2.11)}$$

Where V_0 is the strength in Mpa

A_{cs} = critical section area in mm^2 which is defined as the slab cross-sectional area cut by planes perpendicular to the slab surface at a distance ${}^{d}/_{2}$ from the column face. β_c = ratio of long to short dimensions of the supporting column.

2.4.5 Effect of connection yield

The connection strength provided in equation 2.11 was obtained from experiments in which the connection failed in shear at a load approximately equal to the flexural yield. According to Hawkins and Mitchell (1979), the connection strength in equation 2.11 was proposed from experiments in which shear failure occurred preceding or approximately coinciding with the flexural yield. They suggested that if significant yielding of flexural reinforcements occurs before the shear strength is reached, the shear strength is reduced. Hawkins and Mitchell (1979) have attributed the loss of strength to loss of membrane action around slab to column connection as a result of yielding. Based on this it is recommended that the shear strength of a connection be reduced to three-quarters of equation 2.11 if significant yielding is expected.

2.4.6 Effects of gravity loads

Pan and Moehle (1992) performed an experimental study of Slab-Column connections and the results show that the level of gravity load on flat slab is one of the most critical factors in determining the lateral behaviour of reinforced concrete flat slabs. Similar observation was made by the experimental studies on flat plates by (Akiyama and Hawkins 1984). They concluded that the predominant cause of failure of flat plate connections is attributed to excessive vertical shear stresses that are induced by the combined action of the applied gravity load and moment transfer. Pan and Moehle (1992) observed that when gravity load is increased, there is a significant reduction of the shear capacity of the connection to resist moment transfer due to lateral loads.

2.5.7 Park and Choi Model for unbalanced moment

Park and Choi (2007) carried out a nonlinear finite element analysis to develop a strength model for exterior slab to column connections subject to unbalanced moment developed by gravity and lateral loads. Based on the observation that current design codes do not properly estimate the punching shear strength of exterior slab-column connections specifically ACI318-05 model. The limitation of ACI318-05 was traceable to the use of different critical sections for both shear and flexure in the prediction of punching shear strengths of edge slab-column connections. In the eccentric shear stress model of ACI 318-05 provisions, the total resisting moment is the summation of both moment transfer by the eccentricity of shear and the flexural moment of the slab. Park and Choi (2007) observed that the use of the critical section of $c_2 + 3h$ for flexural moment and the inscription of another critical section of $c_2 + d$ for eccentricity of shear stress induces severe torsional moment by the eccentric shear. This would significantly influence the flexural moment capacity of the slab width $c_2 + 3h$. This observation seems to contradict the design principle that the unbalanced moment of the slab-column connection are resisted by both flexure and shear, since torsional moment due to eccentric shear is transmitted to the flexural moment section. In order to overcome this inadequacy in the ACI318-05 design principle, they adopted the same critical section of 0.5d for both flexural moment and eccentric shear. In order estimate the total resisting moment at the connection, they splitted the moments into various components: moments transmitted at the front and back and at the side (Torsional moment was assume at the side as shown in table 2.2.

2.5 Review on experimental studies on edge supported flat slab

This section examines experimental procedures that have been adopted by previous investigators. It also focuses on the type of boundary conditions and its effects on punching shear capacity of isolated slabs. Difference between isolated slab and the continuous slab was investigated.

2.5.1 Isolated slab

From literature available, most analytical and numerical models on punching shear have relied on experimental results. Very little attention has been given to the deviation of the isolated slab from the real slab, therefore the effects of test set up and boundary conditions need further investigations. The isolated specimen that is

traditionally obtained from the points of moment contra flexure of the real structure has a major disadvantage; it does realistically model the behaviour of a slab-column connection in real structure. According to Alexander (1986), a major advantage of the isolated specimen is that it gives the slab some freedom in determining its own force distribution along the boundary.

2.5.2 Effect of Boundary conditions

Elstner and Hognestad (1956) punching shear test have revealed that the types of boundary conditions adopted could have a significant influence on the punching shear load. According to their report, four square edges were simply supported, two opposite edges are simply supported, and the four corners are simply supported. It was observed that the distribution of shear stresses around column at $^{d}/_{2}$ from for the column face obtained from linear finite element; are roughly identical for the three cases. The tests revealed that shear strength was significantly reduced at the edges there were continuously supported. The moment to shear ratio for the slab supported on its four corners was higher than the simply supported along its four edges therefore, the later experiences higher punching shear strength.

Alendar and Marinkovic (2008) performed experimental studies on punching shear strength of post-tensioned lift slab at edge column. The specimens were obtained from a prototype edge panel at full scale at the points of contra flexure. The boundary conditions that replicate the prototype structure were implemented. The isolated specimens that represent a portion of the prototype edge panel were loaded to failure. The prototype slab was designed based on its spans of 7.5m in both directions with a superimposed dead load of 1.0 kN/m^2 and live load of 2.5kN/m^2. Based on this load configuration, structural analysis was carried out to obtained points of contra flexure and maximum bending moment.

On the lateral sides of the prototype slab where negative bending moments (parallel to the free edge) in a prototype slab are equal to zero, a free edge of the specimen has been adopted. Where the positive bending moments (perpendicular to the free edge of the slab are maximum in the prototype, restraint was adopted. All the three specimens were of the same dimensions (3.5 ×2.8× 0.18m).The layout is depicted in fig 2.12.

Fig. 2.12. Structural layout of the prototype and the specimen extracted (Alendar and Marinkovic 2008).

A test frame made of closely spaced rigid steel girders was used to achieve boundary conditions

This corresponds to the end fixity of the prototype as depicted on figure 2.13

Fig 2.13a boundary condition adopted. Fig 2.13b: Elevation of test set up (Alendar and Marinkovic 2008)

It is definitely impossible to create fixity in the laboratory as they intended to. These boundary conditions are erroneously adopted because a hogging moment may be created close to the mid-span as opposed to the maximum bending moment they intended to create. Elastic analysis would have been conducted to investigate the boundary conditions that create the similitude they intended to achieve.

Moehle and Pan (1992) conducted an experimental study of slab-column connections. The failure of the connection subject to biaxial moment was considered. The core objectives of the experiment were to:

- investigate the effects of biaxial lateral loading
- effects of gravity load on lateral behaviour

In the prototype structure, the column was used as a secondary load transferring mechanism. The shear wall was the primary load transferring mechanism. The specimen was obtained from the points of contra flexure of the prototype. But the boundary condition does not represent the end fixity in the prototype which they aimed to achieve. In addition, no account was given for the in-plane forces (membrane action) and moment redistribution that have unavoidably induced because of the restrained boundary conditions. Sufficient flexural reinforcement was used in the column region. They did not specify the critical or control perimeter for punching shear. Their experimental results show that the gravity load dominated and influences the lateral load behaviour, which agrees with the report of Akiyama and Hawkins (1984) that majority of punching shear failure of flat-slab connections is due to excessive vertical shear stresses that are induced by the apply gravity load and moment transfer. Based on their findings, it was concluded that ACI eccentric shear stress model yields conservative results for both uniaxial and biaxial cases.

Ghali and Dilger (1976) conducted experimental investigation on flat plate subject to static and horizontal forces. The specimen was obtained from the contraflexure bound of a prototype interior column under the effect of uniformly distributed gravity load. The content axial force (V) applied on the specimen is assumed to simulate the effect of distributed gravity load on the slab in the prototype. The test specimens were simply supported on the slab edges. According Criswell (1970) suggested this type of set up does not represent the prototype structure, but the result of their Elastic Finite Element Analysis shows that the stress resultants due to induced load and moment dies out quickly from the column faces and are not affected by the degree of fixity of the slab edges. This claim is theoretical not appropriate because in the prototype, fixity activates membrane actions and redistribution of moment between mid-span sagging moment and support hogging moment.

Vanderbilt (1972) also performed punching shear test to investigate the variation of shear strength with aspect ratio (c/d) column size to depth of the slab, therefore, various column types and sizes were used. He acknowledges the shortfall of the isolated slab-column connections from the real structure as thus;

- In-plane forces which may be present in the real structure are absent in the isolated model.
- Redistribution of forces which can take place in the real structure with progressive increase in load is largely absent in the model.

Following the conventional method, the specimens were obtained from the locations of lines of contraflexure around the column in the prototype structure.

Test results revealed the following;

- The shear strength was a function of column shape, as well as size with higher strength than square columns of equal periphery. This difference is attributed to stress concentrations present at the corners of square columns.
- The available equations for predicting shear strength do not correlate well with test data.

2. 5. 3 Punching Shear Capacity of Real Slab

Evidence from experimental investigations has shown that punching shear capacity of a real slab is significantly higher than that of an isolated specimen. For instance, Ockleston (1955) conducted an experiment on a portion of real continuous slab in a building in South Africa in 1952; and observed that the punching shear failure load was significantly higher than value predicted on an isolated specimen. However, the numerical value was not reported. Chana and Desai (1992) also conducted tests on a full scale shear reinforced slabs supported by a central column and a significant higher punching failure load was reported. Similarly, Choi and Kim (2012) tested a square slab with restrained rotation of the edges, and reported that the reinforcement ratio for sagging moment at the edges of the slab equally influences punching strength as the hogging moment over the support (Choi and Kim 2012)

Based on this significant deviation of the real slab from an isolated specimen as proven by previous investigators, Einpaul *et.al* (2015) performed a through

comparative study to understand the factors influencing higher punching shear in real slab. Their observations were summarised as thus:

- In a real slab, moment redistribution could occur between sagging moments in mid-span and hogging moments around the column which could lead to shifting of the line of contra flexure of the slab and influences its shear slenderness.
- Lateral expansion occurs in the isolated specimens after flexural cracking on the supports. This expansion is constrained in a real slab, which induces axial compression within the hogging moment region and increases the stiffness of the slab in bending.
- Compressive membrane action that may result from restraint against lateral expansion of the slab provided by stiffer support at the corners or edges of the slab, causes expansion of the hogging moment area due to the in-plane stiffness provided by the sagging moment area.

2.5.4 Effects of compressive membrane action

The phenomenon of compressive membrane action is normally considered as a secondary effect, which occurs after cracking of concrete or yielding of flexural reinforcement. Results of tests have confirmed the enhancement of load capacity of continuous slab by compressive membrane action (FIB Bulletin 2001).Attempt to account for the contribution of compressive membrane to punching shear has been investigated by Masterson and Long (1974) in which a rational method was developed. The method considers the portion of the slab inside the nominal line of contra flexure to be laterally restrained by the surrounding zone of the slab inside the nominal line of contra flexure to be laterally restrained by the surrounding zone of the slab and therefore compressive membrane action is induced as the slab

Similarly, Trapani *et.al* (2015) evaluated the effect of compressive membrane action on punching shear of flat slab and observed that membrane action increases both the bending and punching shear capacities of flat slab.

2.6 Review on shearhead systems

It is necessary to review some existing shearhead systems in order to understand their performance. The following shearhead systems are currently in practice.

1. American type cruciforms
2. German type composite cruciform verbundkreuz

3. Swiss type Geilinger
4. Swiss type Tobler-Walm
5. Solid cruciform with staples

A shearhead is designed to transfer forces of the neighbouring concrete slab through shear arms to the column.

The American type shearheads as shown in Fig.2.14a and 2.14b bare made of hot rolled I-section or channel sections. It is usually cast between the flexural reinforcement layers of the concrete slab and connected to the column. Channel section can also be used for RC columns. The closed shearhead type depicted in fig 2.14c is made by connecting a hot rolled steel sections to the ends of the shear arms (This forms a frame). This is analogous to a beam in a frame structure. The close shearhead could have higher stiffness compared to other types of shearheads. The Swiss system Tobler walm depicted in fig 2.14e is popularly applied in Tandem with steel composite columns. From its design, the slab will only sit on the flanges of the tee sections. The T-shapes on the top are connected to a flat steel bar which passes via the column and is meant to resist tensile force, but to achieve equilibrium, it may require concrete compressive struts and tie model but in case where unbalanced moment is present, it would not be suitable because adequate strut and tie model may not developed.

The German system verbundkreuz in fig 2.14g was designed by (Piel and Hanswille, 2006). This shearhead was designed basically for gravity load dominated condition. From this review, the ACI shearhead system is would be modified and adopted to suite the purpose of this research. Shearheads are welded the column section in form of shear reinforcement. It is made of structural steel sections across the column section, also known as shear arm. It was first develop by (Corley and Hawkins 1968). Fig. 2.14f depicts the details of a shearhead system developed by Corley and Hawkins in 1968. It can also be applicable to flats slab system supported on steel tubular columns via shearhead connection.

Fig 2.14. Various shearhead systems (Eder et.al 2010)

Corley and Hawkins (1968) have determined the shear force distribution in a cruciform type shearhead which agrees with the specifications made in the ACI-code. From their results, it was revealed that the shear distribution is constant along the shearhead and it depends on the ratio of the flexural stiffness of the steel section to that of the cracked steel- concrete composite section. However, they assumed that the shear force is transferred from the slab to the column by the tip of the shear arms only.

Cheol-Ho Lee, Jim-won and Song (2008) performed a full scale test on concrete filled tube (CFT) column to RC flat slab connections subject to gravity loading. For shear transfer from slabs, to columns, two types of shear key were used namely; a Tee section and a wide flange section. The wide flange section was designed in accordance to (Corley-Hawkins 1968) and (Wang and Salmon 1979). A wide flange section of H-100mm ×100mm ×6mm with 320mm long was used to ensure punching shear strength was achieved which can be compared to that of Reinforced concrete flat slab structure. The connection detail is depicted in fig 2.15

Fig 2.15.shearhead system (Cheol-Ho Lee, Jim-won and Song 2008)

In order to simulate gravity load on the slab, the slab-column specimens were placed upside down followed by the application of an incremental vertical loading on the column. The edges of the specimen were simply supported and lateral movement of the edges was restrained to mimic the inflection lines as depicted in fig 2.16

Fig 2.16.Experimental set up (Cheol-Ho Lee, Jim-won and Song 2008)

They ACI 318-05 recommendation on shearhead design was not adopted, therefore there is no guarantee that the connection would satisfy the requirements for punching shear. Attempt to create inflection lines by restraining the edges may not satisfy less accurate instead it induces compressive membrane in the slab which was not accounted for.

2.7 identified gaps

From the available literature reviewed, there is a significant dearth of research work on edge connection. Especially edge connection reinforced with shearhead. Few available research works on shearhead ignored the significant effect of bending

stiffness between the shearhead and cracked concrete as recommended by ACI318-05. The use of steel column as alternative to RC column for edge connection is relatively scarce. Furthermore, there is a significant dearth of data on edge connection.ACI 318-05 used the data obtained from interior connection to proposed equation for edge connection; which significantly underestimates the punching shear.

Therefore, test for edge slab-column connection without shear reinforcement was carried out to investigate its punching shear capacity for comparison with existing design codes equations. In addition, this study is focused on the development of a novel shearhead assembly for connecting edge supported steel column to flat slab.

2.8 Summary

The general criteria any model must consider first is equilibrium, followed by assumed constitutive laws, material strengths and failure criteria, most notably the influence of concrete tensile strength. Most empirical models met some of these criteria but ignore the significant aspect of equilibrium. Only the strength criterion for failure loads or shear force is satisfied within the range of experimental verifications.

Drastic simplifications were adopted in various empirical equations to make them easy for codes implementation. Equilibrium could be accounted for in global analysis using linear finite element. However, this cannot completely describe punching shear behaviour. Even though this does not completely undermine empirical equations; they are still invaluable in design codes for other type of shear problems.

Mechanical models could be so complicated therefore; empirical models are preferable in design (Fib Bulletin 2001). Most empirical model ignores the residual tensile strength of cracked concrete.

In order to overcome the shortcomings of empirical model, Fracture mechanics has been used to study the behaviour of the residual tensile strength across crack. Nonlinear Finite element analysis (NLFEA) accounted more on the residual strength of cracked concrete. For this reason, NLFEA was adopted as the dominant methodology.

A comprehensive literature review was carried out to examine theoretical and experimental research conducted on both concentric and eccentric punching shear by previous investigators. Firstly, the relationship between flexural and punching failure was examined, which revealed that flexural failure is preceded by the formation of

yield line mechanism while punching is characterised by an abrupt decline in load value at failure. Based on proven experimental works of previous investigators, design principles on punching shear was provided in the various codes such as BS8110,EC2, CSA, ACI. These codes were compared to examine the one that provides the best approximation for punching shear without partial factor of safety. Comparison shows that ACI318-05 is the only code that provide design guide on the application of shearhead at slab-column connection. However, ACI shearhead systems are limited to Reinforced concrete column; therefore, further modification for its applicability was considered. Various sheadhead systems were compared and contrast. I-section adopted for the experiment was deemed most suitable based on its advantages.

Numerous theoretical models developed on concentric punching shear were examined. These were reviewed to understand punching shear parameters use to formulate analytical equations. Various theoretical models were reviewed such as models based on Fracture mechanics, plasticity, mechanical, strut and tie and empirical.

Eccentric punching shear is the core focus of this research. Punching shear becomes more complicated for edge-supported connections due the presence of unbalanced moment resulting from gravity and lateral load. Because of this, data for edge connections are relatively very limited. In order to deal with the effect of unbalanced moment, ACI 318-05 developed an eccentric shear stress model from data of interior connections. However, ACI model underestimate the strength of edge connections reported by (Moehle 1988) and other investigators. This was traceable to assumption of a uniform shear stress distribution along the asymmetrical critical section, which remains a fundamental shortcoming of ACI model. ACI eccentric shear model is based on the principal that the unbalanced moment is transferred by both flexure and shear in a ratio of 0.6 and 0.4 respectively.

For both concentric and eccentric punching shear, both design codes and previous investigators had neglected the contribution of compressive membrane to punching shear. Due to experimental limitation, test on full-scale prototype is relatively scarce. This is attributed to its cost intensive nature and experimental difficulty. To overcome this difficulty, investigators always use the conventional procedure of obtaining an isolated slab from a prototype structure at the contra flexure bound region. However,

test on isolated slab does not reflect the behaviour of real continuous slab. Therefore, comparison was carried out to sort their difference. It was revealed that the difference is due to contribution of compressive membrane action and redistribution of moment between the hogging and sagging moments lead to higher punching shear capacity in the real continuous slab.

Most investigators reviewed in literature have intended to replicate the boundary conditions of the real slab, which is relatively difficult to implement in the laboratory. Despite the restraints, they failed to account for compressive membrane effect.

From this research, therefore, an unrestrained boundary condition was adopted to avoid the inducement of compressive membrane and moment redistribution on the primary variables under consideration. This solution was envisaged to provide a lower bound solution, which was bench marked for investigating restrained slab. Numerical model is the dominant methodology employed for this study. After validation of the numerical model with experimental results for unrestrained slab, further investigations was carried out to study the effects on the parameters that contribute to punching shear at edge connection.

There is also significant dearth of literature on shearhead system for edge connection, therefore, this study proposed a novel shear head system for connecting flat slab to steel edge column.

Chapter 3: Review of Numerical Modelling

3.0 Introduction

This chapter provides review of previous numerical models, theoretical basis and comparison of various material properties and constitutive models of concrete to support decision on the adopted modelling scheme. Numerical analysis was employed to investigate existing test results in the available literature and the proposed tests that would be carried out as an integral part of this research work. In order to reduced cost intensive laboratory experiments, finite element analysis (FEA) was employed to perform parametric study by using a commercially available finite element programme Midas FEA. This programme was chosen based on the reliability and consistency of the implemented elements and material models in addition to the efficiency of simulating concrete nonlinear properties.

3.1 Review of Previous numerical models on Punching shear failure

Finite element method has been extensively applied to investigate punching shear failure of flat slabs system. Among these, (de Borst and Nauta, 1985), (Menetrey, 1994) and (Hallgren, 1996) have applied two-dimensionally rotationally symmetric elements modelled punching shear failure. Furthermore, numerical studies using three dimension systems were investigated by (Ozbolt and Bazant 1996) and (Staller, 2000). Success in numerical modelling for punching shear cannot be achieved without adequate understanding of material behaviour and failure criteria for concrete as well as steel. The type of failure criterion adopted has a significant effect on the punching shear behaviour. The type of finite element analysis used also plays a significant role. Few researchers such as (Moehle 1996) and (Elgabry and Ghali 1993) have used linear elastic finite element method to study moment transfer between slab and column but did not justify the assumed elastic behaviour of concrete. Linear finite element analysis cannot completely describe the behaviour of concrete, because concrete (as a quasi-brittle material) does not obey elastic law. Linear elastic finite element analysis can be used to study the prescribed boundary conditions.

Eder *et.al* (2010) conducted numerical and experimental investigations on punching shear of a hybrid flats slab with shearheads. The study focuses on the contribution of shearhead to punching shear capacity of the interior slab-column connection not

transferring unbalanced moment. The shearhead was designed based on the ACI 318-05 recommendation. But ACI 318-05 guidance was not strictly applied because the bending stiffness ratio between the shearhead and cracked concrete is less than 0.15. The shearhead was welded to the tubular steel column and inserted between the layers of the reinforcement. It was observed that the shearhead deformed plastically before punching failure occurred. The deformed shape of the shearhead after the test is shown in fig 3.1.

Fig.3.1: Deformed shape of shearhead after punching test (Eder *et.al* 2010).

A quarter of the specimen was model in DIANA commercially available finite element software. A nonlinear finite analysis was performed. Concrete was defined with the 'Total strain crack model' which is based on the modified compression field theory of (Vecchio and Collins 1986).The shearhead was modeled with six-noded triangular and eight-nodded quadrilateral mindlin-Reissner isoparametric shell elements and the mesh was refined around the shearhead. They also investigated governing parameter influencing punching shear of the connection. It was observed that the tensile strength of concrete affects the displacement than the failure load as shown in fig.3. 2.

Fig 3.2: Effects of tensile strength of concrete (Eder *et.al* 2010).

The results, suggest that loads are principally transferred into the shearhead at the tips of the arms if the failure surface lies outside the failure surface.

Eder, Vollum and Elghazouli (2011) investigated the behaviour of ductile shearheads for connecting reinforced concrete flat slabs to interior tubular steel columns. The structural response of the proposed shearheads was compared to the conventional ACI-type shearheads that is fully embedded in the slab. The proposed shearhead was designed as a dissipative element which yields in shear before punching failure occurs in the slab. The configuration of the shearhead is depicted in fig 3.3.

Fig 3.3 Novel shearhead proposed by (Eder *et.al* 2011).

In the conventional ACI shearhead system, a punching failure load of 450kN was recorded while in the proposed shearhead system, a punching failure load of 385kN was recorded. The early failure is attributed to the localised concrete failure at the intersection of the shear arms with edges of the opening near the column.

The load -displacement response curve for both specimens is shown in fig .3.4

Fig 3.4: Load displacement curve for the two specimens (Eder et.al.2011).

The curve revealed that the proposed shearhead exhibits significant ductility before punching shear failure occurred which is desirable under seismic loading.

In order to eliminate the localised concrete failure around the opening, it was recommended that the slab edge should be adequately reinforced around the opening.

To achieve adequate ductility, the connection should have failed above the failure load obtained in the conventional ACI shearhead system. This result suggests that creating an opening near the column aggravates punching shear capacity of the connection which is undesirable.

Based on the shortcomings of the previous test, Eder Vollum and Elgazouli (2012) design a robust shearhead system for connecting reinforced concrete flat slabs to tubular steel columns. In order to eliminate the early localised concrete failure around the edges of the hole in the previous experiment, the hole was adequately reinforced with steel collar. The detail of the connection is shown in fig 3.5.

Fig 3.5: Connection detail of robust shearhead (Eder *et.al* 2012)

The authors also performed tests on several steel sections such as: hollow rectangular section, PFC section, channel and I-section. Results of the tests revealed that I-section is the most suitable due to reduced depth of shear cone punched out of the concrete at failure. And also good composite action was achieved using **I**-section.

Both gravity and cyclic tests were carried failed on the connection, but punching shear did not occurred due the ruggedness of the connection. The detail of the connection is shown in fig 3.5. The load reached 570kN and there was no sign of punching therefore, the test was truncated.

Despite the great effort, punching shear capacity of the proposed shearhead assembly could not be ascertained because the connection did not fail in punching during the test and hence; the contribution of the shear arms was indeterminate. The authors suggested that the contribution of the shear arms could have been determined if the shear arms acted as a cantilever like in the case of the fully embedded ACI shearhead system.

It was concluded that **I**-section performs better as shear arms than any other sections due to improved composite action with the concrete slab. It was impossible to determine the contribution of the shear arms by using the collar, and as such the, attempt to propose design guidance was not achieved.

Genikomsou and Polak (2015) conducted nonlinear finite element analyses of reinforced concrete slab-column connections under static and pseudo-dynamic loadings to investigate punching shear failure. The damage plasticity model implemented in ABAQUS was adopted to define quasi-brittle concrete. Five interior slab-column specimens without shear reinforcement were analyzed. Two specimens of edge slab-column connections were also analyzed.

Damage was introduced in concrete damaged plasticity model in tension according to fig.3.6

Fig 3.6: Tensile damage of concrete (Genikomsou and Polak 2015)

The model was able to predict punching shear failure of tested slabs, but there was no comparison to the predictions of the various design codes for its adequacy. Furthermore, parametric studies on various governing parameters of punching shear were not investigated therefore; the sensitivity of the adopted modelling scheme was not examined.

Wosatko, Pamin and Polak (2015) applied damage-plasticity models in finite element analysis of punching shear. An experimental investigation was carried out on interior column tested in punching for the purpose of validation of numerical models. Two inelastic constitutive models were adopted in the numerical simulations namely:

1. Gradient-enhanced damage plasticity model; and 2. Damaged plasticity model implemented in ABAQUS.

Concrete plasticity model in Abacus incorporates the effect of moderate confining pressure and irreversible plastic damage. In ABAQUS, failure mechanism characteristics for quasi-brittle materials such as concrete is based on concrete plasticity in which yielding and plastic potential functions are used to represent material failure.

The numerical model was not able to capture the post -cracking behaviour of concrete as depicted in fig 3.7

Fig 3.7: Experimental and numerical response of the slab.

Wosatko, Pamin and Polak (2015)

Punching is preceded by tensile cracking. However, aggregate interlock, shear friction due to dowel action of reinforcement withstands substantial amount of the load after initial cracking. Also the numerical predictions suggested a sharp brittle failure after initial cracking; which indicates that the post crack regime was not captured.

3.2 Linear Finite element Analysis (LFEA)

According to Segaseta *et.al* (2014), LFEA could be used to study the shear fields of concrete and the stiffness in torsion due to cracking (in this case the shear modulus is taken as one-eighth of its elastic value as adopted in practice). They adopted Elastic shearfield analysis to study the load carrying mechanism of reinforced concrete flat plate to obtain the shear resisting control perimeter. In this study, linear finite element is employed to investigate the similitude relationship between the continuous slab and the isolated specimen. This would provide sufficient information on the boundary conditions to be adopted.

3.3 Nonlinear Finite element Analysis (NLFEA)

3.3.1 General

Nonlinear finite element analysis was conducted to validate and compare previous investigations in the available literature. This validation and comparison would enhance the selections of material models and element types. The parametric study was used to support decisions on the material parameters that would guarantee an appropriate NLFEA model. The NLFEA model results will also facilitate the validation and calibration of the intended test that was conducted on edge column connections.

3.3.2 Review on concrete NLFEA models

A combination of linear elasticity in compression with a Rankine tension cut off was adopted in the initial stages of Reinforced concrete modelling. Afterwards, elasto-plastic formulations in compression such as Mohr-coulomb, Drucker-Prager and Von mises etc have also been applied in concrete NLFEA. Great efforts have been made on modelling the tension softening behaviour of concrete, which principally led to the smeared crack concept. In the smeared crack concept, the solid (concrete) is imagined as a continuum. The smeared crack concept based on the Rankine failure criterion could be combined with available elasto-plastic constitutive models. The total strain crack model which provides a better description of concrete quasi-brittle behaviour has been introduced. These models were examined and the one that accurately predicted punching shear failure was recommended.

3.3.3 Rankine model

In the Rankine model, the maximum principal stress(σ_1) is used to define the yielding of a material. The tensile behaviour of concrete (tension cut off) is normally modelled with the Rankine failure criterion. According to Rankine criterion, failure occurs in a material if the maximum principal stress σ_1 reaches the uniaxial tensile strength(f_t).

$\sigma_v = \sigma_1 = f_t$ ..... (3.1) $\sigma_1 > 0$

In Midas FEA, the tension cut off is modelled with the exponential, constant and linear functions. If the stress point reaches, the Rankine failure surface cracking is initiated and the tension softening procedure begins. As concrete exhibits a quasi-brittle behaviour, the stress does not suddenly drop to zero, but gradually approaches zero during crack propagation. Material tests revealed that concrete displays different

tension softening behaviour for plain and for reinforced concrete due to the obstruction of cracks propagation by the presence steel reinforcement.

3.3.4 Mohr- Coulomb Model (Non-associative Plasticity model)

Mohr-Coulomb model is mostly applicable to materials that have significant frictional and dilatational effects such as soils and rock. In the Mohr-coulomb model, the yield functions have been established to capture the behaviour of frictional materials. In these materials, the plastic behaviour depends on pressure as opposed to von Mises which is independent on pressure. Mohr-coulomb is a typical example of non-associative plasticity because the direction of plastic flow not normal to the yield surface (Belytschko and Moran 2000). The Mohr-coulomb criterion is established on the principle that yielding in the material occurs when a critical combination of shear stress and mean normal stress is reached on any plane which is expressed as

$\tau = c - \mu\sigma$ ..... (2).

τ Is the magnitude of the shear stress σ is the normal stress on the plane and c is the cohesion.

Fig 3.8 (a) Mohr-Coulomb Yield behaviour; (b) Drucker-Prager and Mohr-Coulomb yield surfaces. (Belytschko and Moran 2000).

From fig.3.8 it is shown that if all three Mohr's circles associated with the principal stresses lie between the failures envelopes, no yielding occur. But when the yield surface is tangential to one of the Mohr's circles, yield takes place

The material yield criterion of the Mohr (1990) model is expressed as

$|\tau| = \mathrm{F}(\sigma)$ ..... (3.3)

The peak strength, τ on a plane is assumed as a function of the normal stress on the same plane. Equation 3.3 relates the yield surface of a Mohr circle and the yield function, F (σ) is determined by experiments. The Mohr criterion assumes that a failure occurs in a material at the instant when the largest Mohr circle meets the coulomb yield surface. This tacitly implies that the middle principal stress σ_2 ($\sigma_1 = \geq \sigma_2 \geq \sigma_3$ does not affect the yield criterion.

According to Potts and Zdravkovic (1999), the Mohr-Coulomb failure model is a linear elastic perfect plastic criterion and is formulated as

$$\tau_f = c + \sigma_{nf.} \tan\varphi \quad \text{..... (3.4)}$$

Where c, φ are shear strength parameters of materials

c = cohesion φ = internal friction angle.

Equation (3.4) is broadly used for materials, which display the property of changing shear strengths with change in compressive stresses. The failure envelop based on Mohr's circle can be express in terms of principal stresses as thus:

$$\sigma_{(\max)} = \sigma_{(\max)} - \sigma_{3\,(\min)} \frac{1+sin\varphi}{2ccos\varphi} = 1 \quad \text{..... (3.5)}$$

Fig.3.9 Mohr-coulomb yield surface (Midas FEA analysis manual)

Failure occurs due to shear if one of the largest of the three stress circles for the corresponding to the three-dimensional stress state touches the failure envelope. The Mohr-Coulomb failure criterion requires just two parameters and allows good approximation of brittle materials such as concrete. The reliance on the hydrostatic pressure p, which takes account of the hydrostatic effect, which is the increase of shear strength when (p) is increased, is a major advantage of this model. In the compressive regime, the failure envelope has a square shape and underestimates the

true compressive strength on the whole, the MC-criterion employed for concrete fundamentally experience 2 major drawbacks

- The MC-criterion ignores the effect of the intermediate principal stress. This suggests that the intermediate stress σ_2 has no influence on the failure. Tests have revealed that σ_2 significantly affects the compressive strength of concrete, concrete strength increases with respect to the increase in σ_2
- The compressive meridians are straight lines whereas tests have shown that the compressive meridians of concrete are curved.

3.3.4.1 Angle of friction

Mohr-coulomb model adopted two parameters namely: angle of friction (ϕ) and cohesion c which are obtained from test data. Based on the unconfined uniaxial compression and uniaxial tension parameters ϕ and c can be estimated from the following formulae;

$$f_t = \frac{2c.cos\phi}{1+sin\phi} \quad \text{..... (3.6)}$$

$$f_t = \frac{2c.cos\phi}{1-sin\phi} \quad \text{..... (3.7)}$$

Where(f_t), represents the uniaxial tension and (f_c) the uniaxial compression strength. The internal angle of friction for plain concrete lies within the range of $30^\circ \leq \phi \leq 35^\circ$. Li et al. (2003) employed the following empirical formula for ϕ which consists of a default value of $\phi = 36^\circ + 1^\circ \ (\frac{f_c}{35}) \leq 45^\circ$

3.3.4.2 Cohesion

The cohesion can be determined as a tangent on the Mohr's circle based on the uniaxial compressive strength as follows.

$$c = f_c \frac{1+sin\phi}{2cos\phi} \quad \text{..... (3.8)}$$

The uniaxial tensile value corresponding to c can be calculated using equation 3.8 obviously; this is a theoretical tensile strength which usually exceeds the true tensile strength of concrete. Therefore, applying Mohr-coulomb plasticity model for concrete.

$$f_t = \frac{c}{tan\phi} \quad \text{..... (3.9)}$$

A tension cut-off should be applied. In order to apply this, a constant tension cut-off criterion such as the Rankine failure criterion.

3.3.4.3 Dilation

The dilation fundamentally an account for the volume change after plastically has been reached. (De Borst and Vermeer 1984) suggested that dilation is caused by frictional sliding, either along particles or along micro cracks.

Dilation occurred when two layers of loose granular material have to undergo both a vertical and a horizontal displacement if these layers slide along each other. This vertical uplift causes the volume increase under plastic deformation. The rate of dilation is found to be constant and can be expressed as thus,

$$\sin \Psi = \frac{{\epsilon_v}^p}{-2{\epsilon_1}^p + {\epsilon_v}^p} \quad \text{..... (3.10)}$$

$${\epsilon_v}^p = {\epsilon_1}^p + {\epsilon_2}^p + {\epsilon_3}^p \quad \text{..... (3.11)}$$

Where Ψ is the dilation angle, (which is constant if $\Psi = 0$ is the plastic potential function is 'associated'). Associative because the vector of plastic strain is always perpendicular to the plastic potential function which means the plastic strains are perpendicular to the Mc-failure surface. For hydrostatic condition, the horizontal component of this vector is the volume change and the vertical component is the deviatoric or distortional strain. If $\Psi = 0$ is assumed, then the plastic potential is non associative and 'nondilatant'. This indicates that no volume change has occurred as the meridian is horizontal and the strain vector is getting closer to the deviatoric strain axis.

3.4.0 Concrete crack models

Concrete crack models can be categorized into discrete crack model (discontinuum model) and the smeared crack model (continuum model). The discrete crack model adopts finite elements at which concrete cracks are separately represented as boundaries. The discrete crack model has the advantage of being able to specifically represent cracks behaviour as physical discontinuity at failure. Nevertheless, it has some demerits in the sense that the accuracy of the analysis greatly depends on the material properties required and the FE modelling can be very complex. The method is computationally intensive since large numbers of degree of freedom are involved (Surendra, Stuart and Chengsheng 1995).

The smeared crack model assumes that cracks generated locally are uniformly scattered over a wide surface. This model is particularly suitable for RC structures with moderate amount of reinforcement and its finite element modelling is comparatively simple. Few advantages of smeared crack concept are

- There is computational convenience and remeshing is not required.
- Cracks generally are not straight but tortuous. Such tortousity can be modelled more readily using the smeared crack concept.

The smeared crack can be further categorized into various models such as the decomposed strain model and a total strain model. The decomposed-strain model computes the total strain in terms of material strain and crack strain. The material strain is further decomposed into other strain components such as: elastic strain, plastic strain, creep strain, thermal strain. The crack strain is further decomposed into non-orthogonal multi-directional crack model. This series of decomposition makes the algorithm very complex and difficult to achieve convergence (Midas FEA, 1989).

The total strain model in the smeared crack model is formulated based on total strain without going through a rigorous method of decomposition into strain components. In addition, its algorithm is quite easy to understand (Midas FEA, 1989). In the total strain model adopts only one stress- strain relationship for tensile behaviour including cracks and one for compressive behaviour. It is also more practical since the input for material properties for defining nonlinear behaviour is relatively simple.

3.4.1 Total Strain Crack Model

MIDAS FEA (1989) adopts the total strain crack model categorized under the smeared crack model. The smeared crack is further classified into fixed crack and rotating crack models. Fixed crack model assumes that the axes of cracks remain fixed once crack axes are defined. It has been observed that fixed crack accurately reflex the physical characteristics of the crack phenomena. The fixed crack model is capable to simulate the physical behaviour of concrete cracks more accurately than rotating crack model because it evaluates both the normal stresses and shear stresses on the crack surface at depicted in figures 3.2a and b. It is also particularly suitable for modelling shear behaviour of concrete. Rotating crack model assumes the direction of cracks rotates continuously depending on the changes in the axes of principle strains when cracks are initiated. In both cases of the fixed and rotating models, the first crack at the integral points always initiates in the direction of the principal strains. Concrete

materials display isotropic properties prior to cracking and anisotropic properties after cracking. MIDAS considers the properties of concrete as orthotropic materials after cracking as well as the normal stresses and shear stresses.

Fig 3.10a: Fixed crack model (Midas FEA 1989) Fig 3.10 b: Rotating crack model (Midas FEA 1989).

A constitutive model based on the total strain expresses the stress as a function of the strain. This phenomenon is known as hypo elasticity, when loading and unloading behaviour is along the same stress-strain path
The basic concept of the Total strain model is that stresses are computed with respect to the crack directions. In Midas FEA, loading and unloading takes place on separate stress-strain paths, especially unloading is modelled with a secant slope. For secant implementation, for both compression and tension, the secant modulus always passes through the origin. This elastic damage approach is dissimilar to elastic-plasticity where the stiffness is fixed, independent of loading and unloading. The tensile behaviour of concrete is considered linear elastic until the peak strength is attained. The constitutive model of total strain is established on the modified compression field theory of (Vecchio and Collins 1986). MIDAS implemented it with a three 3D models based on the theory proposed by (Selby and Vecchio 1993).

3.4.1.2 The Parabolic Compression Model adopted in TS-model

(Feenstra 1993) derived the fracture energy equation of the parabolic model implemented in Midas FEA. The parabolic curve depicted in fig 3.2 accounts for the compressive strength, f_c compressive fracture energy and characteristic element length (h).

The strain ($\alpha_{c/3}$) at which one-third of the maximum compressive strength f_c is reached is given as $\alpha_{c/3} = \frac{1}{3}\frac{f_c}{E}$ ..... (3.12)

The strain α_c at which the maximum compressive strength is reached is

$\alpha_c = -\frac{4}{3}\frac{f_c}{E} = 4\,\alpha_{c/3}$..... ..... (3.13)

It should be noteworthy that $\alpha_{c/3}$and α_c are obtained without consideration of the element size or compressive fracture energy. The ultimate strain α_u at which the Material is completely softened in compression is expressed as thus

$\alpha_u = \alpha_c - \frac{3}{2}\frac{G_c}{hf_c}$ .... (3.14)

Fig.3.11: Parabola curve adopted in the TS-model (Midas FEA 1989)

3.4.1.3. Exponential model (Tension softening)

The exponential softening model assumes that exponential softening occurs when tensile stress exceeds the tensile strength of the material. The slope of the softening is obtained based on the fracture energy, G_f and crack band width, h. The exponential curve is depicted in fig.3.4 as thus

Fig 3.12: Exponential softening curve (Midas FEA 1989).

3.4.1.3 Shear Model

As implemented in MIDAS FEA, in the fixed crack model, the shear stiffness is reduced after cracking as a percentage of the initial elastic shear modulus. The corresponding reduction factor is referred to as the shear stiffness reduction or shear retention factor (β) $0 \leq \beta \leq 1$. The reduced constant shear stiffness is calculated as thus

$G^{cr} = \beta\, G$ ..... (3.15)

Apparently, β depends on the aggregate size and aggregate type amongst other factors of influence. Numerical analysis has revealed that a constant shear retention factor gives a rather good approximation and beta ranges between $0.1 \leq \beta \leq 0.3$. According to Hinton and Owen (1984), the shear moduli can be assumed to degrade linearly with increase in the principal tensile strains.

3.5.0 Comparison between MC-model and TS-model

Mohr -Coulomb-model cannot be apply to concrete modelling because concrete as quasi-brittle material is characterized by its compressive strength and not internal cohesion and angle of friction. Therefore Mohr-coulomb is particularly suitable when friction shear is significant. The total strain model is envisaged to be most efficient in modelling punching shear based on the following justifications.

- It displays the true material behaviour better. Any two different stress-strain curves in compression and tension can be considered, which gives much more flexibility and different elastic moduli in compression and tension are possible.
- It considers the reduction of strength in compression due to lateral cracking.

- It materializes the tension softening behaviour of concrete based on the fracture energy therefore crack initiation and propagation is accurately captured.
- It models the reduction of shear modulus due to the progressive damage of concrete in the post damage regime. This is more accurate because the damage concrete does not have the shear modulus as the original concrete.

3.6.0 Material Characterization

This section examines material parameter that would be suitable for modelling punching shear behaviour. Comes and Regan (1999) carried out tests on material parameters for the total strain model. According to their parametric study, the most influential parameters for modelling punching shear failure are concrete tensile strength (f_t) and shear retention factor (β) other parameters such as compressive strength (f_c) and fracture energy (G_f) also have appreciable effects. Accurate test data must be available if not it could pose some difficulty to compute the tensile strength accurately which governs the initial cracking.

3.6.1 Concrete Compressive Strength

In recent time, prominence is given to the cylinder strength more than the cube strength. Eurocode 2 and ACI adopted the cylinder strength, although BS8110 still retains the cube strength. Therefore, the cylinder strength is considered for this investigation. The cube strength is related to the cylinder strength as thus

$$f_{cylinder} = 0.8\, f_{cube} \quad \text{..... (3.16)}$$

The cylinder strength is used in the parabolic compression model.

The characteristic strength is obtained from the mean strength as thus

$$f_{ck} = f_m - 1.64\sigma \quad \text{..... (3.17)}$$

Where σ is the standard deviation

3.6.2 Concrete Tensile Strength

It has been revealed from sensitivity analysis that the tensile strength of concrete significantly affects the response of the load displacement Curve. Tensile strength can be obtained directly with the compressive strength as provided by CEB (1990) implemented in Midas FEA as thus.

The mean tensile strength $f_{ct,m} = f_{ct,k0,m}\left[\frac{f_{ck}}{f_{ck0}}\right]^{2/3}$ ..... (3.18)

Wheref_{ck0} = 1.40 N/mm^2 and $f_{ck0} = 10\ {}^{N}/_{mm^2}$

The ACI 209 model code recommends an equation relating tensile strength and concrete unit weight w (kg/m^3) as thus

$f_t = 0.0069\sqrt{wf_c}$ ..... (3.19)

Lee *et.al* (2008) have carried out a direct tensile tests on large plain normal weight concrete specimen, According to their test data, the tensile strength varied between

f_t = 0.27 $\sqrt{f_c}$ f_t = 0.37 $\sqrt{f_0}$

Assuming f_c = 35 N/mm^2 with w = 2400 kg/m^3 the tensile strength varies between 3.23 to 1.6 N/mm^2

3.6.2.1 Brazilian Split-Cylinder Test

By comparing all indirect tensile test methods, the split cylinder test is the most popular method. It was introduced by (Carneiro and Barcellos 1953).To conduct the test a compressive line or strip load is applied to a cylinder diametrically along two opposite generators. This condition is sets up by a uniform tensile stress over the vertical diametrical plane and fracture (splitting of the material occurs along this predetermined plane as shown.

The theoretical basis of the formula for estimating the tensile strength of a slit-cylinder test has been derived from the theory of linear elasticity.

The splitting tensile stress is computed with equation 3.20

$\sigma_t = \frac{2P}{\pi dl}$ ..... (3.20)

Where σ_t = tensile strength from split cylinder test.

P = applied load

t = length of specimen

d = diameter of specimen

Basic assumptions of split cylinder indirect tensile Test

- The theory of split-cylinder indirect tensile test assumes that the test material is elastic, homogeneous and isotropic.
- The tensile stress along the centreline is of paramount interest.
- The moduli in tension and compression are equal.

Because of the effect of bearing strips on the cylindrical specimen, the maximum tensile stress $\boldsymbol{\sigma_{max}(\beta)}$ was reduced by (Tang 1994) as thus

$$\boldsymbol{\sigma}^{c}_{max}(P,\boldsymbol{\beta}) = \frac{2P}{\pi BD}\left[1-\boldsymbol{\beta}^{2}\right]^{3/2} \quad \text{..... (3.21)}$$

Where $\boldsymbol{\beta} = \frac{b}{D}$, ratio of bearing strips to Diameter of cylindrical specimen.

3.6.3 Fracture energy – Tension

The fracture energy G_f (N/mm^2) or(J/mm^2) is a material constant and the amount of energy required to create one unit area of crack surface. It can be obtained by integrating the stress-strain softening diagram as follows.

$$G_f = \int_0^{\delta max} f_t\, \delta\, d\ \delta t \quad \text{..... (3.22)}$$

Where $f_{t\delta}$ denotes crack as a function of crack opening. G_f Depends on the concrete strength f_c and the maximum aggregates size d_0, According to CEB (1990), the fracture energy G_f can be obtain as follows

$$G_{f0} = 0.024 + \frac{0.0053\, d_{max}^{0.95}}{8} \quad \text{..... (3.23)}$$

$$G_f = G_{f0}\left[\frac{f_{cm}}{f_{cm0}}\right]^{0.7} \quad \text{..... (3.24)}$$

Where d_{max} is the maximum aggregate size.

Where f_{cm0} is 10 N/mm^2. Table 3.1 shows the value of G_{f0} corresponding to the maximum aggregate size.

Table: 3.1 Fracture energy and Aggregate size

$D_{max}\ (mm)$	G_{f0} (J/m^2)
8	25
16	30
32	58

3.6.4 Fracture Energy-Compression (G_c)

G_c is roughly approximated to value of 100. G_f is used in the parabolic compression model. Although sensitivity studies signified that, this parameter does not influence the punching shear behaviour.

3.6.5 Ultimate Compressive Strain

The peak compressive strain of a constant value ϵ_c= 0.0035 has been used. In the parabolic compression model, concrete completely softens in compression when the peak compressive strain is reached.

3.6.6 Ultimate tensile strain

The ultimate tensile strain at which the tensile stress reaches zero is computed as follows

$$\varepsilon_{nn,ult}^{cr} = \frac{G_f}{\alpha h f_t} \quad \text{..... (3.25)}$$

The coefficient α in equation is defined as follows:

$$\alpha = \int_{x=0}^{x=\infty} y\,(x)dx \quad \text{..... (3.26)}$$

Where $y\,(x)$ is the assumed tension softening function.

3.6.7 Elastic Modulus formulation for the TS model.

Midas FEA (1989) defined the elastic modulus as a function of the mean compressive strength of concrete.

The mean compressive strength is expressed by

$$f_{cm} = f_{ck} + \Delta f \quad \text{..... (3.27)}$$

Where, $\Delta f = 8\ {}^{\mathrm{N}}/_{\mathrm{mm}^2}$

The Elastic modulus is expressed as

$$E_c = E_{c0}\left(\frac{f_{cm}}{f_{cm0}}\right)^{1/3} \quad \text{..... (3.28)}$$

Where, E_{c0} = 2.15 × 10^4 $({}^{\mathrm{N}}/_{\mathrm{mm}^2})$, and the reference mean compressive strength, f_{cm0} is $10{}^{\mathrm{N}}/_{\mathrm{mm}^2}$. This formulation is based on the (CEB-FIP 1990) for material properties.

3.7 Recommendation

Various material constitutive models implemented in Midas FEA have been examined for their applicability and capability to predict behaviour of concrete subject to punching shear failure. Mohr -Coulomb is specifically designed for materials that have significant frictional and dilatational effects (granular materials) and friction shear for concrete. Mohr- Coulomb would be applied to model friction shear induced in concrete due to compressive membrane action.

From this comparison, TS-model was found to be the most appropriate because it provides explicit account of how crack initiation and propagation can be captured using the smeared crack approach. Concrete fracturing is associated with complex mechanism such as: aggregate interlocks, crack branching, crack face friction etc. these mechanisms can be adequately captured using energy approach. More so, T-S model materializes the tension softening behaviour of concrete in terms of fracture energy. The pre-damage and post damage regimes of concrete subject to shear failure can be adequately predicted when combine the tension, compression and shear model implemented in the TS-model. Therefore, TS-model is adopted as the constitutive model for quasi-brittle concrete throughout this study.

4.1 Overview of Research Approach

This chapter presents methods employed to accomplish the outline objectives. Based on the available literature reviewed, experimental and numerical studies were deemed appropriate. These methods would be applied strategically in order to achieve the set objectives. The overall aim of this research is to provide an analytical equation for edge connection reinforced with shearhead.

In line with the objectives, the following research questions are formulated as thus:

- Does ACI 318-05 design code significantly underestimates punching shear capacity of edge connection?
- Can the novel shearhead assembly enhance punching shear significantly beyond the theoretical shear strength of edge connection?
- Does local yielding of the shearhead occur prior to punching shear or punching shear occurs when concrete shear strength is reached?
- Does bending stiffness ratio between the shearhead and the cracked concrete significantly affect the connection behaviour to punching shear?

The research hypotheses that were investigated based the available literature reviews are:

- That the shearhead acts like a cantilever by transferring shear force from the tip into the edge connection.
- Various parameters governing punching shear such as: the effects of reinforcement, fracture energy, tensile strength, and elastic modulus.
- Flexural failure occurs prior to punching shear or both occur simultaneously.
- Punching shear occurs when concrete shear strength is reached or when yielding of shearhead is reached.

To answer research question 1, punching shear test was conducted on slab 1.The result was used for comparison with ACI318-05 and Euro code 2 design codes. The code that provides the best prediction was used in the formulation of the analytical equation for edge connection reinforced with shearhead.

To investigate the fourth hypothesis, Electrical Resistance Strain Gauges (ERGs) were installed on the reinforcement bars embedded in slab 1. ERGs were installed on bars located within the critical section where significant deformation occurred. The load evolution was plotted against the measured strains to capture when reinforcement bars yielded.

To accomplish hypothesis 1 and question 3, the mechanism of load transfer from the shear- head to the connection was investigated. In the experiment on slab 2, ERGs were installed on the top and bottom flanges of the shearhead at 20mm from the intersection between plate and shear arm; to measure the axial strains. Similarly to a beam, the web of the shear arm is resisting shear, therefore, rosette strain gauges were installed on the web of the shear arms. The aim of strain measurements on the shearhead was to investigate if plastic deformation occurs prior to punching shear.

To read strains at every location of the shear arm may be too cumbersome, in addition to the limited channels to the data logger; therefore, numerical analysis was conducted to determine strains and other related parameters such as: shear strains, shear force. The graph of shear force variation along the arm was plotted to clarify hypothesis 1. The load transfer mechanism was used to support decision on the proposed analytical equation.

To deal with question 2, the contribution of the novel shearhead to punching shear capacity of the connection was examined by comparing result with the predictions of design codes without shearheard. And also, compared to previous suggestion that shearhead could contribute up to 75% of the punching shear capacity of the connection.

To provide solution to the fourth question, the effect of bending stiffness ratio between the shearheard and the cracked concrete was examined using numerical analysis. The deformation that occurred at the connection was determined by using discrete interface implemented in Midas FEA. However, ACI 318-05 recommended that bending stiffness ratio should not be less than 0.15. This shows its significance to punching shear capacity of the connection.

The methods employed to accomplish research objectives, questions and hypotheses are described as thus:

4.2 Linear Elastic Analysis

Elastic analysis was employed to study the boundary conditions that produced the closest similitude with the prototype structure. Since it is relative too cumbersome to carry out full scale test on the prototype in the laboratory; a general or common approach of obtaining the representative laboratory specimen from the contra flexure bound region of the prototype slab is adopted. It is a prime requirement that the representative slab should replicate the prototype in flexure and shear; therefore, linear elastic analysis was conducted to create the required similitude between the representative specimen and the prototype especially in terms of bending moments, distribution and deflection. The effect of compressive membrane was ignored to create a lower bound solution. The prescribed boundary conditions were implemented in both the numerical models of the slabs and the experimental set up. Because, elastic theory cannot completely model the behaviour of quasi-brittle concrete; nonlinear finite element analysis was adopted.

4.3 NLFEA analysis

To accomplish objectives I, II and IV, nonlinear finite element analysis was undertaken on slab 1 and slab 2. For slab 1, the aim of the numerical analysis was to investigate the punching shear capacity of the edge slab-column connection without shear reinforcement; in order to compare the results with codes equations. Results obtained from control specimens tests such as: compressive strength, tensile strength and elastic modulus were implemented in the numerical model. Embedded reinforcement concept was used to model reinforcement in the slab.

To accomplish objective IV and hypothesis 2, intensive parametric study was carried out to investigate the influential parameters of punching shear such as: reinforcement ratios, tensile strength, fracture energy elastic modulus on the punching shear capacity of the edge connection. The aim of this parametric study was to examine various divergent views on these influential parameters on punching shear strength. Sensitivity study was also carried out to investigate the influence of various concrete tension softening models implemented in Midas FEA. From this study, the most appropriate models were implemented in the numerical simulation of the tested slabs. Due to the dissimilar materials (concrete and steel section) at the connection, interfacial model was used to capture structural deformation. Discrete crack interface

model was used because it models discrete cracking of concrete when the tensile strength is reached. NLFEA was adopted because it models the softening behaviour and residual strength of cracked concrete.

4.4 Experimental investigation

The experimental work consists of test on both slabs with and without shearheads. The prime rational for the experimental work is to investigate the punching shear capacity of the slab-column connection. The aim of slab 1 is to investigate the punching shear capacity and compare to the design codes equations. This was used to make decision on the code equation adopted in the formulation of punching shear capacity for slab 2.

The aim of experimental investigation on slab 2 is to investigate the contribution of the novel shearhead assembly to the punching shear capacity of the edge connection subject to vertical static loading. The novel shearhead connection developed using the recommendations of ACI 318-05 and New Zealand codes. In order to control the concrete characteristics and quality, specimens were cast for compressive strength, tensile strength and Elastic Modulus test. The specimens were air-cured for 28 days. The experimental results were also used to validate numerical results as proposed in the fifth objective. Experimental method was used because it measured the real behaviour of structural deformation of the edge connections. The test set up was based on the boundary conditions adopted from the elastic analysis. The experiments were also based on the availability of materials and measuring devices.

4.3 Validation

The commercial finite element software Midas FEA was used for the numerical analysis. Prior to implementation, various material constitutive models available in Midas FEA were examined. In addition to material parameters such as: compressive strength, Elastic modulus, tensile strength and fracture energy. The TS-model was adopted based on its merit in modelling shear failure. For instance, it considers the residual tensile stress of cracked concrete after cracking. And also, it models the degradation of shear stiffness due to the progressive damage of concrete. Midas FEA software was validated by Elastic analysis of a square plate which was compared to its analytical solution. The adopted modelling scheme was validated using previous experimental work on punching shear failure of slab-column connection without shear

reinforcement by Eder *et.al*, (2010). The validation procedure is depicted in a flow-chart in fig 4.1

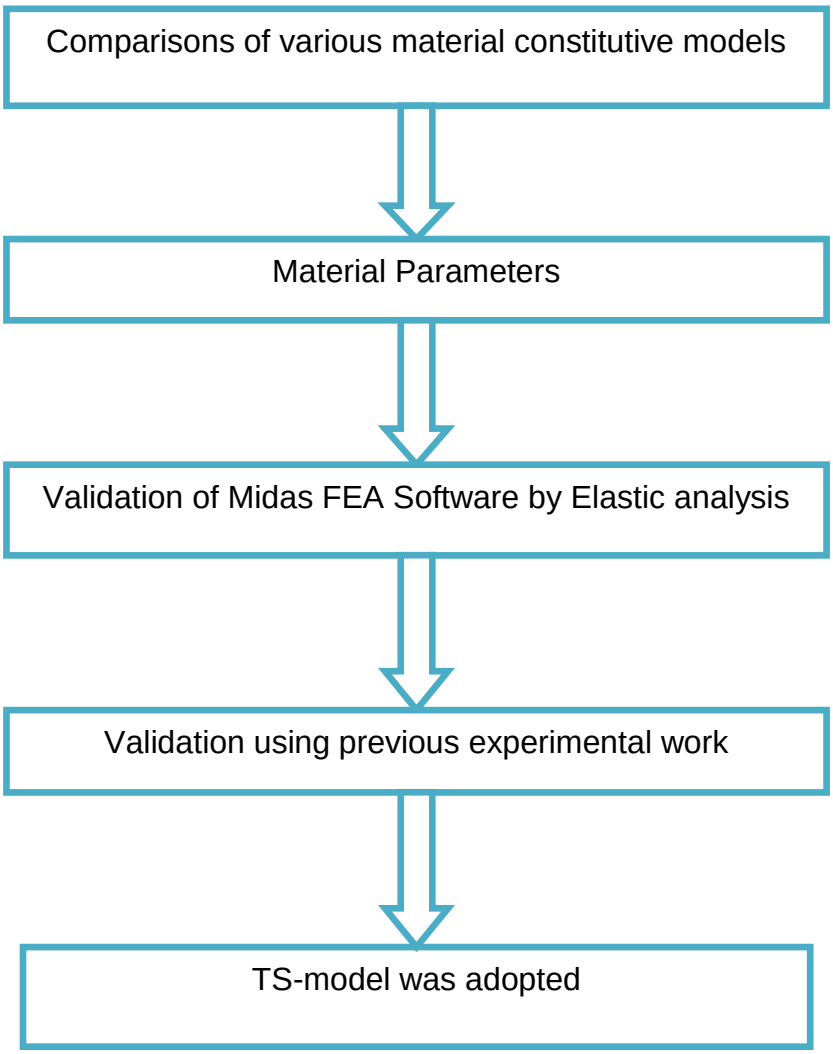

Fig 4.1 Flow chart of the adopted model.

.

The flow chart provided in figure 4.2 shows the nexus of the methods.

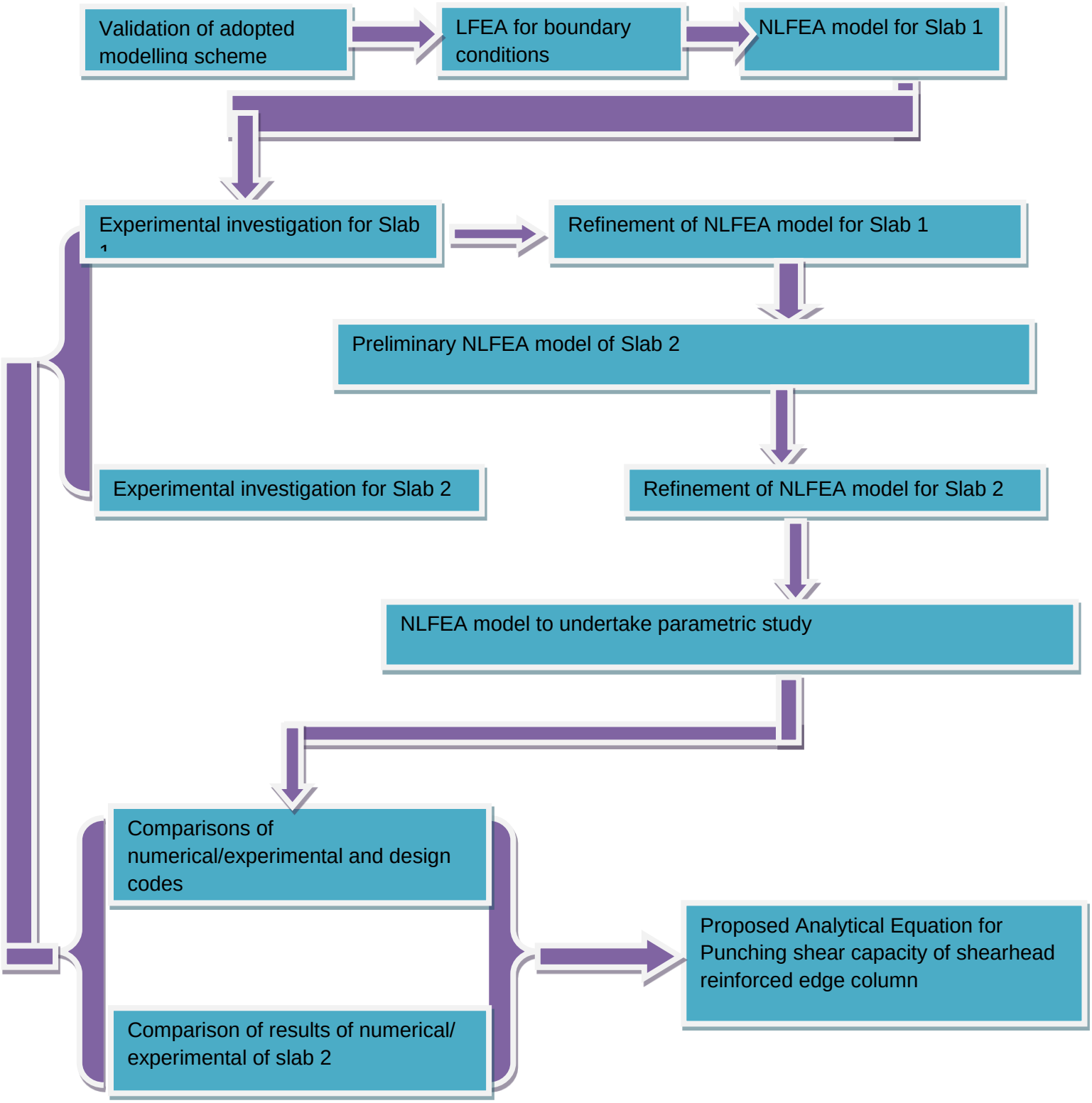

Fig 4.2: Flow chart showing sequential application of methods

Chapter 5: Validation of adopted modelling scheme

5.0 Introduction

For assurance and reliability on the commercial finite element software (Midas FEA) and the adopted modelling scheme provided in chapter 3; validation is carried out. First and foremost, linear elastic analysis is conducted on a simply supported slab subject to uniformly distributed load (UDL) and validated with the analytical solution of Timoshenko plate theory (Timoshenko and Krieger, 1970).

Secondly, the nonlinear finite element analysis (NLFEA) is validated by an experimental investigation of a slab without shear reinforcement subjected to punching shear failure by (Eder et al.2010). Softening behaviour and material parameters of concrete are fully examined and implemented.

5.1 Linear Elastic analysis

Elastic analysis was conducted on a square plate of 4m × 4m by 130mm thick. The plate was characterised with elastic constants such as Elastic modulus of $32800\,N/mm^2$ and Poisson's ratio of 0.2. Linear elastic constitutive model was adopted to define concrete. The slab was modelled as a plate element in Midas FEA. The plate was discretised into 2500 elements and 2601 nodes using element size of 80mm.

All translational degrees of freedom (D.O.F) at supports were restrained but all rotational (D.O.F) was allowed to model a simply supported condition used in the analytical solution.

The self weight of the plate and a uniformly distributed load of $10\,kN/m^2$ were applied. The result of the analysis is shown in fig 5.1

.

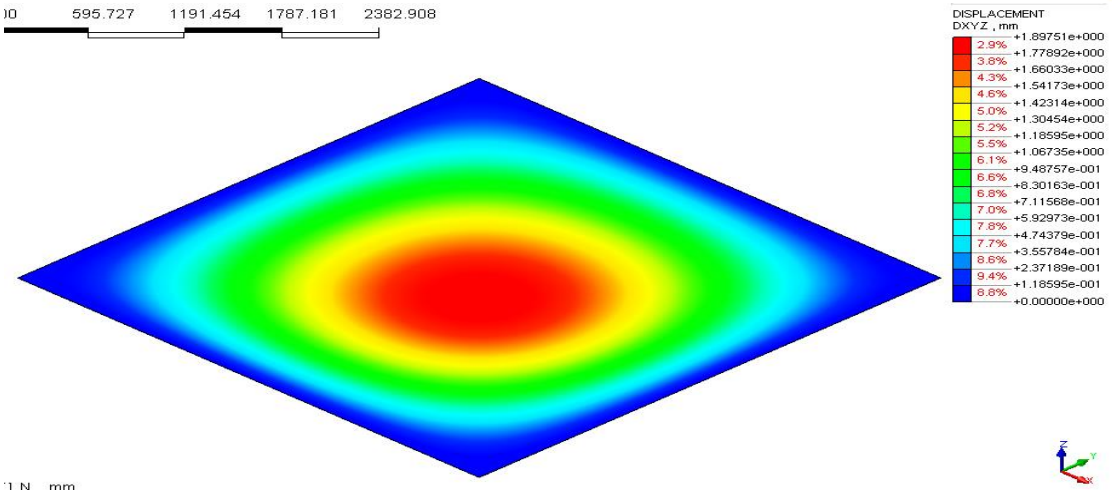

Fig 5.1 deflection contour of the slab with UDL

5.2 Analytical solution

A simply supported square plate supported around the edges subject to UDL was used. It has the dimension and elastic constants of the plate used in the linear elastic analysis. The analytical equation for the deflection function according to Timoshenko and Krieger (1970) is expressed as:

$$W_{max} = \sum_{m=1,3}^{\infty} \sum_{n=1,3}^{\infty} \frac{16q_0}{D\pi^6 mn \left(\frac{m^2}{a^2}+\frac{n^2}{b^2}\right)^2} \; sin\frac{m\pi x}{a} \, sin\frac{m\pi x}{b} \quad \text{.....} \quad (5.1)$$

$$D = \frac{Eh_c{}^3}{12(1-v^2)} \quad \text{.....} \quad (5.2)$$

For a square plate $m = 1$ and $n = 1$

By substituting the geometric and material parameters of the plate into equation 5.1 the maximum deflection was obtained.

Table 5.1: Comparison of results.

Method	Load ($k\,N/m^2$)	Deflection
Analytical solution	10	1.89
Midas FEA	10	1.897

Comparison of both results shows that the maximum deflection was the same. Hence Midas FEA completely satisfied the theoretical equation of plate.

5.3 NLFEA Validation

The slab without shear reinforcement tested by (Eder *et al*.2010) at Structural laboratory, Imperial College was implemented in the NLFEA for validation purpose. The experimental procedure is described as thus,

The slab is made up of 3m × 3m by 220mm thick, and loaded at the centre through a 270mm square plate. 16 ties located around its perimeter were used to restrain the slab in a vertical position as shown in the one quarter view in fig 5.2. The bottom tensile reinforcement was spaced at 90mm centres and were used for tensile reinforcement at each orthogonal direction. The 10mm diameter bars were spaced at 180mm centres and used for compressive reinforcement at each orthogonal direction. Mean cylinder strength of 24Mpa was used.

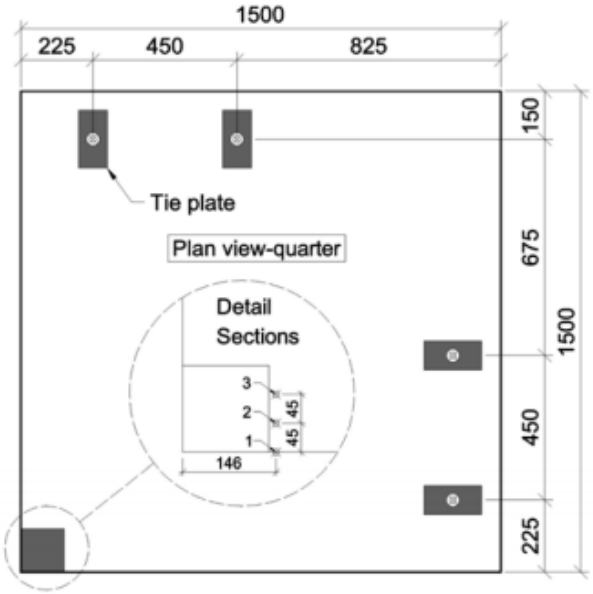

Fig 5.2 Plan view (quarter section)

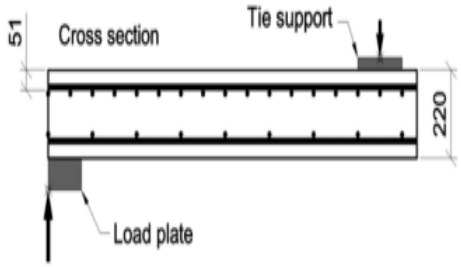

Fig 5.2b Reinforcement detail

5.3.1 Modelling Procedure

Due to symmetry and for computational efficiency, only a quarter of the specimen was modelled as shown in fig 5.2a. The mesh was refined around the column region where structural damages are significant. In order to ensure that the quarter slab replicates the exact flexural behaviour of the full scale slab, horizontal displacements were

restrained in the X and Y directions along the axis of symmetry as depicted in fig 5.3. Vertical displacement was allowed for vertical deflection of the slab. The slab was vertically restrained at the positions of the tie down bars along its perimeter. The concrete and the element representing the steel column were modelled with 8-noded 3D solid element. The steel plate was assumed as linear elastic material. Concrete was defined with the Total strain cracked model. Also, the reinforcement was modelled as elastic-plastic with the Von mises yield criterion. Embedded reinforcement concept was used. The slab was discretised into 19108 elements and 20942 nodes. A full integration scheme was adopted in the solution phase.

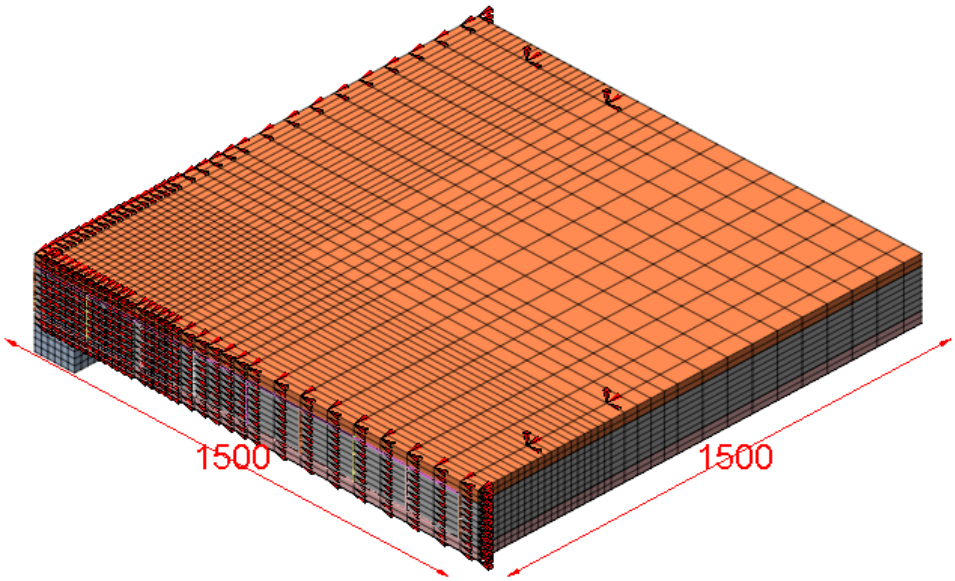

Fig 5.3: Finite elements model of the slab specimen.

Table 5.2 Material properties used in the model

Concrete (MPa)	$f_t = 1.5$	$E_c = 29500$
Steel (MPa)	$f_{yk} = 500$	$E_s = 210000$

Table 5.3 Material models adopted.

	Softening	$G_f(Nmm/mm^2)$	$G_c(Nmm/mm^2)$	β
Concrete in Tension	Exponential	0.074		0.3
Concrete in compression	Parabolic		7.4	0.3

G_f is the fracture energy in tension. G_c is fracture energy in compression.

β is the shear retention factor.

5.3.2 Solution Procedure

In the first phase of the analysis the self - weight was activated to mimic the real life condition. In the second phase of the analysis, an incremental displacement load was applied from the bottom of the steel plate representing the column until punching shear failure occurred. Structural damages are concentrated around the slab-column connection as shown in Fig 5.4. The load displacement evolution is plotted in Fig5.5a.

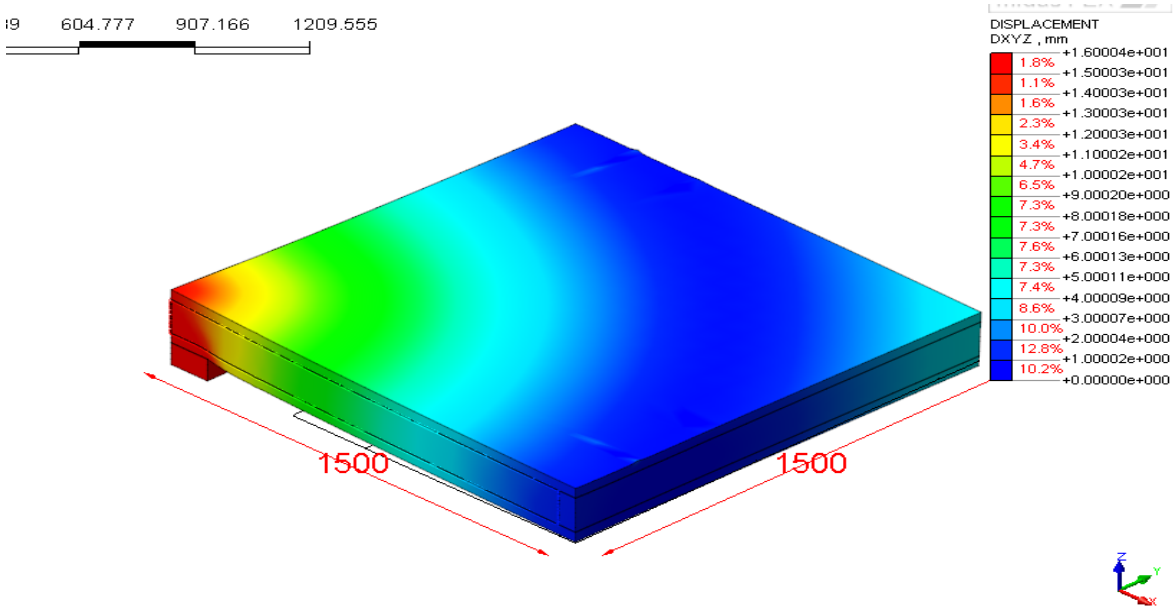

Fig 5.4: Deformation contour of the slab at failure load.

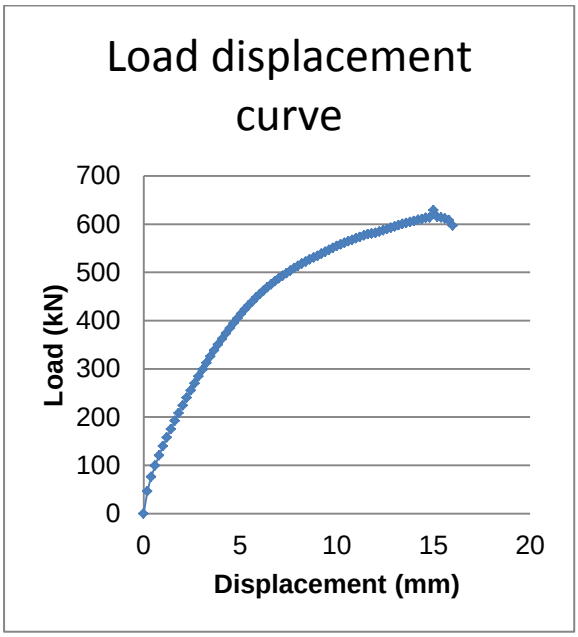

Fig 5.5a: Load- displacement response. at slab-column connection

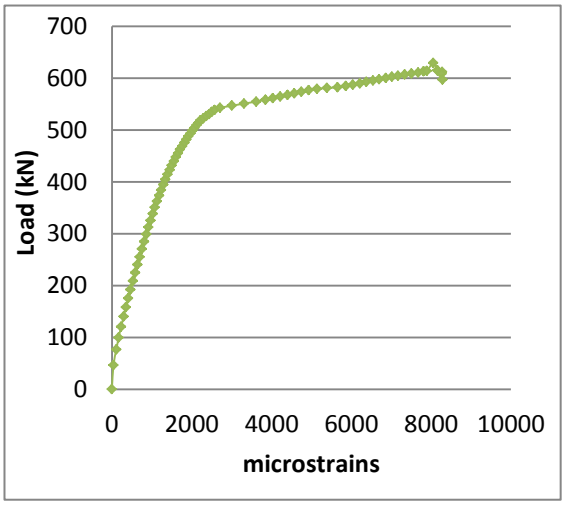

Fig 5.5b: Load- strains on reinforcement

5.4 Comparison of Result

Fig 5.6: Load-displacement curves for the numerical and Eder *et.al* (2010) model

The experimental failure load occurred at 614kN (Eder et.al 2010) while the numerical failure load occurred at 629.08kN.This shows a slight deviation of 2.46% from the experimental failure load. The numerical result in the present study was further compared with previous numerical result of Eder *et.al*. (2010) on the same slab specimen as shown fig 5.6. This numerical failure load deviated from that of Eder et.al 2010 by 2.0% but shows higher deviation in displacements. Fig 5.5b shows that reinforcement yields at a load of 542kN prior to punching shear failure.

From these comparisons, it can be concluded that the software (Midas FEA) and adopted modelling scheme is capable of predicting punching shear failure. Therefore, it is adopted as the dominant methodology in this study. Comprehensive numerical simulations are conducted on the tested slabs in chapter 6.

Chapter 6: NUMERICAL SIMULATIONS

6.0 Introduction

Based on the successful validation of adopted modelling scheme presented in chapter 5, intensive numerical simulation is carried out in this chapter. First and foremost, Elastic analysis is conducted to investigate the relationship between the continuous structure (Prototype) and isolated representative specimen. This investigation evaluates the type of boundary conditions of the representative slab that creates the closest similitude with the prototype slab; in terms of their bending moment distribution and deflections. The prescribed boundary conditions are implemented in the experimental and nonlinear finite element models.

In the second phase, nonlinear finite analysis (NLFEA) is performed to investigate punching shear failure of slab-column connection without shearhead connection. In order to reduce cost intensive laboratory experiments, NLFEA is employed to perform sensitive parameters governing punching shear failure. These numerical results are further validation with experimental results.

In the third phase, numerical simulations were carried out to investigate the structural performance of the shearheads assembly to punching shear capacity of the slab. The main purpose of simulation is to investigate the contribution of the shearhead to the punching capacity of the edge connection; which has been carefully designed. The detail of the shearhead assembly is presented in chapter 7.The results are compared with the measured (experimental) and discussed in detail in chapter 8.

6.1 Elastic Analysis

6.1.1 Extraction of representative slab from Prototype

Elastic analysis is conducted on the full scale continuous slab (prototype) and representative laboratory specimen which is extracted from the prototype slab. As reviewed in the literature, a common approach for selecting a representative specimen size for laboratory test is to determine the location of the line of moment contra flexure by assuming a linear elastic material response of uncracked concrete behaviour. However, the actual response of reinforced concrete is nonlinear.

6.1.2 Description of Prototype Structure

The prototype structure is a multi-story office building hypothesized to be located in a region of moderate seismicity, therefore the columns are designed to resist gravity load only and the lateral load will be resisted by a shear wall. A portion of the prototype that contains the edge slab-column connection to be investigated is extracted from the prototype building as depicted in figure 6.1.Steel columns are used in lieu of concrete column. The dimension of the column is 200mm × 200mm which is scale down to 50 percent in the experiment. The slab is directly supported by steel column without shear capitals or drop panels; instead structural steel shearheads are used to connect the column and the concrete slab. The shearheads connection is advantageous when there is restriction on slab depth and also to achieve an economic design of the slab. But shearhead connection is not considered in the elastic analysis.

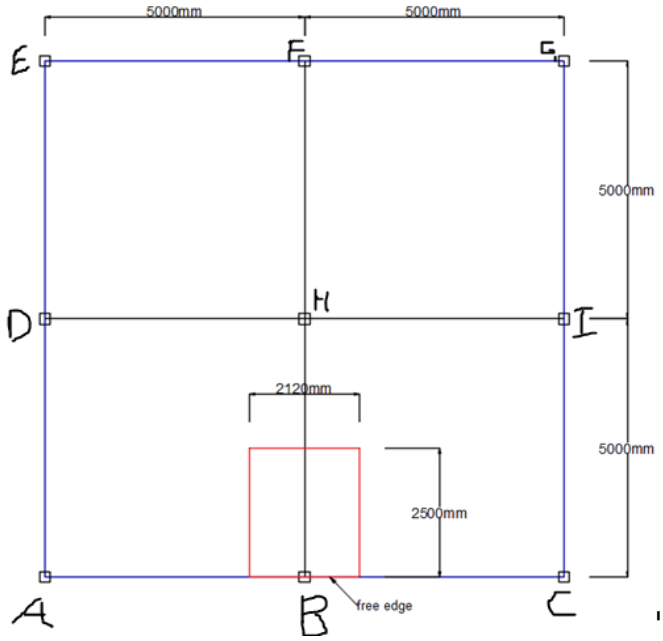

Fig 6.1a: Prototype structural layout

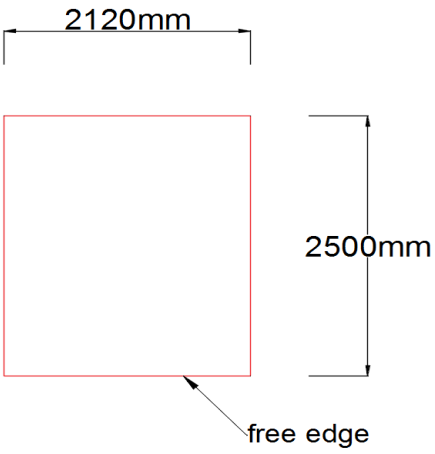

Fig 6.1b: representive slab

6.1.2 Procedure for obtaining representative slab from Prototype

The laboratory specimen was extracted from a portion of the prototype structure. Equivalent frame method was used to obtain the points of zero moments along the free edge and maximum bending moment at the mid-span of the prototype structure. The detail of the structural analysis is presented in appendix 1.

In order to obtain a representative slab from prototype, the following boundary conditions were adopted.

According to Einpaul, Ruiz and Muttoni (2015), it's recommended that for a continuous slab, the radius of the model r_{slab} corresponds to the distance between the column and the symmetry line in the mid-span. Furthermore, the radius of the slab is selected so that in the elastic uncracked phase, the axis symmetric model has to yield the same radius of moment contra flexure of r_s = 0.22L as it is in a regular slab. They also recommended a zero rotation at the edge of the slab as the first boundary condition (at mid-span symmetry). Based on these recommendations, the slab was extracted at the symmetry line at mid-span where maximum bending moment occurs and also maximum deflection occurs because of uniformly distributed load on the prototype.

Secondly, where zero bending moment occurs along the free edge of the prototype, the representative slab was extracted along that line as depicted in Fig 6.1 (a and b)

6.1.3 Drawbacks of the adopted Boundary conditions.

- In the continuous slab (prototype) at mid-span where maximum bending moments occurred and deflection are maximum but for the representative slab, boundary conditions that replicate these behaviour is impossible to achieve in the laboratory, except a full scale test of the prototype is performed.
- At points of zero bending moment along the free edge, from which the slab was extracted, bending moment is assumed zero on perpendicular lines to these point. However, in the continuous structure, bending moment increases linearly to a maximum value at the mid-span.

These assumptions are principally responsible for the 5.85% deviation of the representative slab from the prototype.

6.1.4 Linear Elastic Analysis modelling procedure

Firstly, an equivalent portion of the representative specimen was obtained from the prototype. The extracted specimen with a dimension of 2500mm × 2120mm by 260mm thick was scaled down to 50 percent. The reduced scaled model now has a dimension of 1250mm × 1060mm by 130mm thick. This was done in order to achieve an equivalent manageable laboratory size specimen based on the crane capacity.

Fig 6.2 shows the finite element of the prototype used for the baseline analysis. The edge LO was considered as the free edge of the slab; so that the free edge of the prototype also becomes the free edge of the representative slab. Due to the difference in stiffness between the steel column and the uncracked concrete slab, the stiffness ratio was computed to model the connection.

6.1.4.1 Prototype Slab

An equivalent portion of dimension 1250mm × 1060mm by 130mm thick was considered for elastic analysis on the prototype slab.

All horizontal displacements were restrained along the slab edges LM and ON of zero moment lines but vertical displacement were allowed in fig 6.2. In reality, deflection will continue to increase linearly along LM and ON until it becomes maximum at Mid-span at M and N respectively. Rotational restraints were adopted along the slab edge (MN) at mid-span (symmetry line) in compliance to the first boundary condition recommended for continuous slab. However, vertical displacement (dz) was allowed because deflection is maximum at mid-span (MN) due to uniformly distributed load on the slab.

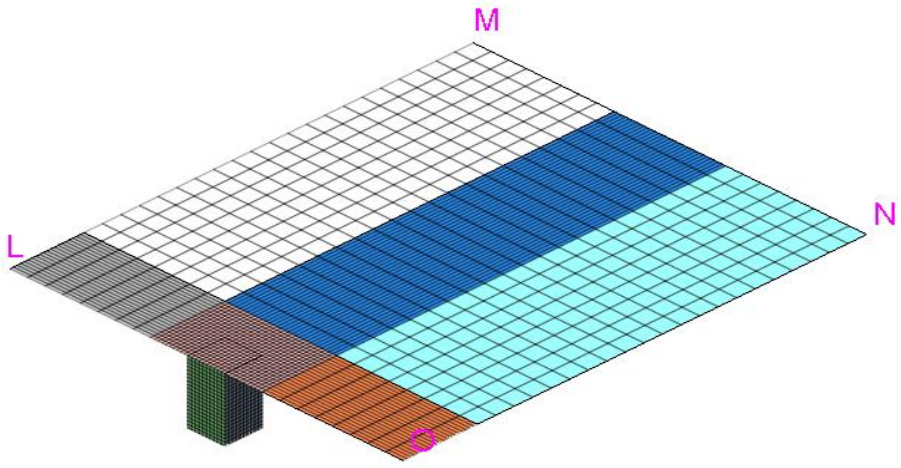

Fig.6.2 finite element discretisation of prototype slab

Both translational and rotational degrees of freedom in all directions were restrained at the base of the column. The detail of the various restraints is provided in Table 6.1

Table 6.1 Boundary conditions adopted.

EDGES	Dx	Dy	Dz	Rotation
LM	Restrained	Restrained	Allowed	Allowed
ON	Restrained	Restrained	Allowed	Allowed
MN	Restrained	restrained	allowed	Restrained
L O	Free	Free	Free	Free

Elastic properties assigned for concrete and steel is depicted in Table 6.2

Table 6.2 Elastic properties.

Materials	Elastic Modulus (N/mm^2)	Poisson's ratio
Concrete	32800	0.2
Steel	210000	0.3

The load applied on the prototype slab is provided as thus,

Unit weight of concrete = $24kN/m^3$

Overall thickness of slab = 130mm 280mm

Slab own weight = $24kN/m^3$ × 0.13m = $3.12kN/m^2$

Live load on slab = $2.25kN/m^2$

Design Load on slab (F) = 1.35 G_k+ 1.55 Q_k to EC2

$$1.35 \times 3.12 + 1.55 \times 2.25 = 7.7kN/m^2$$

This design load was applied on the continuous slab. Elastic analysis was carried out and the shear force transmitted to the edge column was recorded. This shear force was applied at the bottom of the column of representative slab. Since it is difficult to apply uniformly distributed load (UDL) in the experiment, the shear Force roughly represent it. The shear force represents the vertical static load that causes punching shear in the experiment.

6.1.4.2 Representative Slab (Laboratory specimen)

The type of restraints and loading to be adopted in the experiment was examined in the elastic analysis. Firstly, the maximum shear force at the column obtained from the prototype slab was applied as vertical static load from the bottom of the slab, as opposed to the real world upright position .Four vertical supports representing roller supports were applied near the corners of slab by trial and error method until suitable positions that give the closest value of the bending moment distribution as obtained in the prototype. The position is 150mm away from each corner. Excessive rotation was prevented along the mid-span edge (MN) by application of two clamps near the roller supports. The clamps were modelled by restraining the nodes adjacent the supports; in order to reflect similar restraint adopted for the prototype. But this cannot totally eliminate rotation in reality as modelled in the elastic analysis of the prototype.

6.1.5 Results of Elastic Analysis

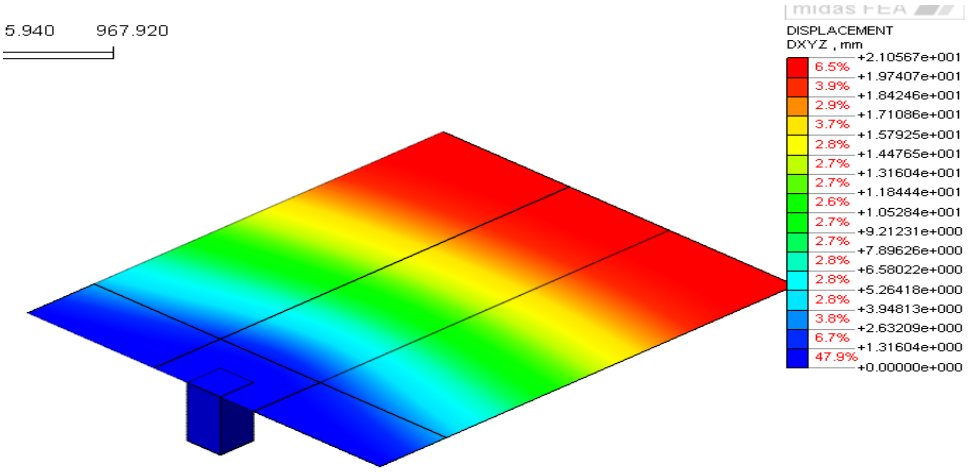

Fig 6.3 Vertical displacement of prototype slab.

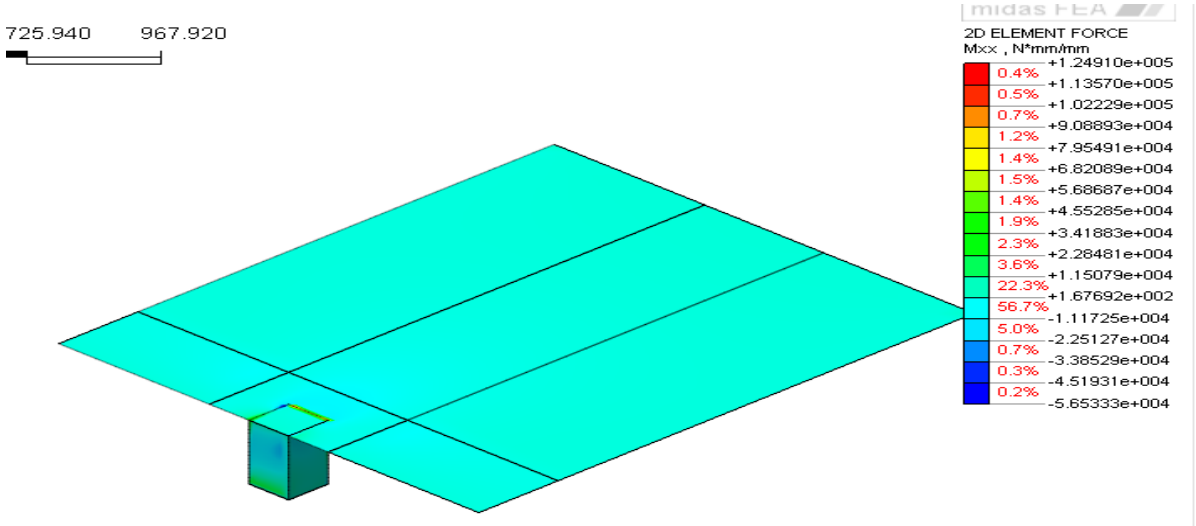

Fig 6.4 Bending moment distribution (M_{xx}) of the prototype slab.

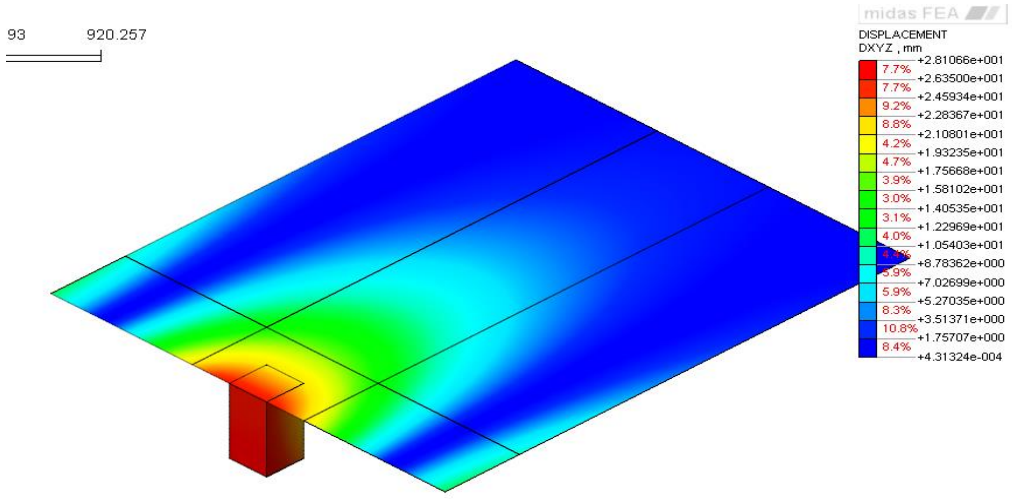

Fig 6.5. Vertical displacement of the representative slab.

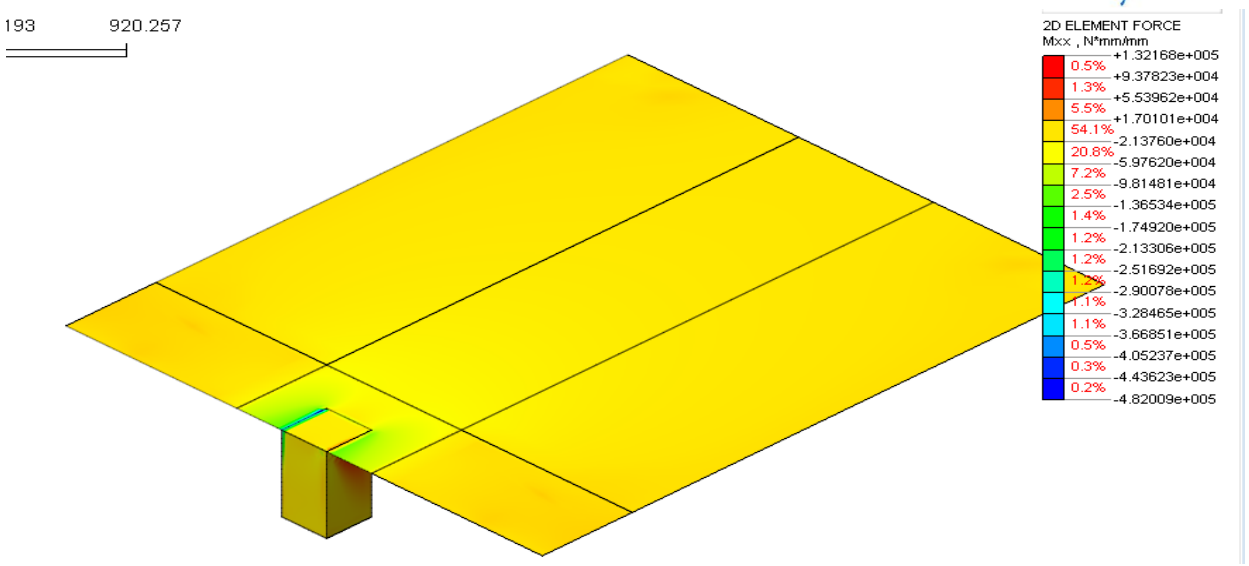

Fig 6.6. Bending moment distribution (M_{xx}) of Representative slab.

Conclusion

The flexural behaviour of the slabs is compared and contrast. Firstly, resultant maximum vertical displacement on the prototype gives 21.06mm which the representative specimen gives 28.11mm. But the values of local deflections at the slab-column connection in both cases are very close. The resultant maximum deflection of the prototype occurs within the mid-span region indicated by the red zone in fig 6.3. This models the real life deflection of the prototype structure, because deflection is maximum at mid-span. Therefore, boundary conditions adopted is very satisfactory.

For the representative slab, maximum displacement occurred at the edge strip of the slab within the vicinity of the slab-column connection due to the vertical load applied from the bottom of the column as shown in fig 6.5

The maximum bending moment that occurred at the slab-column connection of the prototype gives $1.249 \times 10^5\ Nmm/mm$ while that of the representative specimen gives $1.322 \times 10^5\ Nmm/mm$. This shows a deviation of 5.85% from the prototype. It is noteworthy that a closer replication was obtained because of the boundary conditions that was designed to eliminate in-plane forces (axial forces) also known as membrane actions. In addition, the effect of moment redistribution that occurs in the prototype structure was ignored in the elastic analysis. Furthermore, it can be concluded that representative slab replicates the flexural behaviour of the prototype structure.

The prescribed boundary conditions used in the representative slab is deemed adequate therefore, it fully implemented in the preceding nonlinear numerical and experimental models.

6.20 NLFEA modelling of Slab 1 (Slab without shear reinforcement)

This section provides detail of the nonlinear numerical procedure of slab-column connection without shear reinforcement and sensitivity study on parameters that influence punching shear failure.

6.21 Restraints adopted

The exact slab size tested in the experiment was replicated in this numerical model.

The exact restrained adopted in the experimental model was replicated in the numerical model. At 150mm away from each corner, a vertical restrain was applied. Translation in the horizontal direction (dx) was allowed and that of dy and dz were restrained; and rotational restraints were allowed in order to replicate the roller supports. Clamps were modelled by restraining the nodes adjacent the supports as shown in fig 6.8

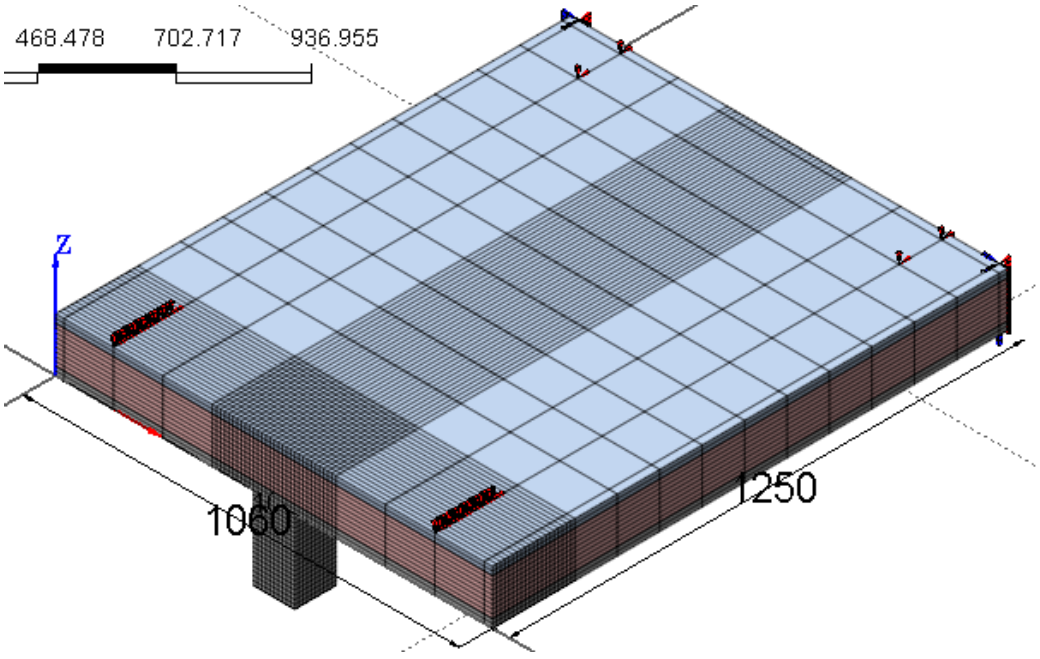

Fig 6.7: Slab model showing restraints adopted.

6. 2.2 Material models adopted

Based on the available literature reviewed in chapter 3 it was deemed suitable to implement material models provided in Table 6.3

Table.6.3 Material models adopted for the slab to column NLFEA

S/N	Materials	Models
1	Plain concrete in Compression	TS-fixed crack model (Parabola)
2	Plain concrete in Tension	TS-fixed crack model (Exponential)
3	Reinforced concrete	TS-fixed crack model (Exponential and parabola)
4	Reinforcement	Von mises (perfect plastic)
5	Steel column	Linear Elastic

6.2.3 Material properties

The material properties obtained from experiment on control specimens and other material parameters computed according to formulae provided in chapter 3 are implemented in Midas FEA as shown in table 6.4

Table.6.4 Concrete material properties adopted for the Midas FEA model are given below

S/N	Properties	Values
1	Elastic Modulus in Compression	$32.82 kN/mm^2$
2	Elastic Modulus in Tension	$16.41 kN/mm^2$
3	Shear Modulus (G)	$12.5 kN/mm^2$
4	Poisson's ratio (ϑ)	0.2
5	Weight Density (ρ)	$2.4 \times 10^{-5} kN/m^3$
6	Compressive strength (f_{cu})	$30 N/mm^2$
7	Fracture energy in tension (G_f)	0.074 (J/mm^2)
8	Fracture energy in Compression (G_c)	7.4 (J/mm^2)
9	Shear retention for Plain concrete (β)	0.3
10	Shear retention for reinforced concrete	0.3
11	Tensile strength (f_t)	$2.49 N/mm^2$

.

6.2.4 Reinforcement Modelling

Embedded reinforcement concept was adopted, in this approach; the stiffness of the reinforcements is added to the stiffness of the continuum elements (concrete) in which the reinforcements are located. Embedded reinforcement in 3D solid element is represented in Midas FEA as depicted in fig 6.8.

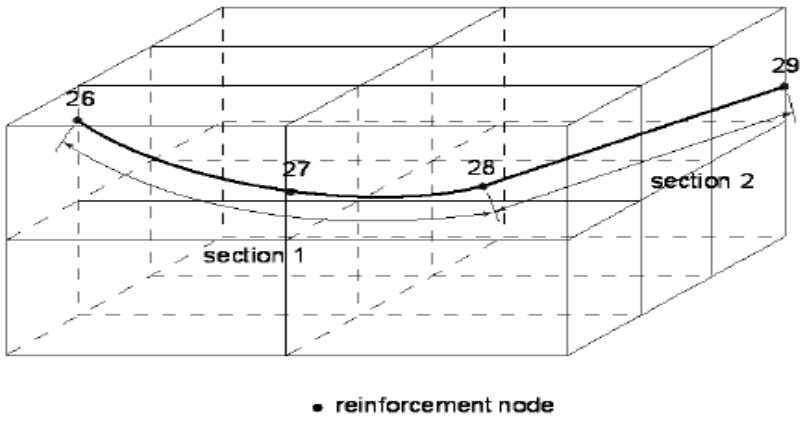

Fig 6.8 embedded reinforcement in solid element

The reinforcements were inserted along the edges of the continuum elements and divided into segment in which the nodes correspond to the nodes of the continuum elements. The reinforcement does not have a separate degree of freedom; its strains are obtained from the displacements of concrete. Reinforcement and concrete were assumed to be perfectly bonded. The reinforcement bars were represented a line, its material property and cross-sectional area were defined. The Auto mesh function was used to assign material properties and division of the reinforcement bars into segments. The material properties and reinforcement ratio is shown in Table 6.5.

Table 6.5: Numerical simulation data

Elastic constants	Young modulus (N/mm^2)	Poisson's ratio
Concrete	32.82	0.2
Steel	205	0.3

Concrete strength (N/mm^2)

Tensile (f_t) = 2.49	Compressive (f_{cu}) = 30

Rebars	Spacing (mm)	Cover (mm)	Sectional area (mm^2)	Yield strength (N/mm^2)
In Slab				
Tensile	102 (long)	20	50.27	500
	110 (Trans)	20	50.27	500
Compressive	204 (long)	20	50.27	500
	220 (Trans)	20	50.27	500

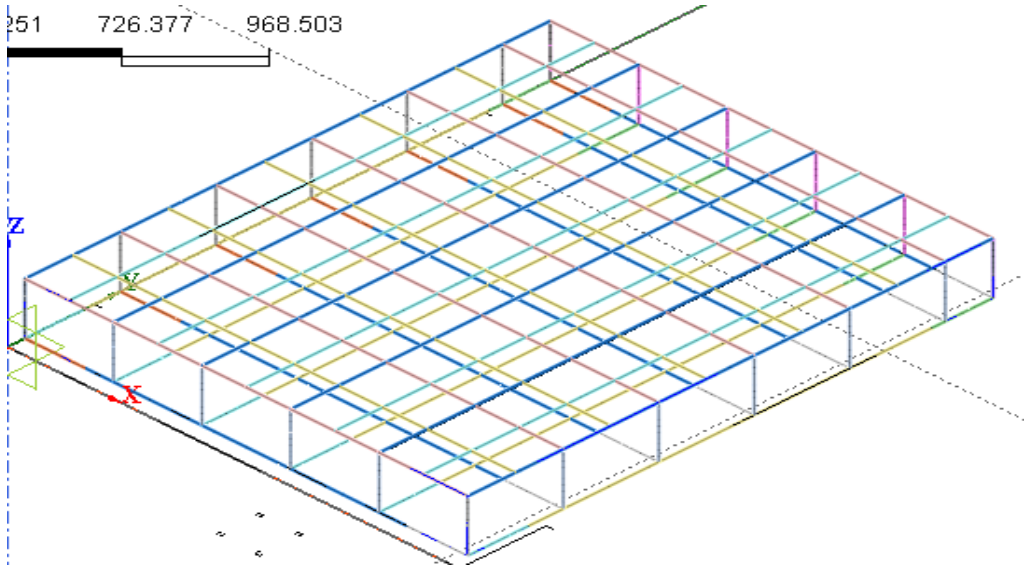

Fig 6.9 model showing reinforcement grid embedded in the slab.

6.2.5 Modelling Procedure

The full scale of the slab specimen was modelled. The slab specimen was discretised into 19771 elements and 21981 nodes as shown in fig.6.10. The mesh was refined in

plane within the vicinity of the column and included five layers of elements through the slab depth. A full integration was used throughout to avoid convergence problems. Embedded reinforcement was used. Perfect bond between reinforcement and concrete was assumed. The Von Mises yield criterion with isotropic hardening was adopted for reinforcement. Clamps were simulated by supporting nodes near the corners of the slab.

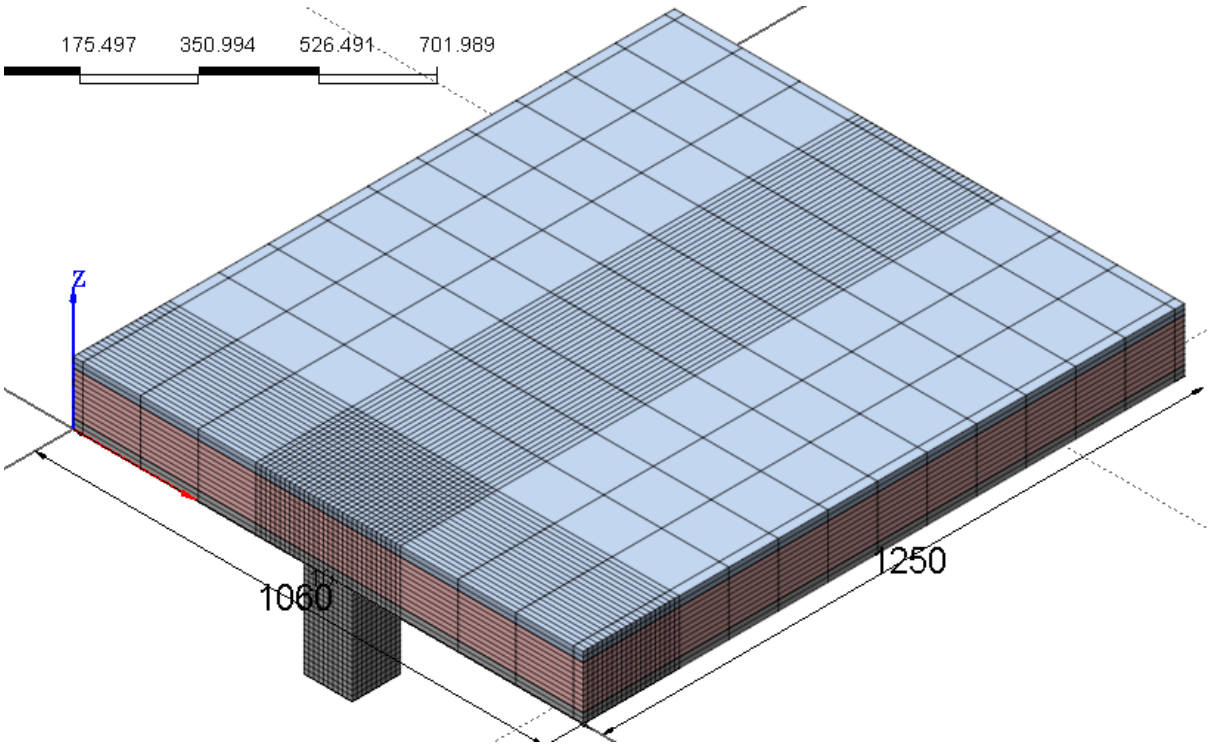

Fig.6.10. Full scale discretization of slab specimen into finite elements.

Table 6.6: Material model implemented in numerical analysis

Model	$G_f\ (Nmm/mm^2)$	$G_c\ (Nmm/mm^2)$	(β)	(Tensile softening)	(compr softening)
Slab	0.074	7.4	0.3	exponential	parabolic

Since there is no recommended relationship between elastic modulus in tension and compressive, elastic modulus in tension was assumed half of the value in compression.

6.2.7 Solution Procedure

Regular Newton-Raphson iteration scheme was adopted. In the regular Newton-Raphson method, the stiffness matrix represents the tangential stiffness of the

structure. The stiffness matrix is evaluated each iteration. The method yields a quadratic convergence characteristic, which means that the method converges to the final solution within little iteration. Despite the time consuming nature of its convergence, the quadratic convergence is guaranteed if a correct stiffness matrix is used and if the prediction is already in the neighbourhood of the final solution. It needs little iteration as opposed to the modified Newton-Raphson method that requires more iterations (midas FEA 1989).full integration scheme was adopted, results are evaluated at the integration points. The solution is carried out in an incremental step-by-step analysis with the total applied load divided into a number of load steps. According to Davison and Owens (2012) when the stiffness matrix approach is used in the method, there are no significant limitations on its applicability.

6.2.8 Numerical Results

In order to mimic the experimental procedure, the loads were applied in two phases as thus.

1. The self-weight was activated in the first phase of the analysis. A maximum deflection of 0.0058mm occurred at the centre of the slab, as shown in fig 6.11.

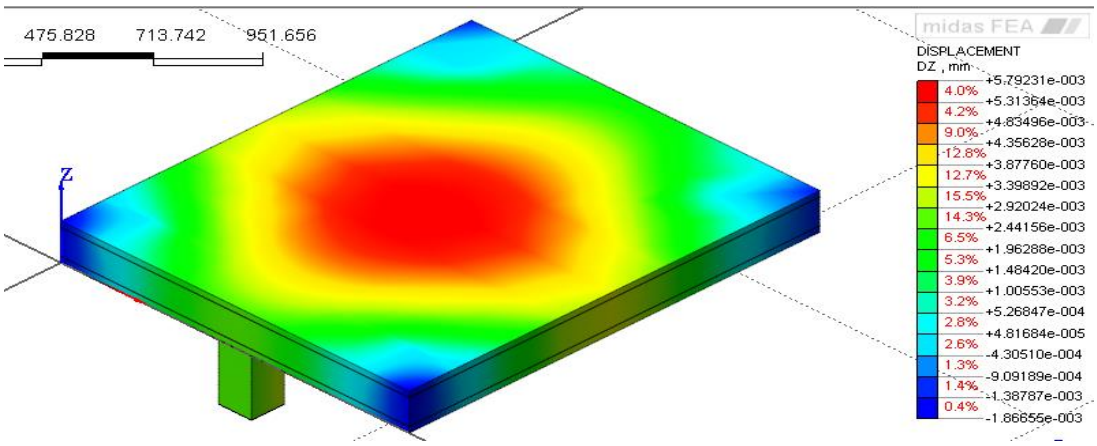

Fig.6.11: Deformation of specimen under self-weight.

2. In the second phase of analysis, a nonlinear displacement-controlled Quasi-static load was applied from the bottom of the column. Effect of material nonlinearity was accounted for by activating Second Piola-Kircchoff stress,

Lagrangian strain, and cracks stresses. The displacement was applied from the bottom of the column; although in laboratory experiment, incremental step load was applied. Incremental step load was avoided in this numerical modelling because it provides very large unacceptable displacement evolution. In all iterations, force and energy norms were used for convergence criteria, and a maximum tolerance of 2.0% was set for the out-of-balance forces. The deformation profile of the slab-column connection at failure load is depicted in fig 6.12.

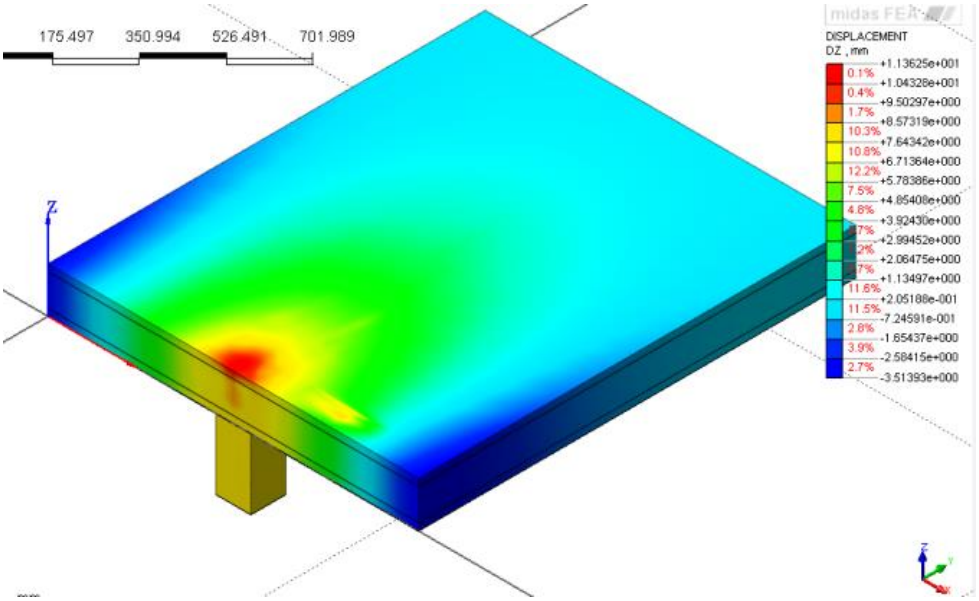

Fig.6.12 slab deformation at failure load.

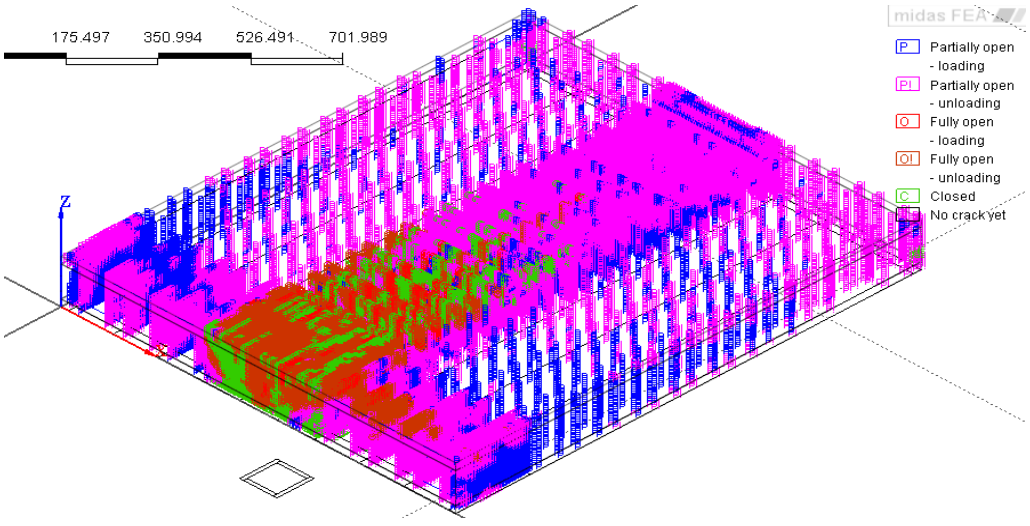

Fig.6.13 crack propagation in the slab specimen.

6.2.9 Theoretical assumption adopted

- One way shear failure was assumed. According to Kupfer (1969), the compressive strength under biaxial compression is not greater than 15% of the uni-axial compressive strength. In addition, the tensile strength of concrete under biaxial compression-tension may deviate very slightly from that of the uni-axial compression. Based on this, one way shear was assumed

  Moreover, research has shown that shear strength two-way exceeds one-way by 15 percent.
- The same rotation was assumed for the slab - column connection. The same rotation was assumed for the slab-column connection in order to achieve uniform displacement at the joint.
- Membrane effect (in-plane forces) is considered absent.

  Compressive membrane action was neglected in various design codes. It is relatively difficult to investigate in the laboratory. A lower bound solution is proposed. Compressive membrane contributes significantly to punching shear.
- Redistribution of mid-span sagging moment and hogging moment over the support is avoidably absent. Moment redistribution contributes to punching shear strength. Moment redistribution occurs when the slab is restrained laterally which contributes to punching shear strength of the connection

6.2.10. SENSITIVITY STUDIES

Concrete material properties such as compressive strength, tensile strength and fracture energy are interdependent; however, parametric analysis is undertaken by considering each parameter independently in order to investigate their effects on punching shear failure process.

6.2.10.1 Effect of concrete Tensile strength

Concrete tensile strength was varied between 1.0 to 2.49 MPa. The tensile strength of 2.49 was used for the baseline analysis. The effect of concrete tensile strength is investigated by varying the tensile strength as depicted in Fig 6.14

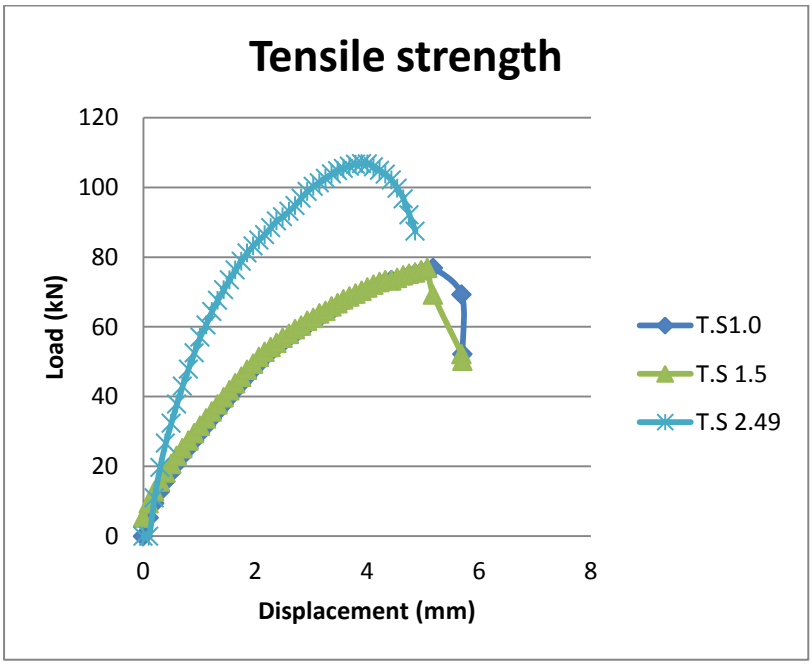

Fig 6.14. Variation of concrete tensile strength.

The graph presented in fig 6.14, shows that increasing the concrete tensile strength increases the punching shear strength. It could also be observed that increasing concrete tensile strength affects both displacement and to the failure load slightly. The most appropriate equation for predicting concrete tensile strength is still not provided. However, empirical an equation has been provided by (Bresler and Scordelis,1963) which relate tensile strength to the square root of cylinder compressive strength of concrete as thus ; $f_t = 0.33\, {f_c}^{1/2}$ which has been applied by (Vecchio and Shim,2004) and many others. The tensile strength used for the baseline analysis was measured from experiments on control specimens. Detail is provided in chapter 7.

It can be concluded that punching shear failure is principally due to tensile failure of concrete along the inclined punching crack as observed in the experiment and not due to compressive failure of concrete. This observation agrees with the observation of (Moe 1961) that suggested that punching shear failure is usually a splitting type of failure which is comparable to the type of failure observed in specimens subject to

tension. This significant influence of tensile strength was adopted as the basis for the analytical equation of punching shear capacity of an interior connection by (Menetrey, 1996). However, Menetrey assumed a uniform tensile stress distribution across the inclined crack profile which was seen as a drastic simplification of his model.

Hallgren (1996) has also shown that tensile strength has a major effect on punching shear capacity of a slab-column connection than compressive strength. He also observed that increase brittleness of higher concrete grades reduces the punching shear strength.

2. Shear Retention Factor (β)

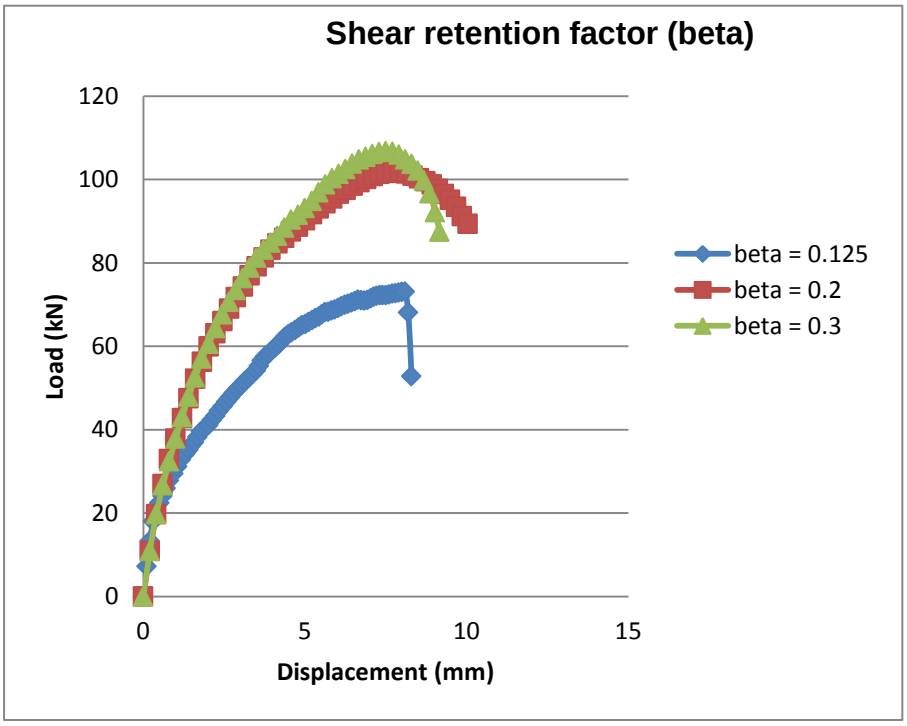

Fig 6.15. Variation of shear retention factor (β).

In order to account for the degradation of shear stiffness due to the progressive damage of concrete in the post-damage regime, the shear retention factor was used. Vaz Rodrique (2007) recommended that one-eighth of the value of shear modulus of the uncracked concrete should be used. Rot (1988) suggested that a low value of

shear retention factors should be used in fixed crack models to eliminate stress locking. In this study, the value of β was varied between 0.125 and 1.0 on the response of slab 1 tested without shearheads. The choice of β could also depend on the structural type and concrete properties. Fig 6.15 shows that increasing β could lead to an increase in failure load because it delays the fracture process and thereby alleviating shear stresses in the uncracked concrete. For this study, $\beta = 0.3$ correlate very well with experimental measurement of load and displacement.

3 Effect of Mesh Density

For the baseline study a coarse mesh was used in the vicinity of the column with a size of 10 × 10 mm and 10mm thick and 150 ×150 mm and 10mm thick was used on the remaining area. A less coarse mesh sizes of 20 × 20 mm and 20 thick in the vicinity of the column was used.

From comparative study, the result shows that decreasing mesh density increases the punching shear capacity of the connection. The coarse mesh used for the baseline study provides the best fit when compared with the experimental result. However, it involved too many elements and nodes, which becomes too cumbersome to deal it and also required great computational time.

4. Effect of Fracture Energy of concrete.

From Equation 3.21 it shows that fracture energy depends on the aggregate size

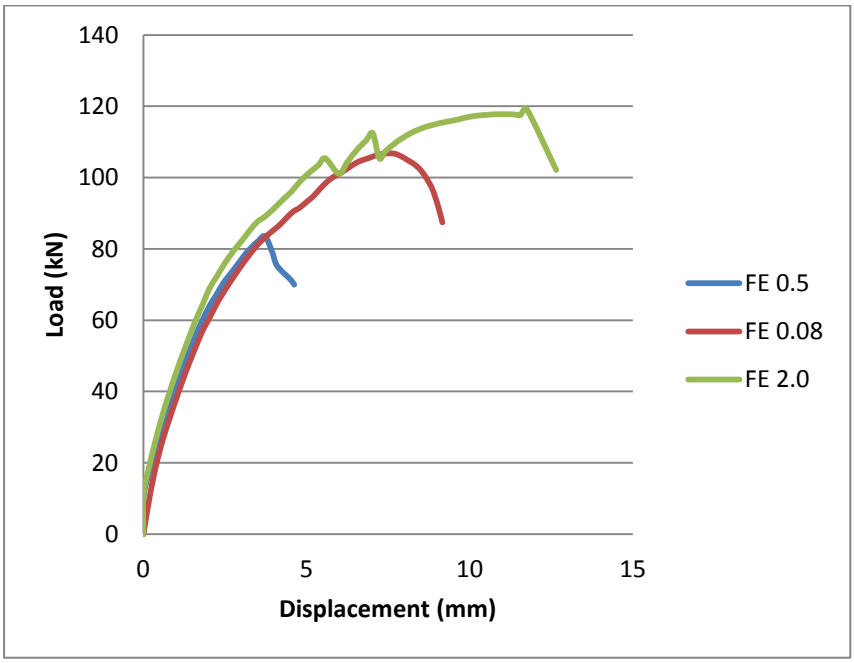

Fig 6.16: Variation of Fracture energy of concrete.

The influence of the concrete fracture energy is investigated. The graph in fig 6.16 shows it influences the failure load and the ductility of the response as it increases with increasing fracture energy.

Concrete Tension Softening Behaviour

Various tensions softening response implemented in Midas FEA were examined using slab 1. The Brittle, Hordijk and exponential softening response functions were compared as shown in fig 6.17

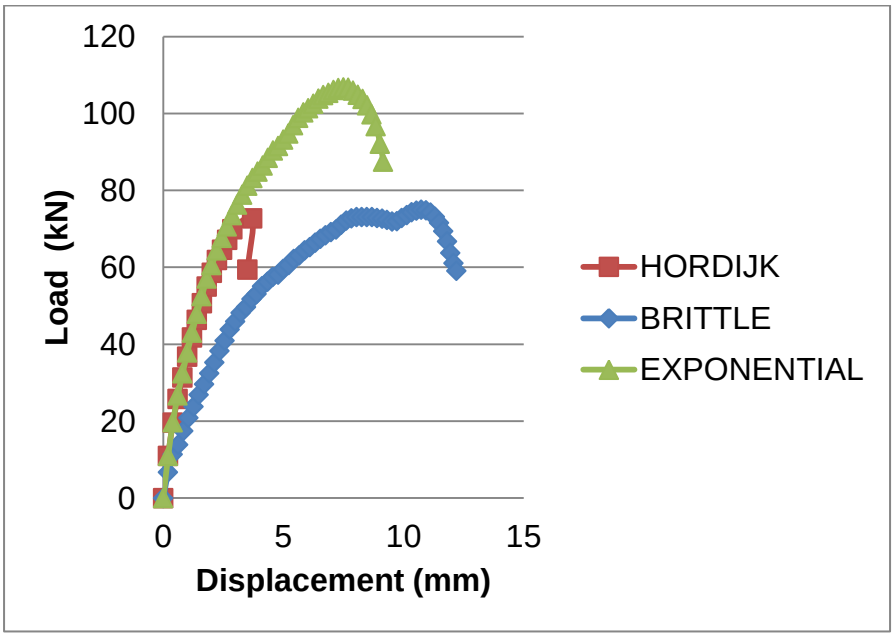

Fig 6.17: Variation various Tension softening model.

The Exponential softening response is represented as thus.

$f_t(\varepsilon) = f_t\, e^{-\varepsilon/k}$ ..... (6.1)

$k = \frac{G_f}{h f_t}$ ..... (6.2)

Where ε represents the tensile crack strain

Cracking occurred when the maximum tensile stress is reached and exponential softening begins. The area under the tension softening diagram is calculated as $\frac{G_f}{h}$ in the exponential Hordijk model. In the brittle model ($G_f = 0$) because once the tensile strength is reached, the stress drops abruptly to zero.

Effects of Concrete Elastic Modulus

From fig 6.18, it could be observed that increasing the elastic modulus slightly increase the punching shear failure Load. Moreover, elastic modulus is directly influenced by compressive strength. As compressive strength increases, the elastic modulus increases. The influence by compressive strength is included in the EC2 equation; which indicates the punching shear capacity as a function of the cube root of concrete compressive strength.

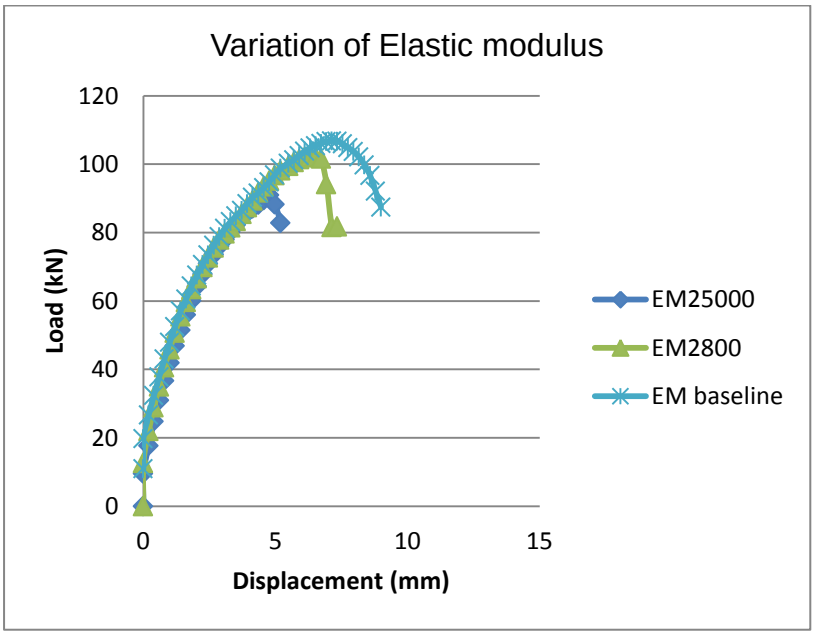

Fig 6.18: Variation of Elastic modulus of concrete.

Effects of Reinforcement Ratio

As provided by EC2 and BS8110, the reinforcement ratio has a significant influence on the punching loads. But ACI 318-05 ignore this significant influence of Reinforcement ratio in its punching shear capacity equation. In EC2, punching shear capacity increases approximately as the cube root function of reinforcement ratio. According to Ozbolt *et al*. (1986) suggested that increase in reinforcement ratio lead to a higher height of the compression zone which increasing the punching failure load associated by more brittle failure. In furtherance, reinforcement ratio may increase the shear strength due to the dowelling action.

Increase in tensile reinforcement ratio also increasing the height of the compression zone leading to higher punching shear failure loads which is accompanied by more brittle failure.

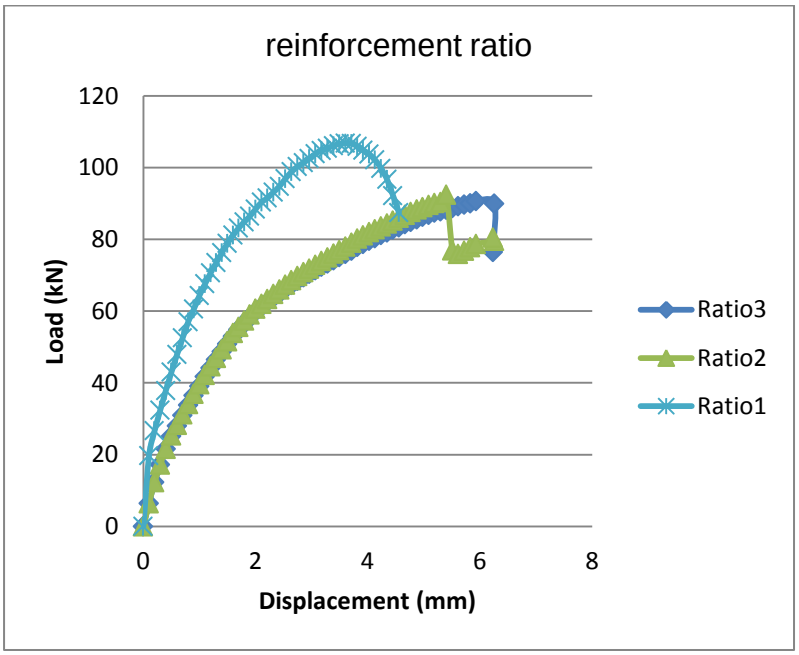

Fig 6.19: Variation of Reinforcement ratio

The effect of the reinforcement was investigated by varying three ratios, 0.02, 0.04, and 0.06. A similar cracking mechanism was observed in all the variation. Fig 6.19 shows the influence of ratio on the Load- deflection response. It could be observed that increasing the reinforcement ratio increases the failure load. However, there is no significant influence on the displacement even though the ductility decreases. It is noteworthy to mention that the numerical model could not capture the dowelling actions of the reinforcement which remains one of the shortcomings of the numerical simulation. Provided the reinforcement ratio is sufficient to delay flexural failure (yielding of reinforcement), the compressive strength does not lead to significant increase in the peak load. This is due to the fact that the shear capacity of the compression zone grows with the compressive strength. However, it does not contribute to more stable growth of the cracks of the tensile zone. Fig 6.20 shows that reinforcement yielded prior to punching shear failure of the connection. Yielding is significant in the vicinity of the connection.

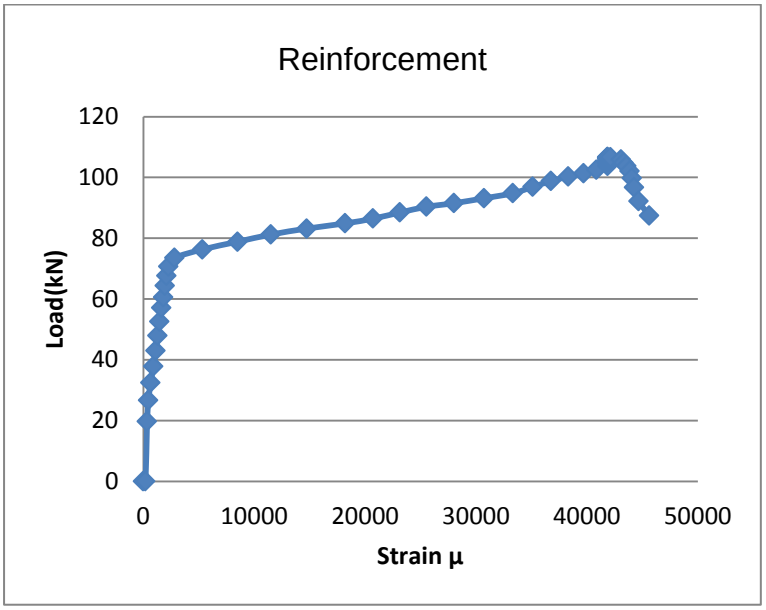

Fig 6.20: strain on reinforcement at failure load.

6.30 NUMERICAL SIMULATIONS OF SLAB WITH SHEARHEAD (SLAB 2)

6.3.1 Modelling Procedures

.

The concrete slab is model with the 'Total strain crack model' which is based on the modified compression field theory of (Vecchio and Collin, 1986) and its 3D extension by (Selby and Vecchio,1993) to account for the effect of lateral cracking. The original compression field theory ignores the tensile strength of cracked concrete, which the modified compression field accounted for. The concrete compressive behaviour is modelled with the parabolic softening model proposed by (Feenstra ,1993). In order to account for the degradation of shear modulus due to progressive damage of concrete in the post damage regime, a shear retention factor of 0.3 was adopted. But Vaz Rodrigues (2007) suggested that shear stiffness should be reduced to one-eight of its original value to account for stiffness degradation in the post crack regime. The fracture energy in compression was taken as $G_c = 100\, G_f$ where G_f is equal to fracture energy in tension computed based on equation 4.20

The tensile behaviour of concrete was modelled with the exponential softening model in which the area of the softening zone equals G_f / h , where h is the crack bandwidth

which is taken as $\sqrt[3]{V}$ (V = volume of element). The concrete tensile strength was taken as $f_c = 0.8\, f_{cube}$ in accordance with EC 2.

The structural steel (shearhead) was modelled with four nodded isoparametric shell elements. Discrete embedded reinforcement concept was used to model the reinforcement. The steel was defined as perfectly elastic-plastic with the Von mises yield criterion. A perfect bond was assumed between the reinforcement, embedded shearheads and concrete.

6.3. 2 RESTRAIN ADOPTED

For computational efficiency only half of the slab was modelled. The restraints capture the flexural behaviour of the isolated slab 2. Horizontal displacements were restrained in the X and Y directions on the axis of symmetry which is perpendicular to the free edge of the slab (BD) and (CE). Vertical displacement was allowed because the slab is expected to undergo a vertical deformation under the static load. Horizontal displacements were also restrained in the X and Y directions along the edge of the slab parallel to the free edge; which represents line of symmetry where maximum deflection occurred in the prototype slab (DE). Vertical displacement (Dz) was also allowed. The clamped was modelled by restraining the s nodes near the supports. The restrained adopted is depicted in fig 6.21.

Rotational displacement was also applied on top of the column above the slab. At 150mm away from the right edge of the slab, a horizontal restrain in the Y-direction and vertical restrain were applied. Horizontal displacement in the X direction was allowed to replicate the behaviour of a roller support implemented in the experiment.

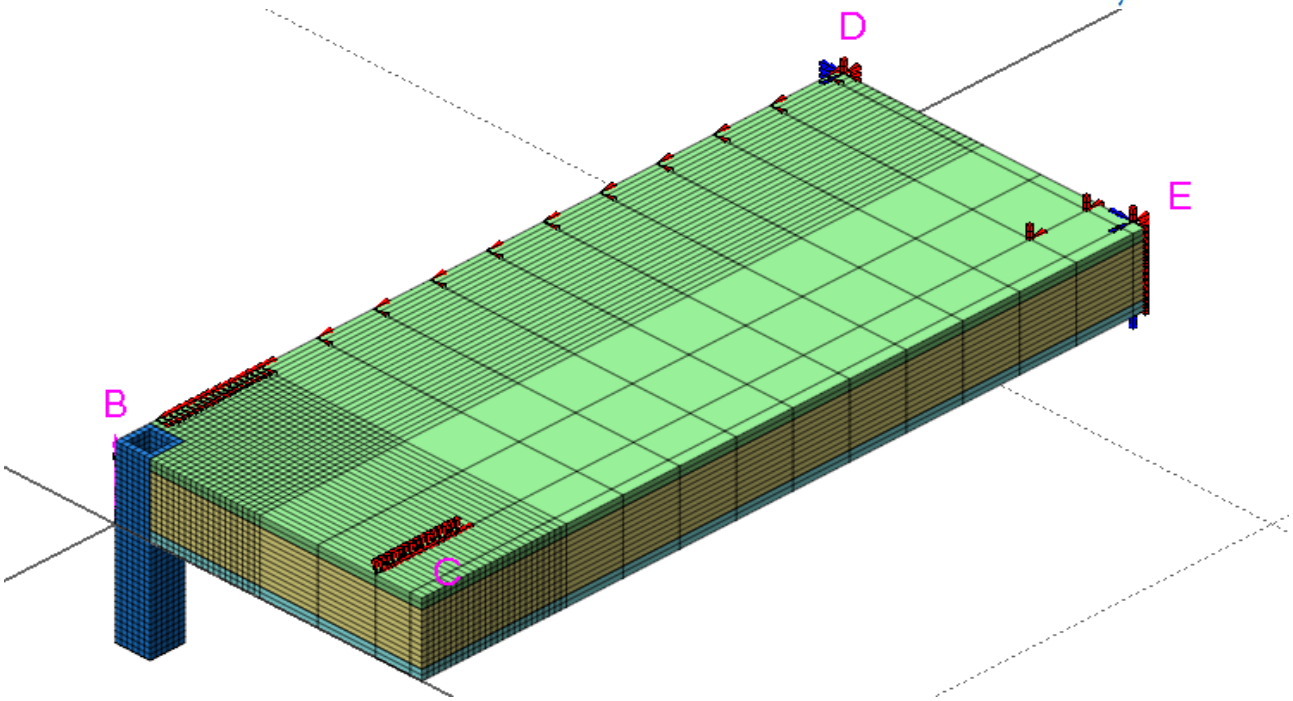

Fig 6.21 finite element model of slab2 showing restraints adopted.

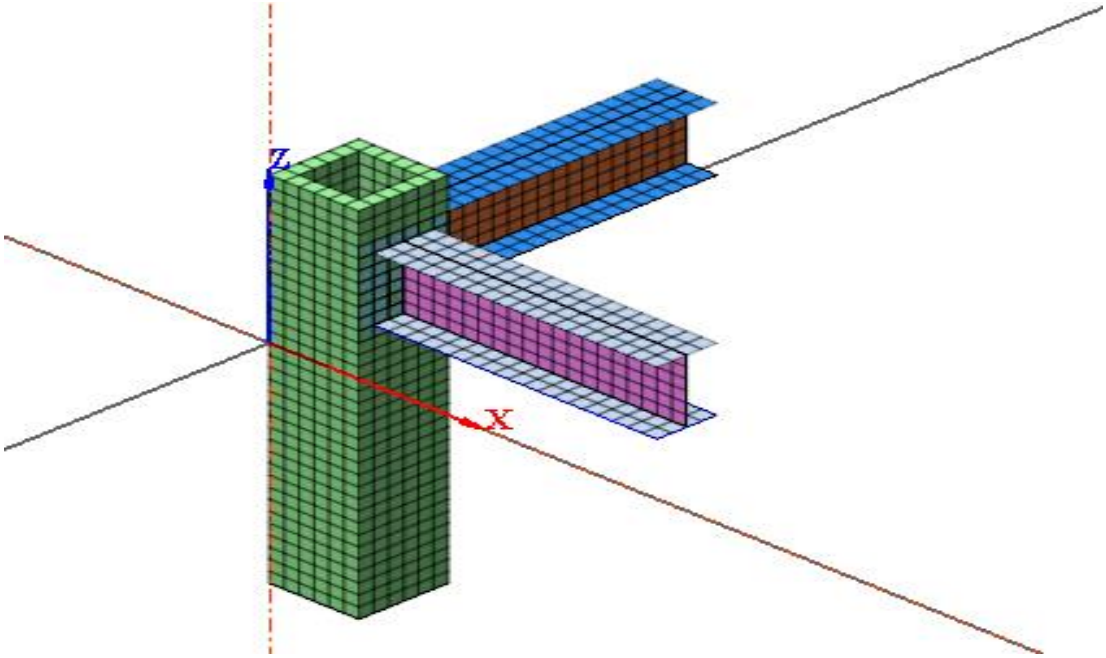

Fig 6.22 finite element model of shearheads assembly

The specimen was discretised into 16386 elements with 17693 nodes. The mesh was refined in the plan around the column and shearheads and included seven layers of elements through the slab depth.

The material model properties and shearheads section geometry are presented in Table 6.7a and b.

Table.6:7a Material model implemented in NLFEA.

Model	$G_f\ (Nmm/mm^2)$	$G_c\ (Nmm/mm^2)$	(β)	(Tensile softening)	(comp softening)
Slab	0.074	7.4	0.3	exponential	parabolic

Table 6.7b Section dimensions used for Shear arms in NLFEA

Section	h (mm)	w (mm)	t_f(mm)	t_w(mm)
I	76	3	3	3

6.3. 3 Interface

In order to capture the interfacial mechanism of the shearheads and concrete, interface concept was adopted. The interface element was introduced to account for discrete cracking of concrete and loss of bond between the steel shear arm and concrete. The thickness of the interface was assumed zero. In order to overcome numerical instability associated with zero thickness interfaces, penalty stiffness is assigned to the interface element. To ensure that the penalty stiffness does not caused numerical instability, Midas FEA recommended the following formula.

$K = 1000 \times E \times d$ ..... (6.3)

Where K = penalty stiffness. E =Elastic modulus of the most stiff element used in the model, in this case steel was used.

d = representative element size.

The interface element was assigned material properties, and then point interface type was adopted as shown in fig 6.23

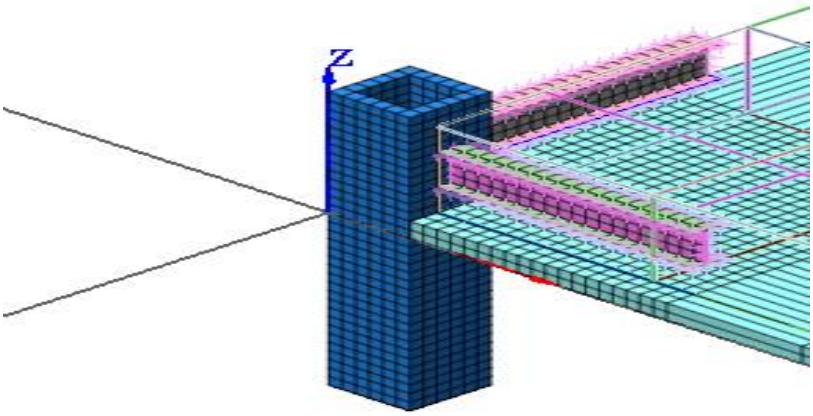

Fig 6.23. discrete interface model for shearheads to concrete interface.

discrete crack interface was adopted to model the interfacial mechanism between the shear arm and the concrete; because discrete cracking of concrete could occur around the shearheard. Both secondary transverse and longitudinal cracks could occur within the vicinity of the sheararm, this behaviour is best modelled using discrete crack model..The interface was characterised with the tensile strength of concrete. normal and shear modulus of steel section.Mode II failure mode was adopted to capture the shear failure. The secant unloading type was also applied at the interface.

6.3. 4 Solution Phase

1. The self-weight was activated in the first phase of the analysis to check the deflection induced by self weight. Fig 6.24 shows the deflection was maximum around the centre of the slab.

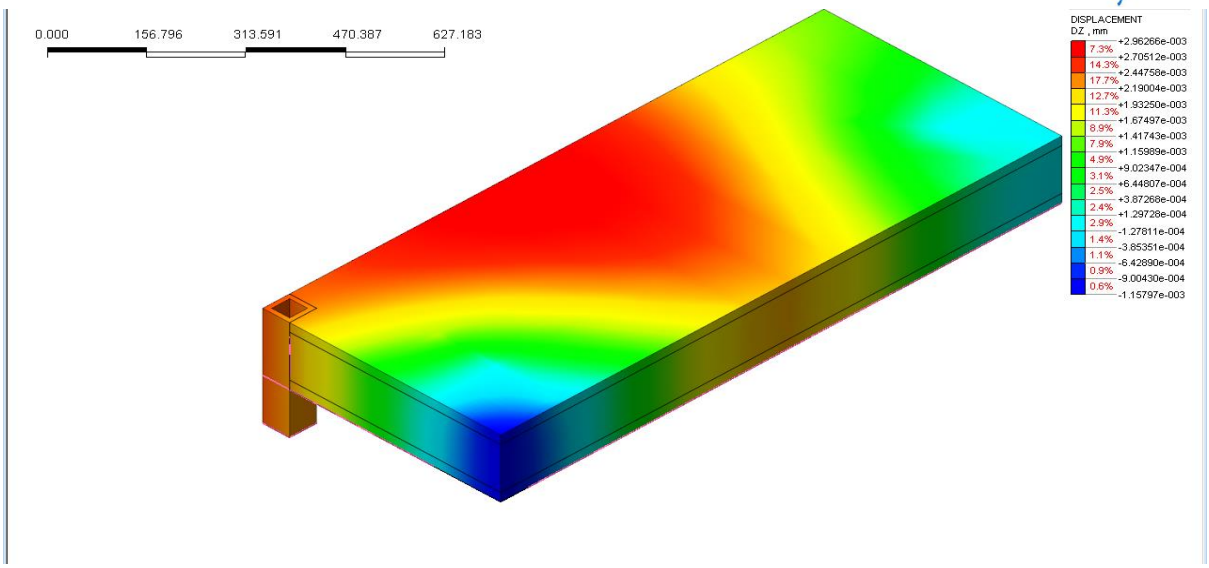

Fig 6.24: displacement contour under self weight.

2. I n the second phase of analysis, an incremental displacement load was applied from the base of the steel column, until punching shear failure of the slab occurred. Local deformation was very significant at the slab-column connection as depicted in fig 6.25.The slab-column connection shows a stiffer response than Slab1 without shearheads. The shearheads deformed plastically prior to punching shear failure.

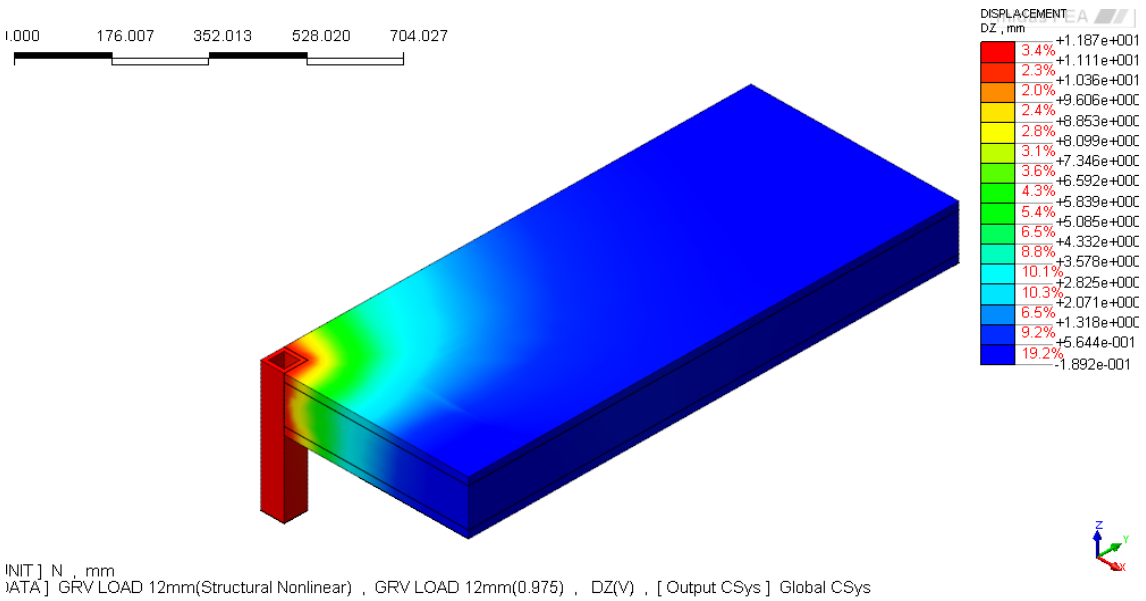

Fig 6.25: displacement contour for slab 2

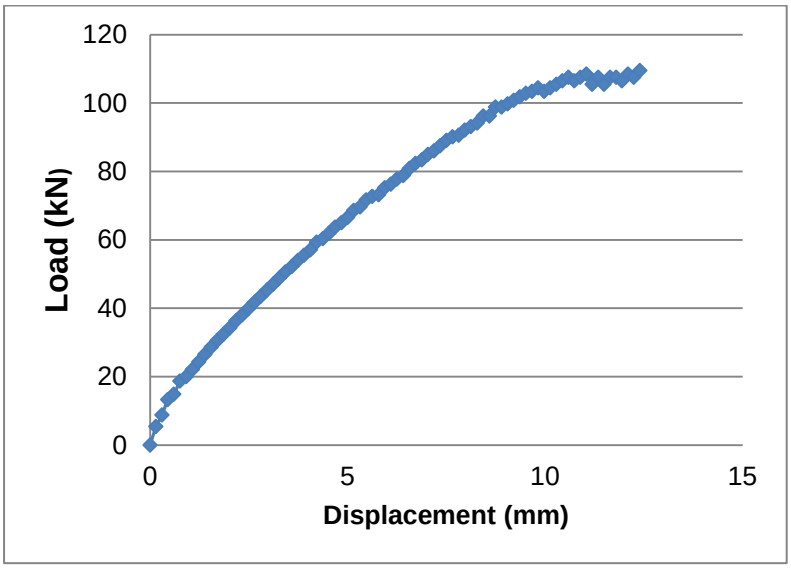

Fig 6.26: Load displacement curve for slab 2.

Fig 6.26 shows the load evolutions and the vertical displacement at the support. The summation of the self weight and peak supports reaction equal to the punching shear failure load.

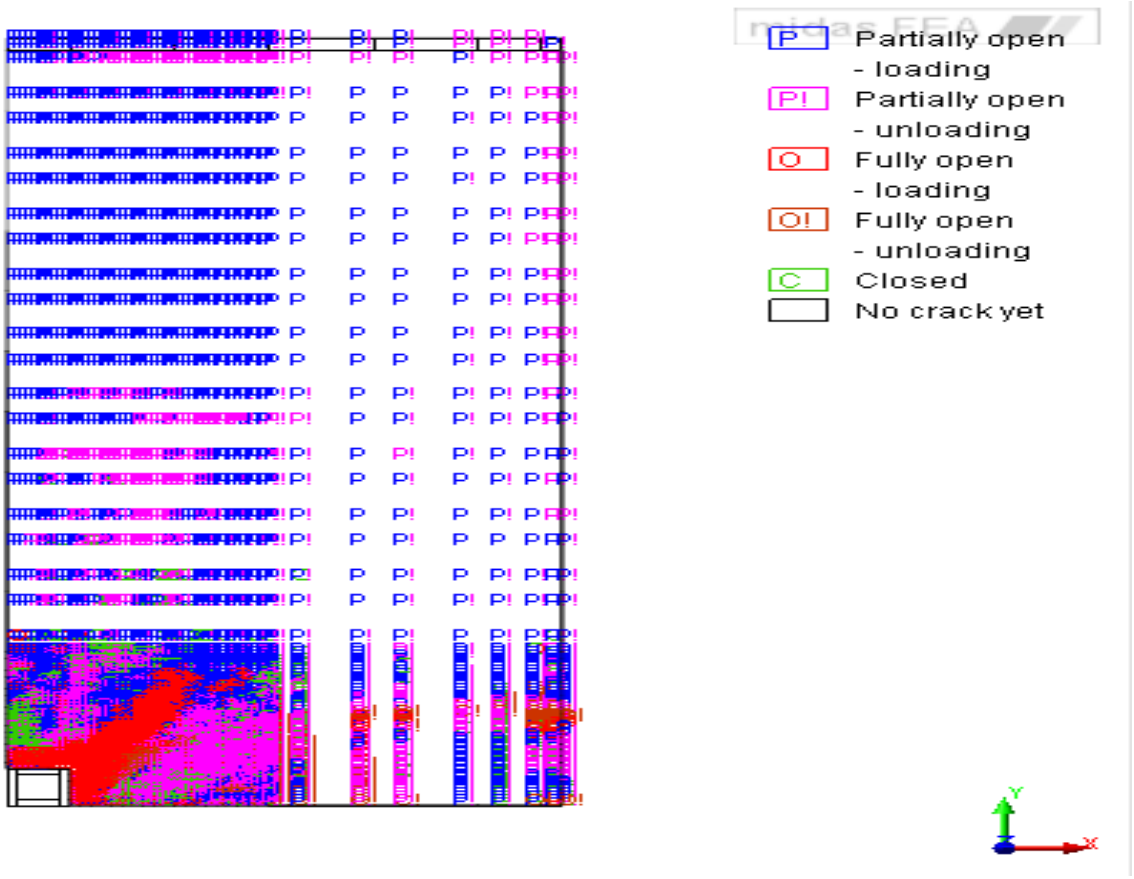

Fig 6.27: cracks on concrete at the tension bottom of the slab.

As shown in fig 6.27, the red zone indicates the region where cracks have fully opened. This is consistent with the experimental observation. The dark blue region indicates where cracks are partially opened during loading. The pink region shows where cracks are partially opened during unloading. The red region shows where cracks are opened during loading and unloading.

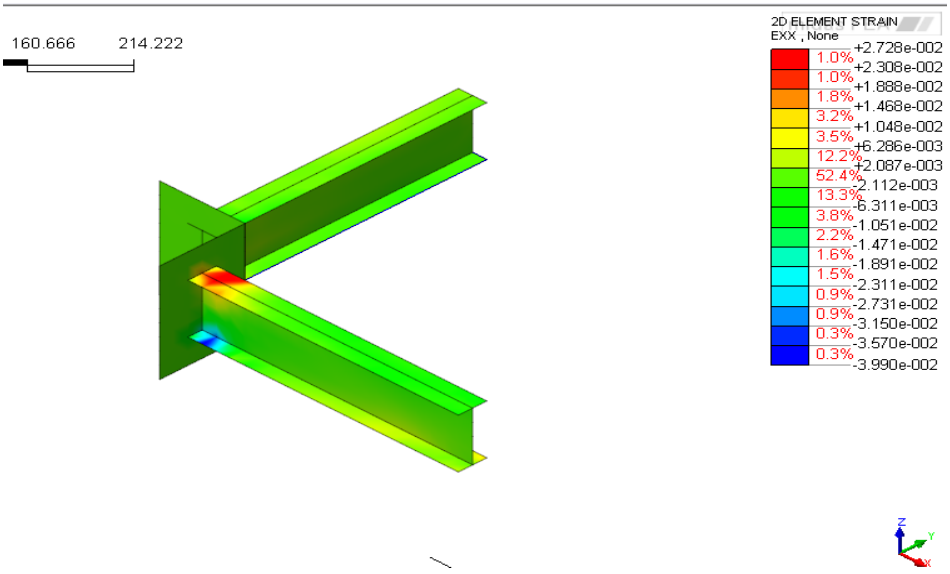

Fig 6.28: Strain ε_{xx} on the shearheads.

6.3. 5 Conclusion

The outcome of these numerical models show that the modelling scheme adopted is an appropriate approach for modelling punching shear failure of connection with and without shearheads. Slab 2 shows a stiffer response and higher failure load than slab due to the contribution of the shearheads. Comparisons for all measured parameters (experimental) and their corresponding numerical values are carried out in chapter 8.Detail parametric study on the shearheads is also presented.

Chapter 7: Experimental studies

7.0 Introduction

This chapter presents test procedures and results of experimental investigations of punching shear behaviour of flat slab to steel column connection with and without shearhead. This investigation focuses on punching shear failure of the slab-column connection subject to vertical static load only. The slab-column is design as a secondary load resisting mechanism, based on the assumption that location of the structure is subjected to high seismic activity in line with ACI design guideline. The lateral load is resisted by the shear wall which is the primary load resisting mechanism. The gravity load is investigated because it dominates the unbalanced moment transfer at the slab-column connection in the direction perpendicular to the free edge of the slab within the critical section. This experiment does not impose any lateral restraints on the slab in order to minimise compressive membrane action. These experiments are performed in line with the outline objectives.

The test is conducted in two phases, firstly slab-column connection without shear reinforcement and secondly slab-column connection reinforced with shearheads.

The material components and other specimens required in the experimental programme were prepared and tested at the Structures Laboratory, department of Civil Engineering, Building and Architecture, Coventry University.

7.2 Objectives of the experimental Programme.

The core objectives of experimental investigations are:

- To study the deformation behaviour of the slab-column connection subject to punching shear.
- To investigate punching shear capacity of the steel edge supported slab without shear reinforcement for comparison with design codes equation. This comparison would be used to support decisions on the slab2 tested with the proposed shearhead assembly.

- To measure critical influential parameters governing punching shear failure at the connection such as: strains on concrete and reinforcement and shearheads at locations where stresses could be significant
- To obtain the punching shear capacity of the proposed novel shearhead assembly.
- To use these measurements to calibrate and validate numerical models.

7.3.0 Experiment on Slab 1 (slab without shear reinforcement)

7.3.1 Experimental set up

The control specimen that was cast on the laboratory floor (subject to 28 days of air curing) was lifted by means of crane to a test rig with a self resistant system built in the structural laboratory as shown in fig 7.1. The hydraulic jack was attached tightly to the top cross beam that connects the column, followed by the installation of the plate and load cell. Four roller supports were inserted on the top of bottom beams supporting the specimen. The rollers were placed exactly 150mm away from the slab corners. After completion of the test set-up, instrumentation of the specimen was carried out at locations where significant deformations were expected.

Fig 7.1: Photo of Test set up for slab 1. .

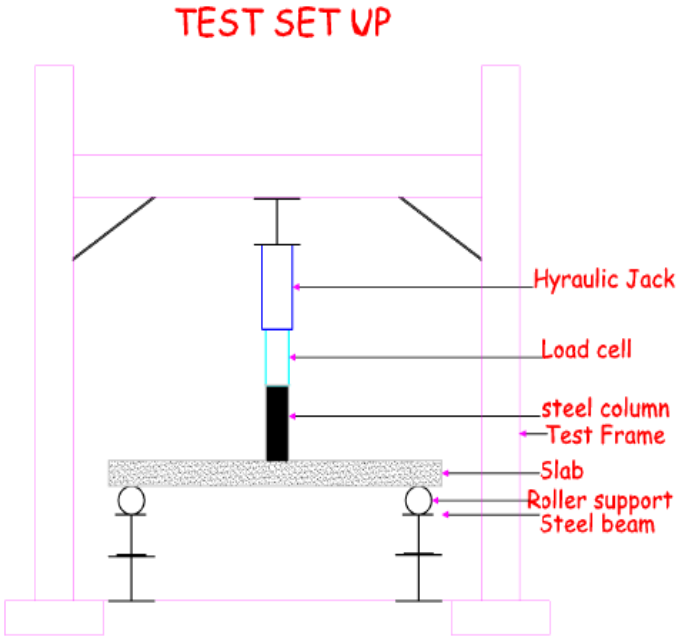

Fig 7.2: Diagrammatic elevation view of test set up.

7.3.2 Restrains adopted

To ensure that slab edges are not restrained, four roller supports were inserted at 150mm away from the slab edges. Horizontal movement was allowed, in order to prevent possible membrane action (in-plane forces) prior to the formation of full yield line mechanism. The unconstrained shear strength is the most critical to punching shear failure.

The edge parallel to the free edge was clamp at points near the roller supports to maintain equilibrium with the applied vertical load and to prevent excessive rotation at the mid-span edge as described in elastic analysis in chapter 6. The rationale for the boundary conditions has been provided in chapter 6.

7.3.3 Material properties

7.3.3.1 Compressive strength test

Concrete strength of C30/37 was targeted. Trial mixes were made of Portland cement, sand and coarse aggregate (granite) of maximum size of 20mm. 3 cubes of dimension 100mm were cast from the same batch used for casting of specimen. The wet concrete has a slump value of 41mm showing good workability. The cubes were air cured for 28 days. The detail of the mix design and cube test result is presented in

appendix II. Compressive strength test was carried out on the cubes on the day of testing; using the Avery-Denison 2000kN machine as shown in fig 5.6

Fig 7.3 Cube under compression in Avery- Denison machine.

7.3.3.2 Splitting Tensile Test

Three cylindrical specimens of dimension 100mm × 200mm were made from the same batch used for casting the slab specimen. They were also air cured for 28 days, followed by a splitting tensile test. The Brazilian tensile test apparatus was used; the specimens were inserted in mould and a metallic rectangular strip of breadth 26mm was inserted for the load distribution and was tested in the Avery-Denison 2000kN machine on the day of punching shear test. At failure the specimens fail in compression along the centre line. The test arrangement is shown in fig7.4.

Fig 7.4: Splitting tensile test

The failure load (P) obtained from test was substituted in equation 3.20 to obtained the tensile stress. The tensile strength was further reduced due to the strip effect by equation 3.21

The detail results and calculation of the splitting tensile test is presented in appendix III,

7.3.4 Control Specimen connection and reinforcement detail

The specimen is made of 1250mm × 1060mm ×130mm thick slab supported at the edge by a 100mm × 100mm ×4.5mm square hollow section (SHS) representing the steel column. Tensile reinforcements consisted of 11T8 bars at 102mm centres in the orthogonal direction and 11T8 bars at 110mm centres in the longitudinal direction. Compression reinforcements consisted of 6T8 bars at 204mm centres in the orthogonal direction and 6T8 bars at 220mm centres in the longitudinal direction. The minimum 20mm cover for the reinforcement was used in compliance to minimum design requirements (EC2).in order to connect the steel column to concrete, 12 shear studs of 10mm diameter, 80mm long and 22.5mm spacing were welded to the interior of the hollow steel column and inserted vertically. It was propped to ensure verticality during and after casting.

The sectional view and reinforcement detail is provided in figure 7.5 and 7.6 respectively.

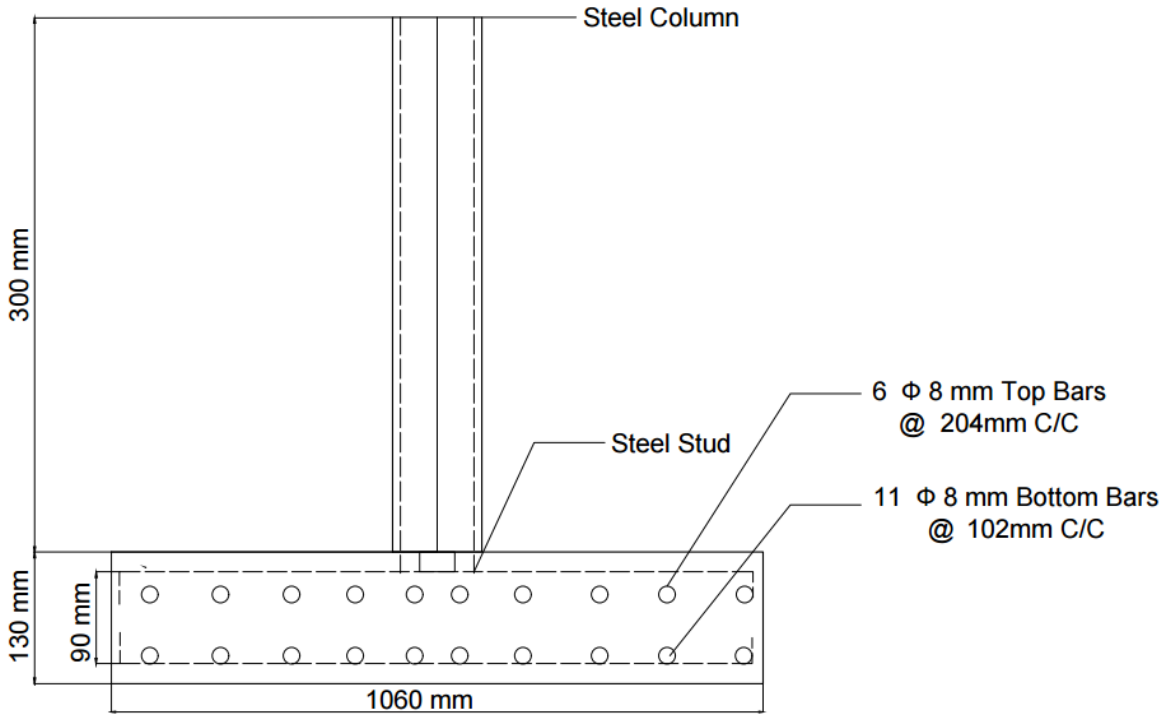

Fig 7.5 section detail of control specimen

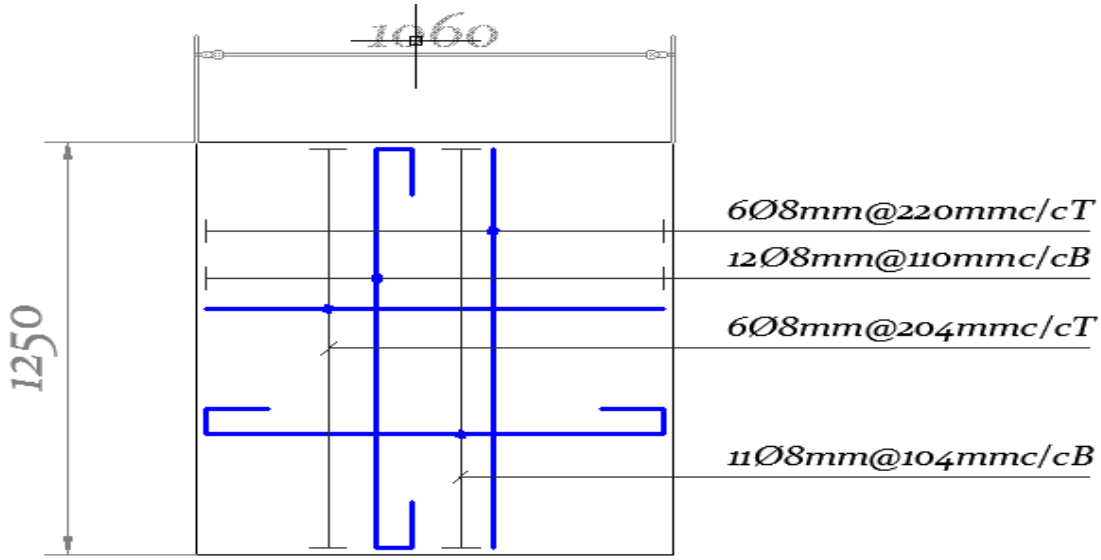

Fig 7.6: Reinforcement detail

7.3.5 Instrumentation of specimen

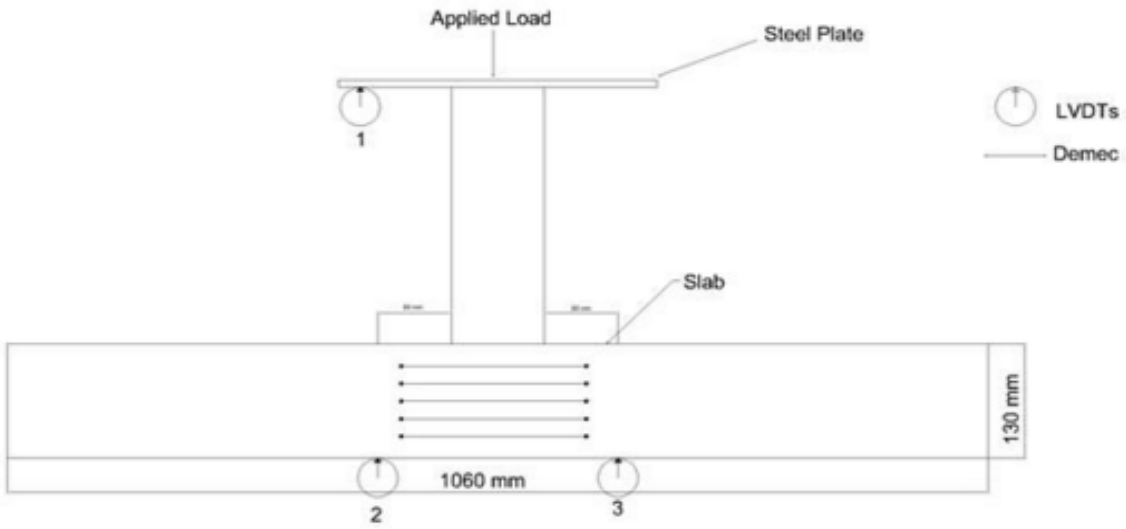

Fig 7.7: LVDTs and DEMEC positions on specimen.

7.3.6 Calibration of LVDTs, Load cell and Strain gauges

7.3.6.1 Strain gauges

The electrical resistance strain gauges (ERS) is simply a length of wire formed into the shape of a continuous grid sealed to a non-conductive backing. The ERS gauges were bonded to the surface of the bars using araldite adhesive. The strain gauges have the properties listed in table 7.1.

Table 7.1 Strain gauge properties

Strain gauge type	Electrical resistance
Gauge Length (L)	60mm
Gauge Resistance	120 $\pm$0.3mm
Gauge Factor (G.F)	2.13

The ERGs is very sensitive to any change in length or cross-sectional area of the reinforcement, any slight change in these bars gives a corresponding change of resistance. The ERS gauges were connected to a Data logger system. This received electrical data from these instruments, which is automatically recorded. A gauge factor of 2.13 was provided by the manufacturers. The gauge factor value was adjusted to 2.13 and the shunt resistor set to 59kΩ on the data logger; the logging system was used for the calibration of strain gauges and reported in micro strains. The strain gauges from the specimen were installed to strain gauge cards (quarter bridges) and subsequently connected to the data logger as shown in figure 5.12.

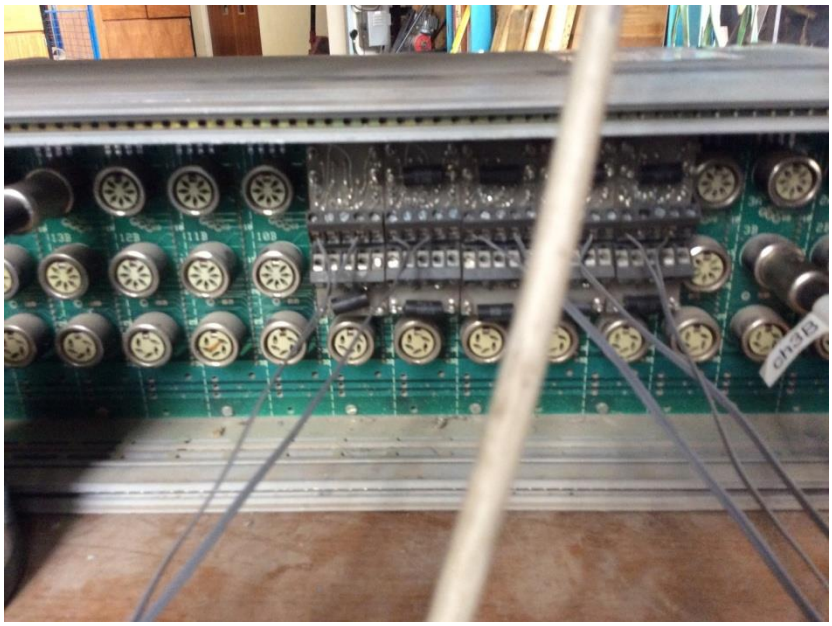

Fig 7.8: ERGs strain gauges connection to data logger.

The strain gauges were labelled as thus

SG1: strain gauge on embedded bottom rebar in the longitudinal direction

SG2: strain gauge on embedded bottom rebar in the orthogonal direction

SG3: strain gauge on the embedded top rebar in the longitudinal direction

SG4: strain gauge on embedded top rebar in the orthogonal direction

SG5: strain gauge on the compression face of concrete.

The ERGs were calibrated with the formula given in equation 7.1.

The strain reading changes according to the following formula.

$$\varepsilon = \frac{R_g}{G.F \times (R_g + R_S)} \quad \text{..... ....} \quad (7.1)$$

Where R_g = gauge resistance, R_S = resistance of the shunt (59kΩ)

By substituting the strain gauge properties into equation 7.1 the strain reading of 953 micro strains was obtained.

This value was used to calibrate all the channels. A strain gauge was installed on a flat steel bar at its centre and connected to each channel followed by the application of a

compressive or tensile load until a reading of or very close to ±953 micro strains for tension and compression were obtained.

7.3.6.2 Linear Variable Displacement Transducers (LVDTs)

To obtain utmost accuracy, the LVDTs used in the test were calibrated with slip gauges from a block-set. The calibration procedure provided in the data-logger instruction manual was adopted. Three measurements were taken. The first was a LVDT reading on a 10mm invar slip gauge. A reading of 0.01 which is very close to zero was recorded on the data-logger. The second measurement was taken on a 50mm invar slip gauge and a final reading was taken on a 30mm Invar slip gauge. The Data-logger automatically calibrated the LVDTs to a plus or minus in mm. The load cell used was already calibrated but it was still checked for accuracy.

7.3.7 Self Weight Measurement

In order to account for the self weight imposed on the connection, the mass of the column, hydraulic jack, Load cell and the reaction plate were recorded. The total combined self weight gives1.21kN and added to the self weight of the slab. This initial load was used as starting point for all the load measurements).

7.3.8 Test Procedures and Observation

A load cell of 500kN capacity was attached centrally on top of the hydraulic jack to simulate vertical static load on the slab-column connection. The load was applied through the column in an upside down position. Prior to load application, the number of repeats was multiply by the time lapse between consecutive readings. The load was applied incrementally at the rate of 10kN per minute. At intervals, strains across the slab depth were read using DEMEC strain gauge. The first vertical flexural crack occurred at a load of 80kN. The cracks become wider with increasing load until the slab-column connection fails in punching. A diagonal shear failure was observed on both sides of the column. When the load reaches 93.2kN, there was a rapid propagation of radial, tangential cracks until the slab failed in punching at a load of 106.33kN (fig 7.9a). Cracks periphery formed at a distance of 320mm away from the free edge of the slab as depicted in fig 7.9b.

Fig 7.9 a: Punching shear of the connection Fig 7.9b: crack periphery (bottom)

7.3.9 Test results and Discussion

7.3.9.1 Displacements

Figure 7.10 and 7.11 shows the load displacement evolution measured from the experiment .Load- displacement response for LVDT 1 is presented in Fig 7.10 .The Load-displacement response between loads zero and 10kN shows a slightly linear behaviour. At load levels less than 80kN, there was no visible crack. However, micro cracks might have developed.

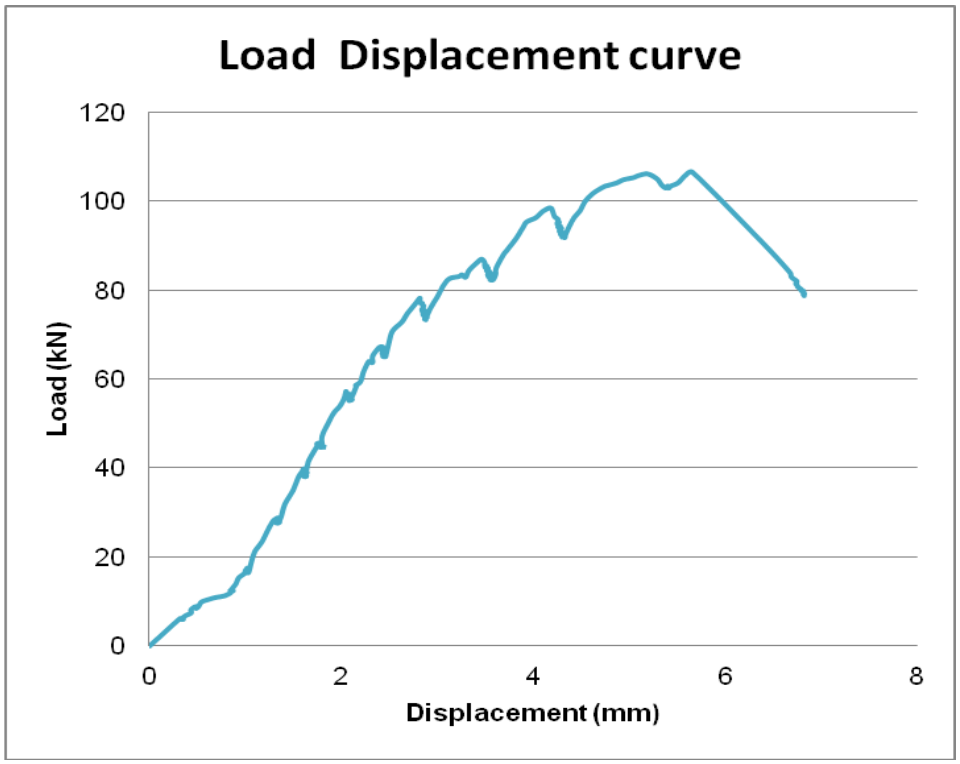

Fig 7.10: Load -displacement curve for LVDT1

After the appearance of the first incipient flexural crack at a load of 85.0kN, there was a slight increase in displacement up to a load of 93.6kN this indicates a region of rapid initiation and propagation of micro cracks spreading outward from the region of load application. Within a load of 93.6kN, large cracks were observed which indicates that rapid spreading micro cracks begin to localise into major cracks. At a load of 102kN large crack opening were observed, at this stage, very complex mechanisms such as aggregate bridging, crack face friction, micro cracking and crack branching have occurred. At the peak load of 106.3.kN which is the load at which the tensile stress exceeded the tensile strength of the concrete, a sharp drop in the load to 79.65kN which indicates brittle punching.

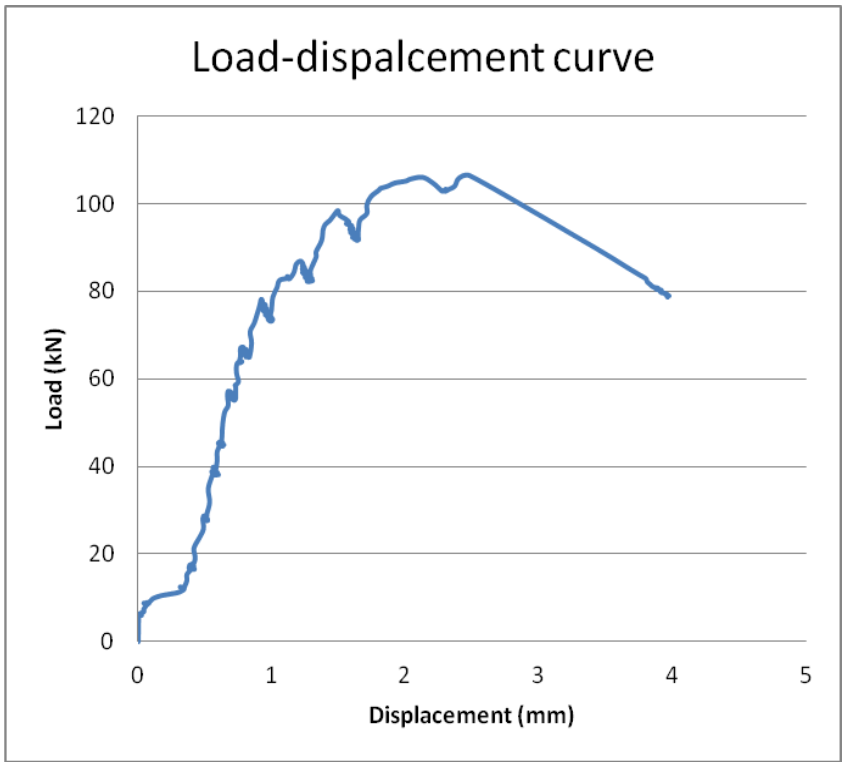

Fig 7.11: Load -displacement curve for LVDT2

Fig 7.11 provides a stiffer response compared to LDVT 1 although similar load-displacement evolution occurred. The stiffer response indicates that deformation was more significant at the slab-column connection at the compression face of the concrete than the tension bottom.

7.3.9.2 Strain measured on the reinforcement

2. 1 Strain measured on flexural reinforcement (Tension)

Electrical resistance strain gauges were attached to the flexural reinforcement located in the critical section. SG1 was attached to the longitudinal tension reinforcement at the bottom of the slab. And SG2 was attached to the orthogonal reinforcement on the tension bottom of the slab. Their response with respect to load increments is depicted in fig 5.15 .The strains on SG1 were significantly higher than those of SG2, this indicates that the longitudinal reinforcement dominate bending (the shorter span). Strains on SG1 very small and gave a haphazard response, therefore, was disregarded. Large increase in strain was observed between loads of 65.74kNand 82.3kN. This indicates points where severe flexural cracks have caused loss of bond. At this point there was a sharp switch from tensile to compressive strains without any increase in load level as depicted in fig 7.12

Maximum values recorded were $SG1_{max}$ = 989$\mu\varepsilon$ and $SG2_{max}$ =468 $\mu\varepsilon$. The modulus of elasticity for steel is E_{steel} = 210kN/mm^2 and yield strength of 450kN/mm^2 $were$ assumed. From the graph, it could be observed that the reinforcement yields before punching failure occurs. Reinforcement yields approximately 82.33kN after the first visible crack occurred. The strain remains constant at -17842 $\mu\varepsilon$ until the connection fails in punching.

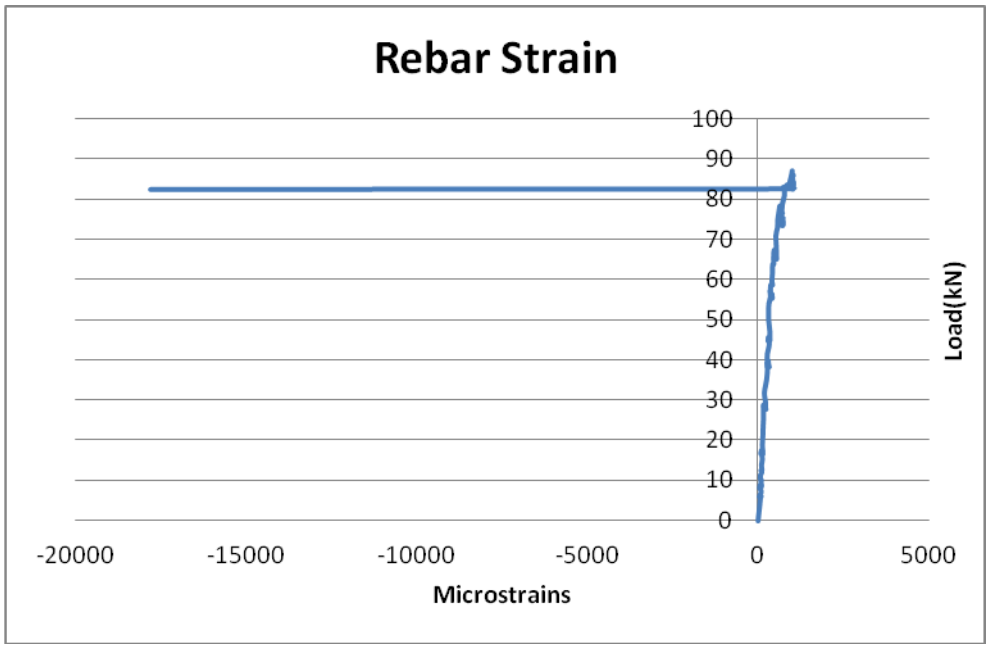

Fig 7.12: Tensile strain on embedded reinforcement.

2.2 Strain Measured at the compression reinforcement

Electrical resistance strain gauges (ERSGs) were also attached to the flexural reinforcement located in the compression zone of the critical section. SG3 was attached to the longitudinal reinforcement located in the compression zone of the critical section and SG4 to the orthogonal reinforcement. Strains' reading on SG4 were very haphazard and was disregarded. The reading is plotted in fig 5.16.

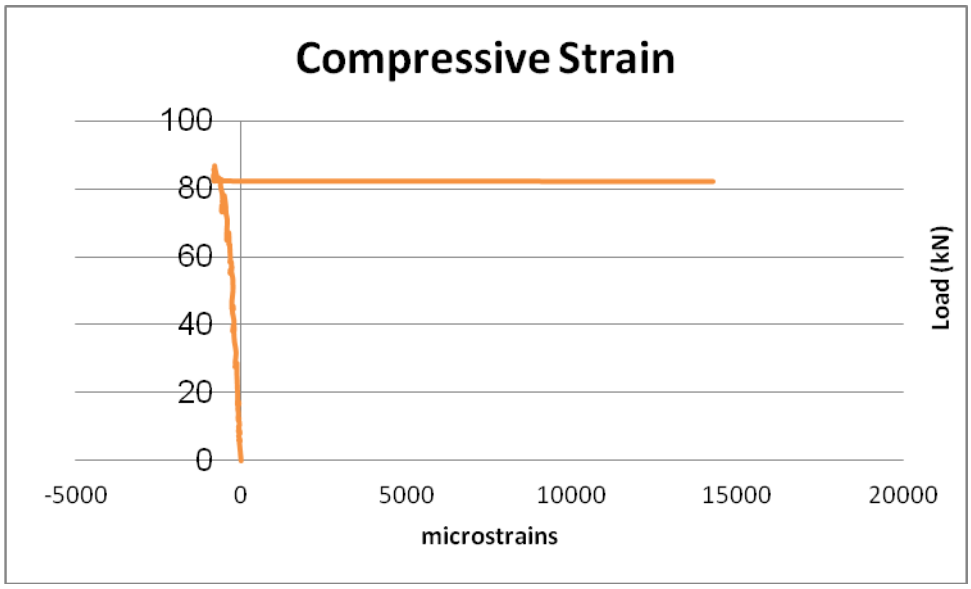

Fig 7.13: Compressive strain on embedded reinforcement.

7.3.9.3 Strain across the depth of slab (DEMEC)

by membrane action which contributes significantly to higher punching shear DEMEC strain gauge was used to measure strains across the depth of the concrete slab. The variation of strains with increase in strain in load measured across these points is plotted in fig7.14. Tensile strain recorded by the D4 shows that concrete yielded locally before punching failure occurs. The D2 also recorded higher values of strains after the tensile zone has sustained severe flexural cracks. Demec (D3) which was located close to the neutral axis (axis of zero strain) reads more of tensile strain from the beginning and switch to compressive strain as shown in fig 7.15. This could be attributed to the fact that under the gradually increasing load, the formation and propagation of flexural cracks in the slab sections in addition to the yielding of the longitudinal reinforcing bars reduce the depth of the compression zone. As a result, the section axis of zero strain shifted to the tensile zone which Lead to the formation of compressive strain at that point. Because the slab is simply supported, horizontal elongation occurred. In real slab this tendency to elongate is constrained strength.

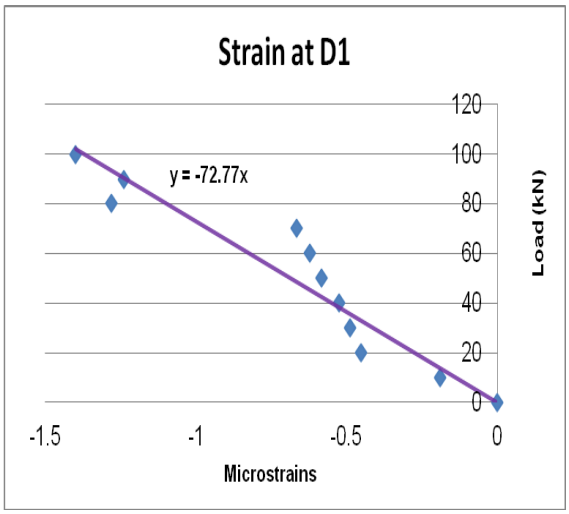

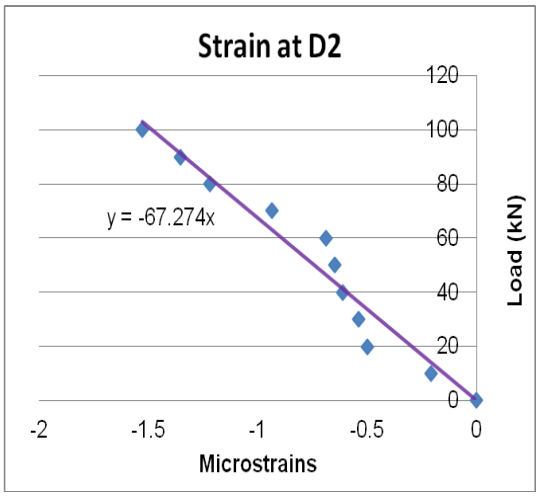

Fig 7.14 a and b: compressive strain across concrete of concrete.

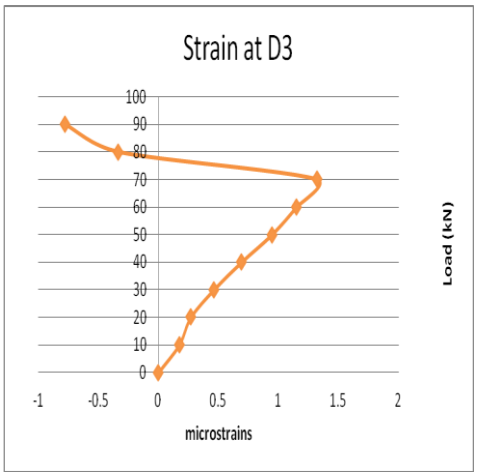

Fig 7.15 (a) strain at D3

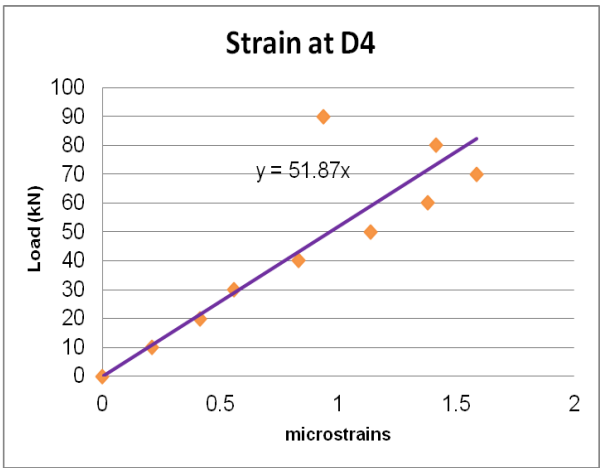

Fig 7.15 (b) strain at D4

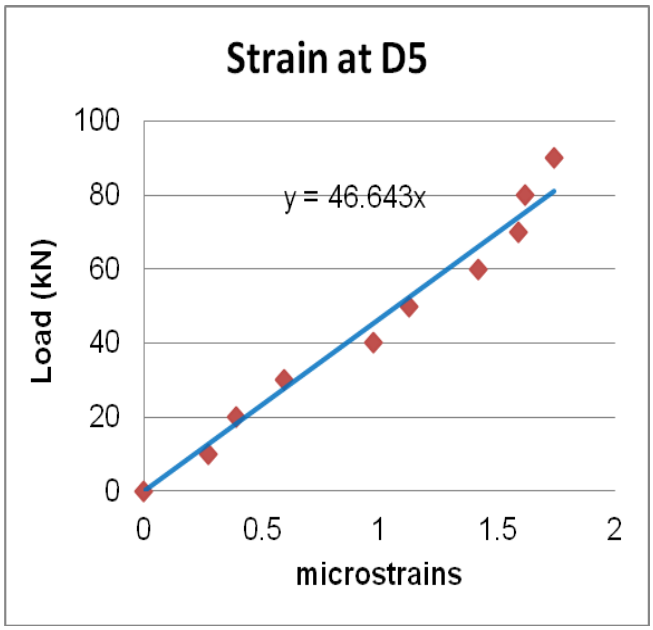

Fig 7.16 strain at D5

7.4.0 Design and experimentation of specimen with shearheads (Slab 2)

This section provides detail procedures of the design of the shearhead assembly and reports experiment conducted on it.

The slab-column connection was connected with a shearhead. The steel column assembly consist of a steel column fabricated from a square hollow section (SHS) of size 100 × 5mm. and the shear arms were made of steel I-sections.

The shearheads were fillet welded to an end square plate of 10mm × 10mm and 5mm thick. The end plate was then welded to the steel column. The detail of the shearheads assembly is depicted in fig 5. The sections were filled welded to the column. The most influential factor that governs the dimensions of shearhead is the bending stiffness of each shearhead arm and that of the surrounding composite. Based on this recommendation, computation of the flexural stiffness ratio between shearheads and cracked concrete was undertaken

7.4.1 Design Procedures for the Shearhead Assembly.

In order to enhance punching shear capacity of the edge connection that is more vulnerable to punching shear failure; the design guidance was carried out in strict compliance to design recommendations of ACI318-02 and standards of New Zealand for concrete structure.

The structural design is premised on the following principles.

- ❖ The moment capacity of the shearhead must be greater than the moment applied to the shearhead.
- ❖ The shearhead must extend to the critical shear perimeter to avoid any need for conventional shear reinforcement.
- ❖ To calculate the flexural stiffness ratio between the shearhead and the neighbouring concrete, it should be assumed that the concrete is partially cracked.
- ❖ Each shearhead shall consist of steel shapes fabricated by welding with full penetration welds.

Other commentaries relating to the design principles are provided in the sequential design procedure as thus;

7.4.1.1 Section adopted

In the shearheard assembly, the I-section is used based on the recommendation that only PFC, I and H sections should be used for structural shearheads which is hinged on the observation that good composite action is easily achieved with the concrete. The concrete will fill around the sections and hold the members in place.

7.4.1.2 Shearhead Section Properties and input data

D = 76mm

B = 60mm

t = 3mm

$I_{x-x} = 5325684mm^4$

$Z_{x-x} = 14014.95mm^3$

$$S_{xx} = 16248mm^3$$

$C_1 = \mathbf{100mm}$

$C_2 = \mathbf{100mm}$

h = 130mm

Concrete cover = 20mm

$f_{cu} = \mathbf{32.72\ N/mm^2}$

$$f_y = \mathbf{275\ N/mm^2}$$

Detail is shown in figure 7.25

7.4.1.3 Maximum Shear Force at slab-column connection.

$V_u = \mathbf{1.15\ \times 102.38 = 117.73kN}$

ACI 318-02 recommends that the maximum shear Force to be factorised. Therefore, a factor of 1.15 was used. The maximum shear force of 102.38kN was computed using theoretical shear strength equation of ACI318-05.

7.4.1.4 Computation of Basic Shearhead Perimeter

Concrete shear strength should be computed and substitute into equation 7.3 as thus.

(a) Concrete Shear Strength

$V_c = \boldsymbol{v_c\phi}$ ..... **(7.2)**

$\boldsymbol{\phi}$ = shear reduction factor $\boldsymbol{\phi = 0.85}$

$\boldsymbol{f'_c = 0.8f_{cu}}$ = 0.8× 40.17 =32.14N/mm^2.

$v_c = 0.33\sqrt{32.14}\ = 1.87\ N/mm^2$

$\boldsymbol{\phi v_c} = \mathbf{0.85} \times 1.87 = 1.59\ N/mm^2$

$\boldsymbol{\phi v_c} = 1.59\ N/mm^2$

(b)Shear Perimeter Required

$\boldsymbol{b_0} = \frac{\boldsymbol{V_u}}{\boldsymbol{\phi V_n d}}$ ..... **(7.3)**

$\boldsymbol{b_0} = \frac{\mathbf{131.1}\times 10^3}{\mathbf{1.59\times 106}} = 777.85mm$

This shear resulting from moment transfer by eccentric shear shall be assumed to vary linearly about the perimeter for connection without shear reinforcement.

7.4.1.5 Computation of Shearhead minimum length

Assuming the shearhead is centrally placed.

Computation of the perimeter is based on the configuration of fig 2.11

$d = 130 - {}^{8}/_{2} - 20 = 106$

$$b_0 = 2\left[\left(\frac{3}{4}\left(l_v - \frac{C_2}{2}\right) - \frac{d}{2}\right)^2 + \left(\frac{100}{2}\right)^2\right]^2 + 2d + 2\left[\frac{\frac{3}{4}\left(l_v - \frac{C_1}{2}\right) - \frac{d}{2}}{Cos45}\right]$$

$$777.5 = 2\left[\left(\frac{3}{4}\left(l_v - \frac{100}{2}\right) - \frac{106}{2}\right)^2 + \left(\frac{100}{2}\right)^2\right]^2 + 2 \times 106 + 2\left[\frac{\frac{3}{4}\left(l_v - \frac{100}{2}\right) - \frac{106}{2}}{Cos45}\right]$$

By solving this quadratic equation,

$$l_v = 123.73mm$$

Having computed the minimum length of $l_v = 185mm$ was adopted

7.4.1.6 shearhead moment required

$$\phi M_p = \left(\frac{V_u}{2\eta}\right)\left[h_v + \alpha_v\left(\ell_v - \frac{c}{2}\right)\right] \quad \text{..... (7.4)}$$

$$\alpha_v = \frac{E_s \times I_s}{I_{CR} \times E_C} \quad \text{..... (7.5)}$$

$$\alpha_v \leq \mathbf{0.15}$$

$$\phi = 0.9 \qquad 2\eta = 6$$

Second moment of area of the shearhead I-section is calculated as thus,

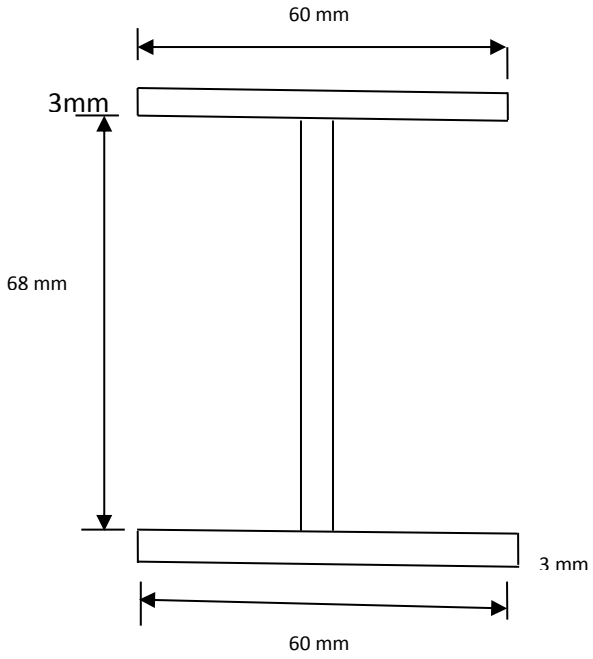

1. Position of plastic neutral axis $Z_{plastic}$

$A = [2(60 \times 3) + 68 \times 3] = 564\ mm^2$

For equal area $\frac{A}{2} = 282\ mm^2$

For equal area axis

$(Z_{plastic} - 3)3 + (60 \times 3) = 282$

$Z_{plastic} = 37mm$

It is concentric with the elastic neutral axis at the mid-height for a symmetrical section.

Plastic section modulus ($W_{pl,xx}$)

$W_{pl,xx} = 2[(60 \times 3 \times 3.5) + 34 \times 3 \times 17] = 16248\ mm^3$

Elastic Section Modulus

$$I_{xx} = 2\left(\frac{60 \times 3^3}{12} + 60 \times 3 \times 35.5^2\right) + \frac{3 \times 68^3}{12} = 532568mm^4$$

$$W_{el,xx} = \left(\frac{I_{yy}}{Distance\ to\ extreme\ fibre}\right)$$

$$W_{el,xx} = \left(\frac{532568}{76/_2}\right) = 14014.95mm^3$$

$$Shape\ Factor\ (\mathrm{V}) = \left(\frac{W_{pl,yy}}{W_{el,yy}}\right) = \frac{16248}{14014.95} = 1.16$$

The concrete is assumed to be half cracked

When concrete is assumed to be half-cracked, the value of I_{CR} is exactly half between the maximum and minimum cracking values. The empirical derivation according to New Zealand code is given as thus.

Fully cracked > half cracked >Uncracked

$\frac{(C_2+d)T_s^3}{24} \geq \frac{(C_2+d)T_s^3}{18} \geq \frac{(C_2+d)T_s^3}{12}$ (Newzealand code)

$I_{CR} = \frac{(C_2+d)T_s^3}{18}$ ..... (7.6)

$I_{CR} = \frac{(100+106)130^3}{18} = 2.51 \times 10^7 mm^4$

I_s Of steel

$\alpha_v = \frac{210000 \times 532568}{2.51 \times 10^7 \times 29500} = 0.151$

$\alpha_v = 0.151 \leq \mathbf{0.15}$

Hence, section is adequate.

$\phi M_p = \left(\frac{117.73}{6}\right)\left[130 + 0.151\left(185 - \frac{100}{2}\right)\right]$

$$\phi M_p = 2.95kNm$$

7.4.1.7 Shearhead Moment Capacity

$\phi M_p = \phi\, s_{xx} f_y$ ..... (7.7)

s_{xx} = plastic section modulus of the section.

$\phi = 0.9$ For tension controlled section

$\phi M_p = 0.9 \times 16248 \times 275 = 4.02kNm$

The moment capacity is greater than the moment due to applied load;

Therefore, the section used for the shearhead is satisfactory.

7.4.2 Construction of shearheard

By considering the stated design recommendations, the shearhead was constructed as thus, 5mm thick end plate was fillet-welded to the top and bottom flanges of the I-section as shown in fig 5. The end plate was designed to transfer forces uniformly from the flanges of the shearhead to the steel column. The shearhead was embedded in the slab between the top and bottom reinforcement grids as shown in fig 7.17 the bars that intersected with the shear arms and steel column were discontinued.

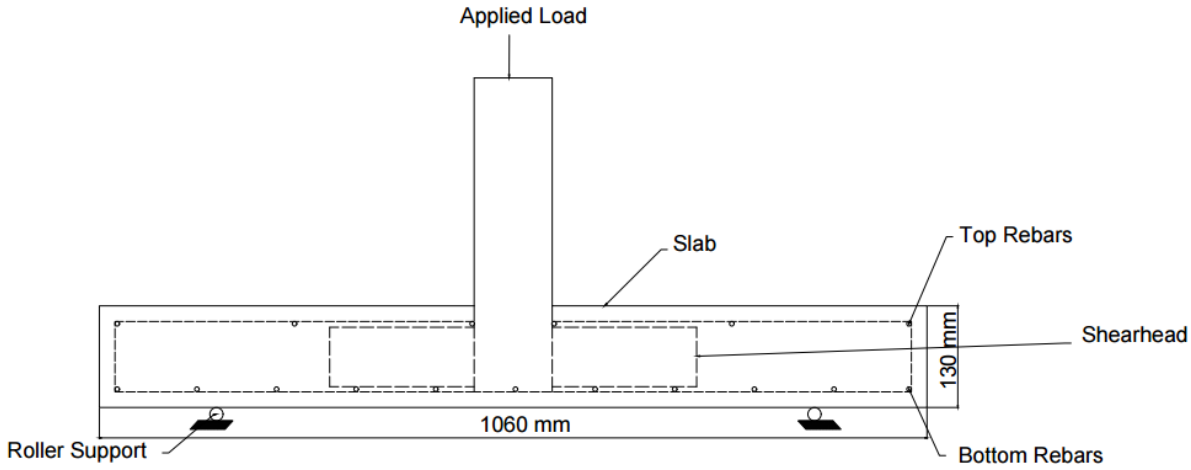

Fig 7.17: shearhead inserted between reinforcement grids

Fig 7.18: photo of shearhead inserted between reinforcement grids

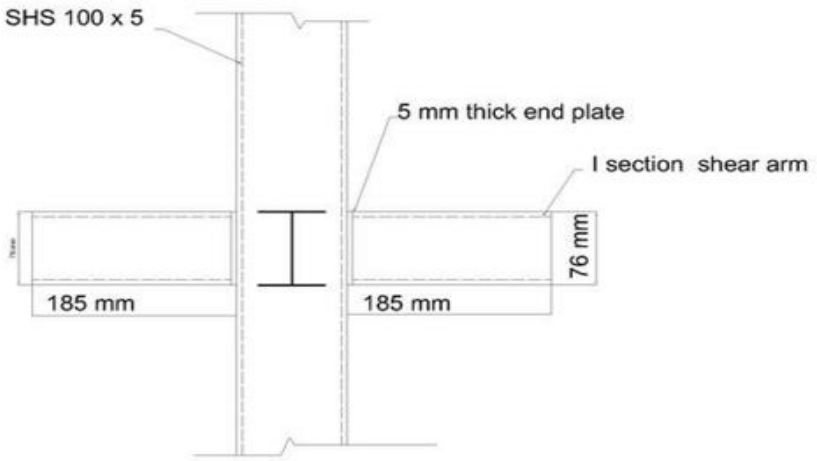

Fig 7.19: Sectional view of the shearhead assembly.

7.4.3 Materials and properties

Normal concrete was made from Portland cement, sand and granite with a maximum aggregate size of $d_{max} = 20mm$. The mix proportion is shown in fig7. Detail calculation of the mix design is presented in appendix 5. Three cubes of dimension $100mm \times 100mm \times 100mm$ were cast from the same batch used for the slab specimen with slump value of 48mm .The cubes were subjected to 28 days of air cure along side with the slab specimen; Compressive strength test was carried out on the day of the punching shear test as shown in fig 6.

The mean cylinder compressive strength value of $\boldsymbol{f'_c = 32.17}\, N/mm^2$ computed from 80 percent of the cube compressive strength.

In the absence of the coupon test to determine the elastic modulus and yield strength of steel reinforcement and shearhead; values were assumed according to BS EN 10002. The elastic modulus of steel was assumed as $210\, kN/mm^2$ and a yield strength of $500\, N/mm^2$ for reinforcement.

Table 7.2: Concrete mix proportion (kilogram per cubic metres).

Slab 2	Proportion
Cement	327
Fine sand (0/2)	673.62
Coarse aggregate (10/20)	1249.14
Water	170.04

7.4.3.1 Concrete Elastic Modulus Test

Elastic modulus test was performed according to BS1881: part 121:19831.

Three identical control cylindrical specimens were cast from same batch of the concrete mix for the tested slab. The specimens were aired cured for 28 days before testing; in order to maintain consistency the air cured slab. Prior to testing, DEMEC points were attached to the specimens by means of araldite adhesives for strains measurement using DEMEC. Six DEMEC points were attached at equal distance around the circumference of the cylindrical specimens. Two DEMEC points were placed at a vertical spacing of 200mm that will accommodate the strain gauge. Then the specimen was capped with steel plate and placed centrally in the compression-testing machine.

Before the compressive load was applied on the specimen, for each specimen the initial strain was measured using DEMEC strain gauge. One third of the value of cylinder compressive strength was used as the upper loading stress. The strains was read using DEMEC strain gauge .Upon completion of the static elastic modulus, the specimen was loaded to failure, to confirm if the failure load is eighty percent of the cube strength. From the results, the mean value of Elastic modulus was calculated for the control cylinder specimens.

The calibrated electronic DEMEC has a scale of 0.403×100000

DEMEC strain reading was taken as thus,

Reading at zero Loads was taken.

Strain = (reading at point 1 - reading at zero)* Scale value

The mean Elastic modulus calculated gives 29500

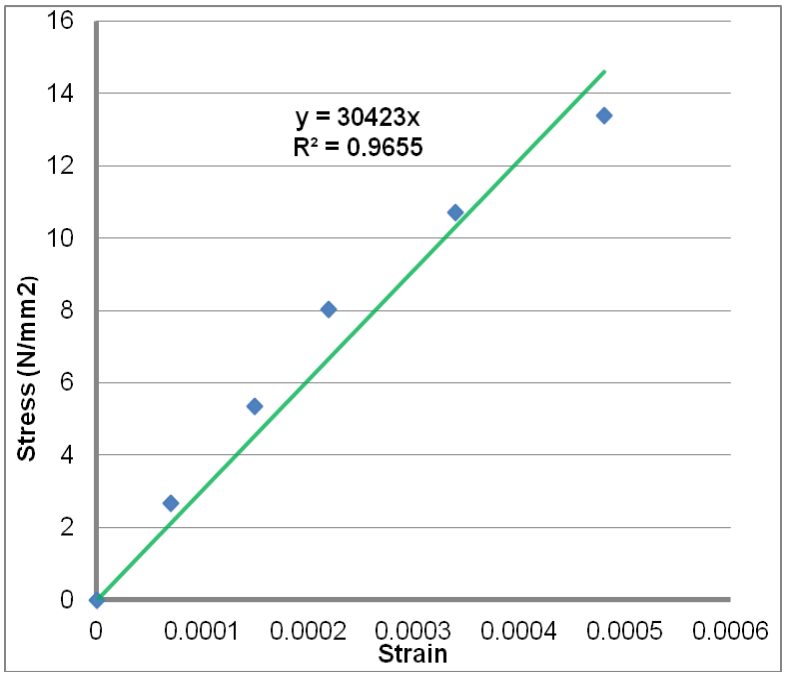

Fig 7.21: Elastic modulus for control specimen 1.

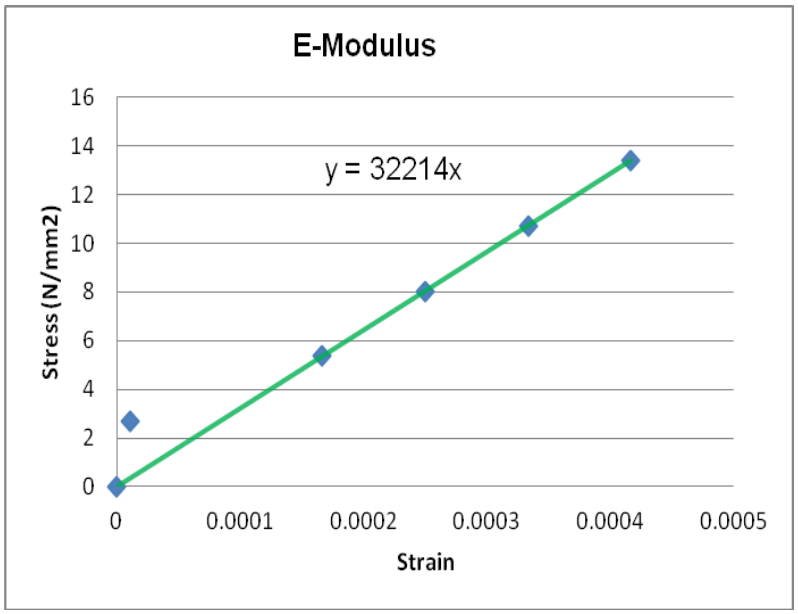

Fig 7.22: Elastic modulus for control specimen 2.

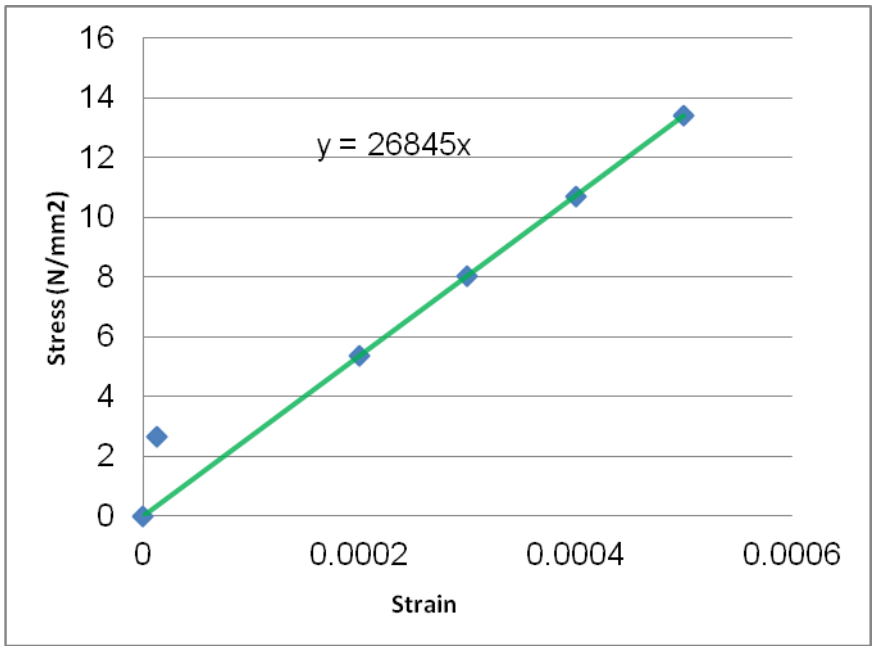

Fig 7.23: Elastic modulus for control specimen 3.

7.4.3.2 Concrete Tensile Strength

The same procedure described section 7.3.3.2 was adopted.

Table 7.3: Result of tensile test on control specimens

S/N	Failure load (P) in kN	Tensile stress (σ_t) in N/mm^2	Corrected value
1	73.78	2.35	2.12
2	83.43	2.66	2.39
3	74.06	2.36	2.12

Average Tensile strength = $2.21 N/mm^2$

The tensile stress is calculated using equation 3 as thus

$$\sigma_{t1} = \frac{2P}{\pi dl} = \frac{2\times 73.78 \times 1000}{3.142 \times 100 \times 200} = 2.35 N/mm^2$$

$$\sigma_{t2} = \frac{2\times 83.43 \times 1000}{3.142 \times 100 \times 200} = 2.66 N/mm^2$$

$\sigma_{t3} = \frac{2\times74.06\times1000}{3.142\times0.1\times0.2} = 2.36N/mm^2$

Because of the effect of strip, the tensile strength is reduce as thus

$\boldsymbol{\beta} = \frac{b}{D} = \frac{26}{100} = 0.26$

$\boldsymbol{\sigma}^{c}_{max}(P,\boldsymbol{\beta}) = \frac{2P}{\pi BD}[1-\boldsymbol{\beta}^2]^{3/2} = 0.9$

By substitution $\boldsymbol{\sigma}^{c}_{max}(P,\boldsymbol{\beta}) = 0.9$

This is used to reduce the original tensile stress in column 3.

7.4.4 Test Set up and Instrumentation

The test was set using the same boundary conditions used in Test1 based on its rationale provided in the elastic analysis.

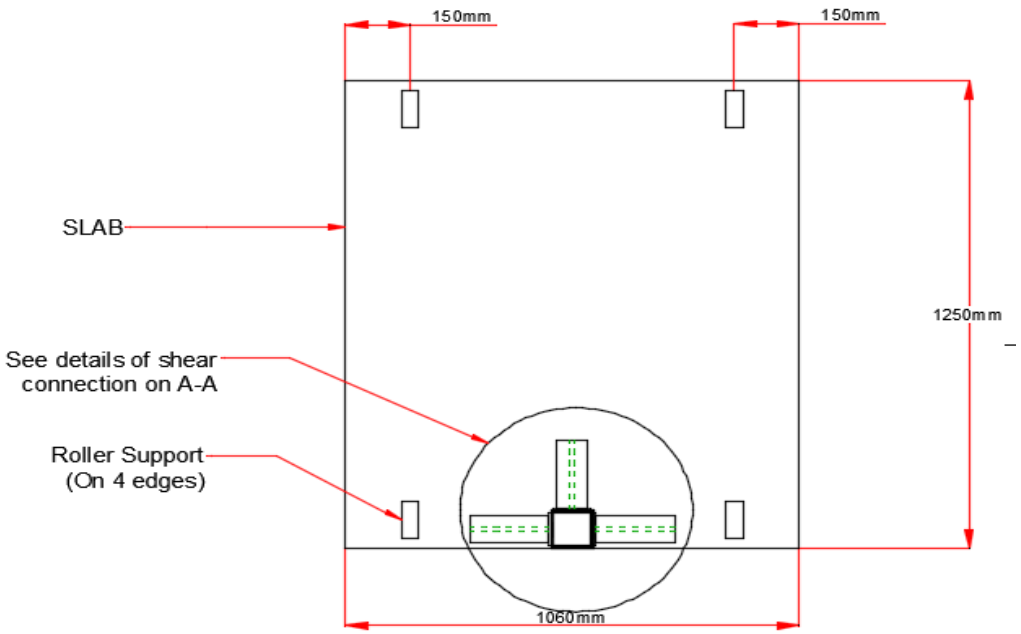

Fig 7.24: Plan view of test set up.

The slab specimen was cast in an oily plywood formwork and demoulded after 3 days. The slab was subjected to 28 days of air cure and lifted to the test frame.

Strains were measured in the longitudinal direction of the shear arm using electrical resistance strain gauges (ESG). Axial strains were measured in the top and bottom flange with gauges positioned at 20mm away from the intersection of the plate and shear arms. Shear strains were measured with strain gauge Rosettes positioned in the

web of the shear arm. Concrete surface strains were measured with a Demec strain gauge. Strain across the concrete depth was also measured using Demec strain gauge as shown in fig 7.25

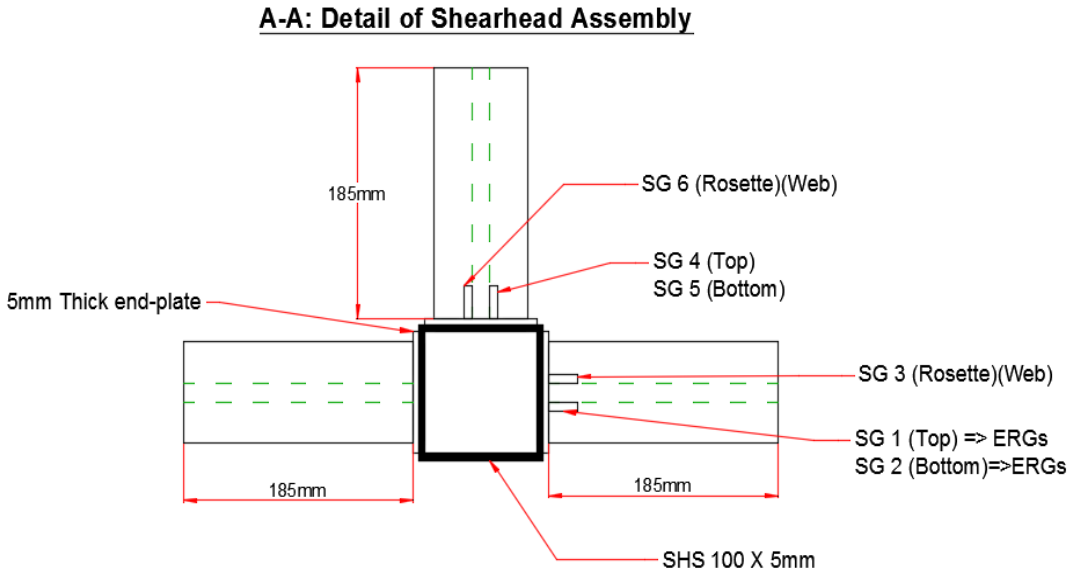

Fig 7.25: shearhead assembly instrumented with strain gauges

As shown in fig 7.26 the piston of the jack was aligned with the centre of the steel column. A circular plate of diameter 150mm and thickness of 20mm was positioned between the jack and the steel column to ensure uniform distribution of load to the slab-column connection. The slab specimen was tested in the upside down position as opposed to the normal position in reality.

Loads, displacements and strains were the measurable quantities from the experiment. The Load cell inserted under the hydraulic jack, LVDTs and ERGs strain gauges from the specimen were connected to an electronic data acquisition device which is synchronized with a computer for their measurements respectively. As shown in the first experiment. The applied load was measured with a load cell (capacity 500kN) positioned between the hydraulic jack and the steel plate. It was a load control experiment. Prior to load application, the number of repeats was multiply by the time lapse between consecutive readings. The load was applied incrementally at the rate of

10kN per minute. At the intervals strains across the slab depth were read using DEMEC strain gauge.

Three linear displacement transducers (LVDTs) were used to measure vertical displacements at critical locations as shown in figure 7.26.

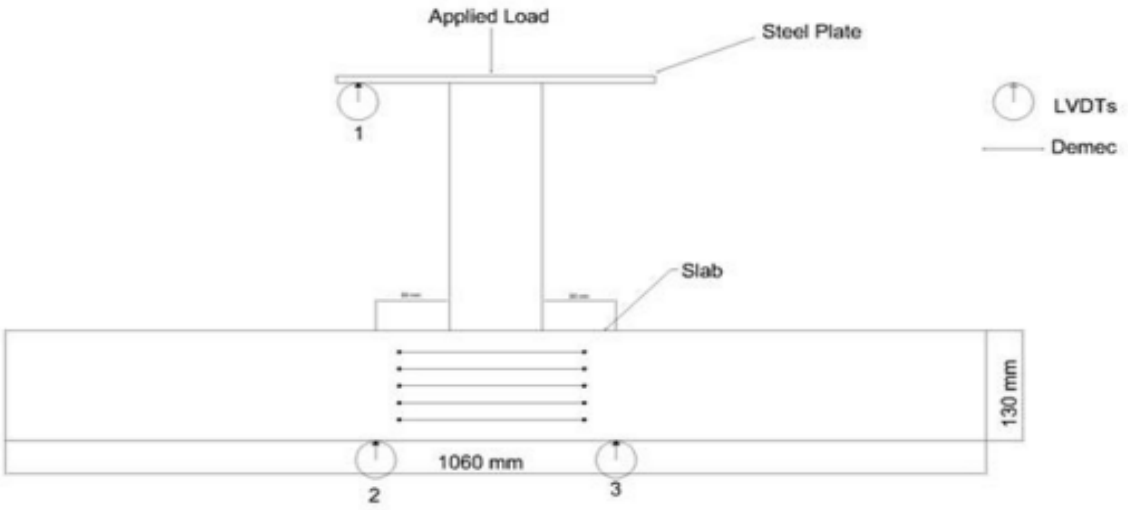

Fig 7.26: LVDTs Positions and DEMEC position on specimen

LVDT1 was placed directly underneath the plate that distributes the load uniformly from the hydraulic jack to the column which is indicted as position 1 in fig 7.26. And two others were placed at the bottom of the slab indicted as 2 and 3 respectively. They are positioned exactly 80mm from the column edge. These are positions where deformation could be significant.

7.4.5 Sources of Error in the experiments

Before presenting the results, some errors that may limit the accuracy of experimental results are examined. The most significant source of error resulting was observed during the unloading and reloading of the slab specimen. Unloading and reloading may influence the deformation behaviour and thus the punching shear resistance of the connection. Additional deformations emanating from the fluctuating loading pattern

may reduce the punching shear resistance of the connection. Koppitz, Kenel and Keller (2014) suggested unloading and reloading cycles influence the deformation behaviour by affecting the bond properties between the reinforcing steel and surrounding concrete. The initial deflection due to the specimen's self-weight was assumed as zero due of the relative difficulty in measuring during calibration of LVDTs. In reality, this initial deflection contributes specimen to the overall deflection of the specimen. Material defects such as residue stresses in steel and void present in concrete, initial micro cracking due to shrinkage may also limit the accuracy of the result. The result was also affected by the effective in situ tensile concrete, which is reduced by tensile stresses induced by restrained shrinkage.

7.4.6 Result

7.4.6 .1 Load – Displacement curves

The Load displacement evolution measured by means of the LVDTs is presented in fig 7.27

Load-displacement response becomes stiffer prior to the initiation of flexural cracks.

It was observed that there was an abrupt increase in strain value for a load level corresponding roughly to the initiation of flexural cracks.

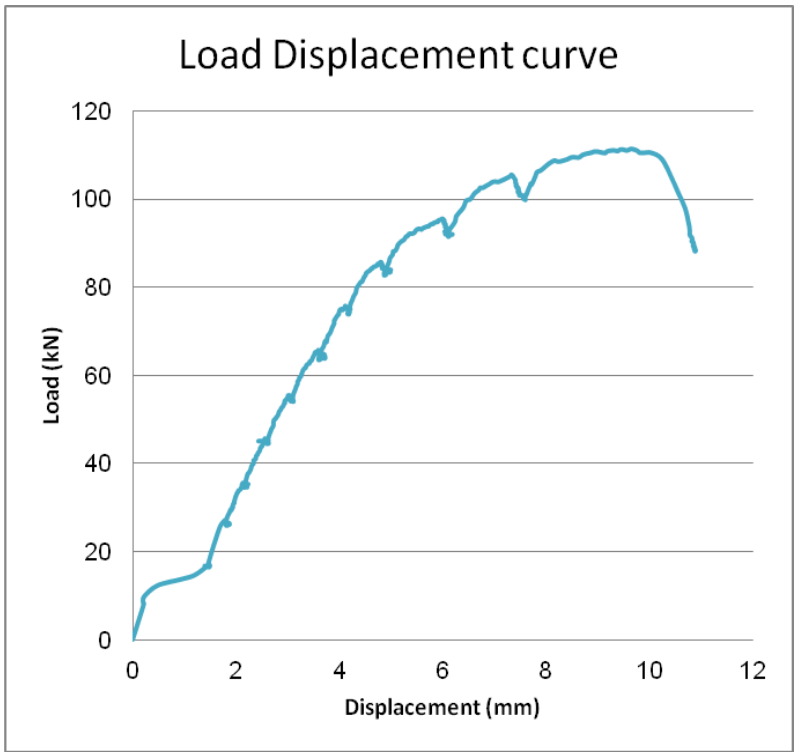

Fig 7.27: Load-displacement curve for LVDT1

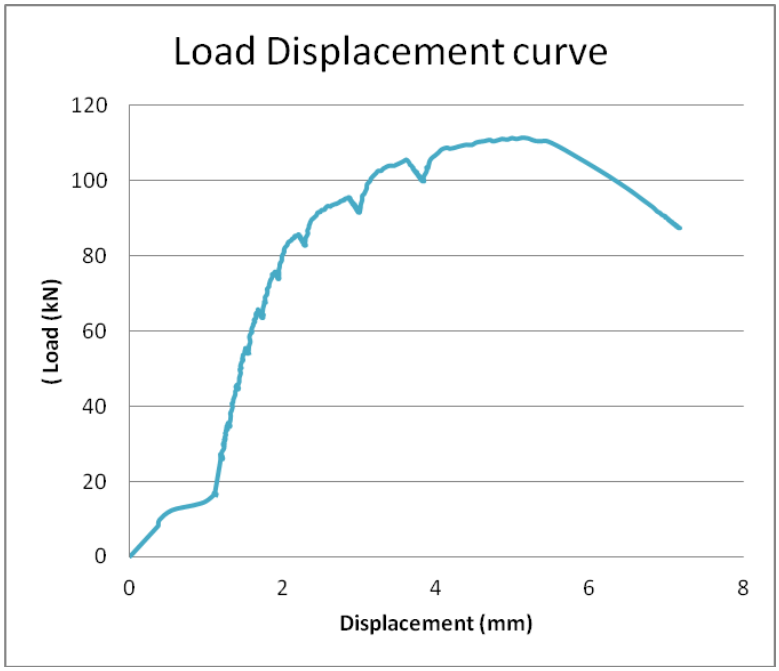

Fig 7.28: Load-displacement curve for LVDT2

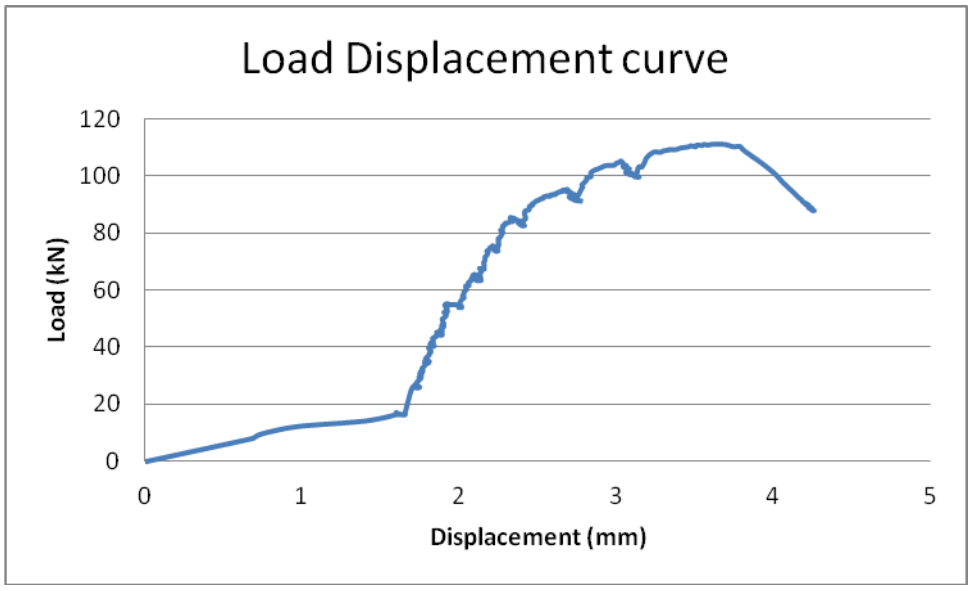

Fig 7.29: Load-displacement curve for LVDT3

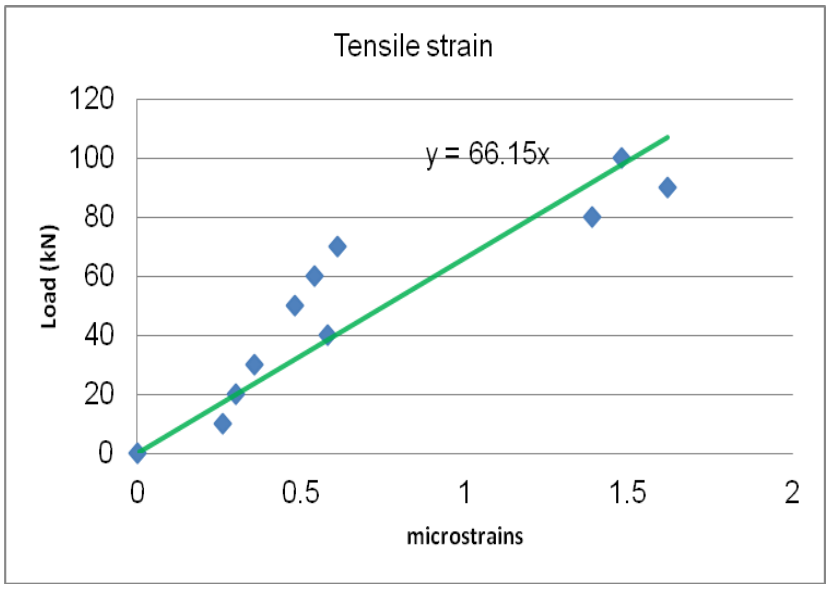

Fig 7.30: Tensile strain across concrete depth

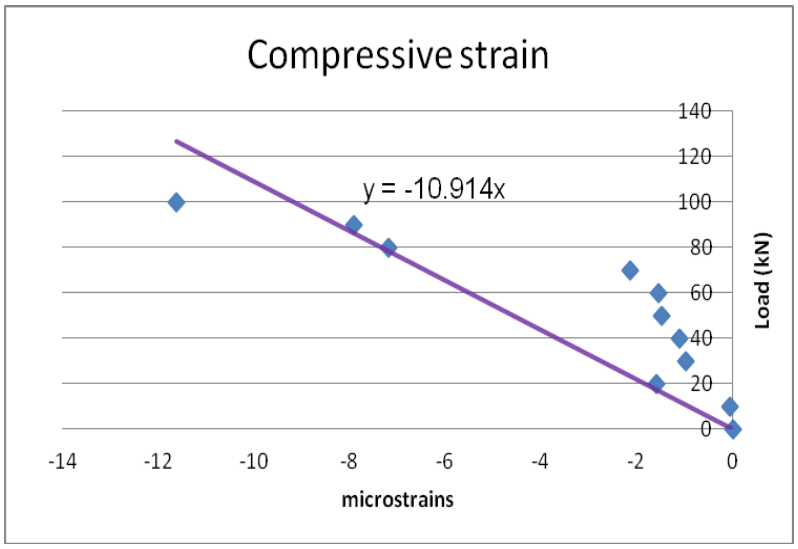

Fig 7.31: compressive strain across concrete depth

7.4.6 .2 Strain Readings on the Shear arms

7.4.6.2.1 Shear Strain on Web for shear arm 1 at Failure Load of 111.08kN

As a result of the shear being principally resisted in the web, therefore, the shear strain is computed with the following equations

Rosette readings on shear arm 1 are: $\varepsilon_0 = 49\ ms$, $\varepsilon_{45} = 0\ ms\ and\ \varepsilon_{90} = 0$

$\varepsilon_\theta = \varepsilon_x cos^2\theta + \varepsilon_y sin^2\theta + \gamma_{xy} sin\theta cos\theta$ ..... (7.8)

For θ = 0 $\varepsilon_x = \varepsilon_0 = 49\ microstrain$

For θ = 45^0 $\varepsilon_{45} = 0$

$\varepsilon_{45} = \varepsilon_x cos^2 45 + \varepsilon_y sin^2 45 + \gamma_{xy} \sin 45\, cos45$

$0 = 0.5 \times 49 + 0.5 \times 0 + 0.5\gamma_{xy}$ ..... (7.9)

$0 = 24.5 + 0.5\gamma_{xy}$

$\gamma_{xy} = -49\ microstrain$

For θ = 90

$\varepsilon_{90} = \varepsilon_x cos^2 90 + \varepsilon_y sin^2 90 + \gamma_{xy} \sin 90\, cos90$

$\varepsilon_{90} = \varepsilon_y = 0$

Substitute into equation 5.2 to obtain the shear strain.

Calculate the principle strain as thus.

Rosette readings on shear arm 2 are: $\varepsilon_0 = -39\ ms$, $\varepsilon_{45} = -12\ ms\ and\ \varepsilon_{90} = 70\ ms$

Using similar approach, the strain strain in the web of sheararm 2 is calculated as

$\varepsilon_\theta = \varepsilon_x cos^2\theta + \varepsilon_y sin^2\theta + \gamma_{xy} sin\theta cos\theta$ ..... (7.10)

$-39 = \varepsilon_x cos^2 0 + \varepsilon_y sin^2 0 + \gamma_{xy} sin0 cos0$

For θ = 0 $\varepsilon_x = \varepsilon_0 = -39\ ms$

For θ = 45^0

$\varepsilon_{45} = \varepsilon_x cos^2 45 + \varepsilon_y sin^2 45 + \gamma_{xy} \sin 45\, cos45$

$-12 = 0.5 \times -39 + 0.5 \times 70 + 0.5\gamma_{xy}$

$\varepsilon_x + \gamma_{xy} = 15$

For θ = 90

$70 = -39\, cos^2 90 + \varepsilon_y sin^2 90 + \gamma_{xy} \sin 90\, cos90$

$70 = -39 \times 0 + \varepsilon_y \times 1 + \gamma_{xy} \times 0$

$\varepsilon_y = 70ms$

By substituting into equation

$\gamma_{xy} = -55ms$

The readings show that very small deformation occurred on the shearhead due to the high moment of resistance of the shear arms.

7.4.6.2.2 Tensile strain at the bottom flange of the shear arm 1

The reading of tensile strain becomes very haphazard due to fluctuation of the loading rate on shear arms.

7.4.6.2.3 Compressive strain at the Top flange of the sheararm 1

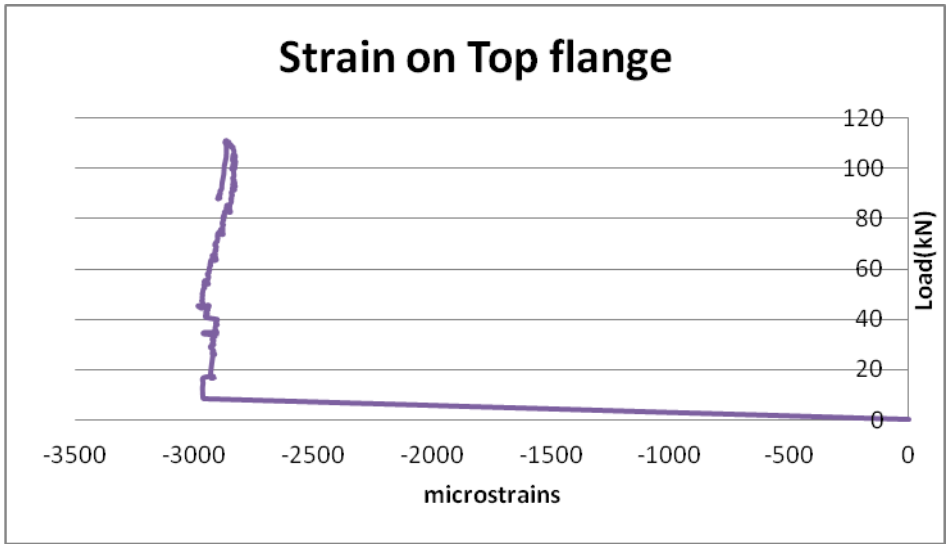

Fig 7.32: Load -strain graph for Top flange of shear arm1

7.4.6.2.4 Compressive strain at the Top flange of the sheararm 2

The axial compressive strain in the top flanges of the shear arms reached a strain of approximately, 0.003 at a load of 8.25kN; the strain remains approximately steady with increase in load until failure occurred.

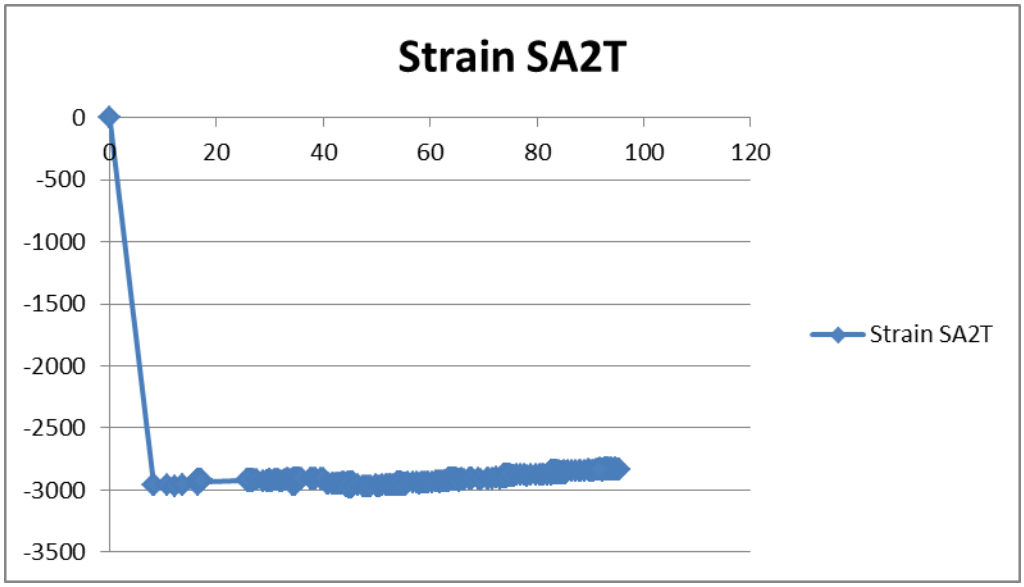

Fig 7.33: Load -strain graph for Top flange of shear arm2

The failure perimeter was difficult to measure in test because crack propagated towards the column edges .The compressive face of the slab was almost intact; there was no significant crack propagation. The values obtain for both axial and shear strains on the shear arms reveal that plastic deformation occurrred. For instance, the measured axial compressive strain (ε_x) -0.003 exceeded the theoretical yield strain of -0.015. This indicates that the shearheads only deformed plastically before punching shear occurred which is desirable.

From the test observation, it could be tacitly assumed that punching shear failure occurs approximately when the shear strength of concrete is reached. This indicates that, regardless of the connection rigidity, punching shear failure may occur predominantly when the shear strength of concrete is reached.

Earlier tests for shearhead connected to interior column performed by Corley et at (1968) revealed that shearhead increases punching capacity by enlarging the critical shear perimeter in similar way as the enlarge column. In addition, shearheads was defined as over-reinforcing if its flexural capacity is not reached when the connection fails and under-reinforcing if the flexural capacity is reached before the end of the test. Following these definitions, it means that previous design of shearheads was probabilistic because it is relatively difficult to control the outcome of the design. But the design procedure that combined the recommendations of ACI 318-05 and Newzealand codes adopted herein enhances an authoritative of the exact type of shearhead needed.

Summary

Two experiments that investigated the punching shear capacity of a slab with and without shear reinforcement have been performed. Measured values of concrete material properties such as: compressive strength, elastic modulus and tensile strength have been implemented in the numerical analysis.

The design guidance gave a satisfactory performance of the shearheads. Measured values of strains on the tensile bottom of the shear arms poorly captured are complimented in the numerical analysis. Both experimental and numerical results are

compared in the next chapter. These results are further compared to design codes predictions; leading to the formulation of an analytical equation for punching shear at edge supported connection reinforced with shearhead.

Tabular summary of how 7.2 was achieved is needed here:

Table 7.4: Tabular summary on how section 7.2 was achieved

Objectives	**Outcomes**
1. To study the deformation behaviour of the slab-column connection subject to punching	Punching shear test was carried out on slab1 and slab 2; in which load was applied and the evolution of displacements were measured at specific locations as depicted in Figures 7.10, 7.11, 7.27, 7.28
2. Investigate punching shear capacity of the steel edge supported slab without shear reinforcement for comparison with design codes equation.	As presented in chapter 8, the punching shear capacity obtained from the experiments Slab 1 was compared with analytical equations of ACI 318-05 and EC2; to support decision in the formulation of New analytical equation for punching shear capacity of edge slab-column connection reinforced with shearhead.
3. Some influential parameters governing punching shear failure at the connection such as: strains on concrete and reinforcement and shearheads at locations where stresses could be significant	Strains on embedded reinforcements were measured to investigate if flexural failure occurred before punching shear and the influence of reinforcement ratio as depicted on figures 7.12 and 7.13. strains on the shear arms at top, bottom flanges and web were measured using strain gauges and rosette as presented in figures 7.4.6.2, 7.32 and 7.33.
4. The proposed novel shearhead assembly was subjected to punching shear experiments.	Design guidance/procedure for shearhead assembly has been proposed. The design guidance was used to select the structural steel sections that provided adequate enhancement of punching shear capacity of the connection
Tests on control specimens were performed to measure compressive strength, tensile strength and Elastic Modulus of concrete, which were used to calibrate, refine and validate numerical models	Compressive strength, tensile strength and Elastic Modulus tests were used calibrate concrete nonlinear properties implemented in the numerical model

Chapter 8: Analysis of Results and Discussion

8.0 Introduction

This chapter provides detail comparison of all the experimental and numerical results. Firstly, the numerical results for slab 1 are compared with the experimental results for further validation. The validation further confirms the adequacy of the adopted modelling scheme. The results are used to evaluate the predictions of ACI 318-05 and Eurocode codes for punching shear without shear reinforcement. The code that provides the best correlation would be used to support decisions in the modification of existing design code for shearhead reinforcement.

Secondly, numerical model of slab 2 (slab with shearhead) is validated with the corresponding experimental results. Detail parametric study on factors that influence the structural response of the sheadhead is conducted. This would provide useful information for the formulation of an analytical equation for punching shear capacity of the edge connection reinforced with shearheads.

8.1 Comparison of Numerical and Experimental results on slab 1

The Load –Displacement response of the experimental investigation and numerical model are shown in fig.8.1.The measured experimental failure load occurred at 104.98kN including the self-weight of the slab specimen, while the numerical failure load occurred at 106.79 kN. A slight deviation of 1.69% was obtained which could be attributed to micro cracking due to shrinkage that degrades the original initial elastic stiffness.

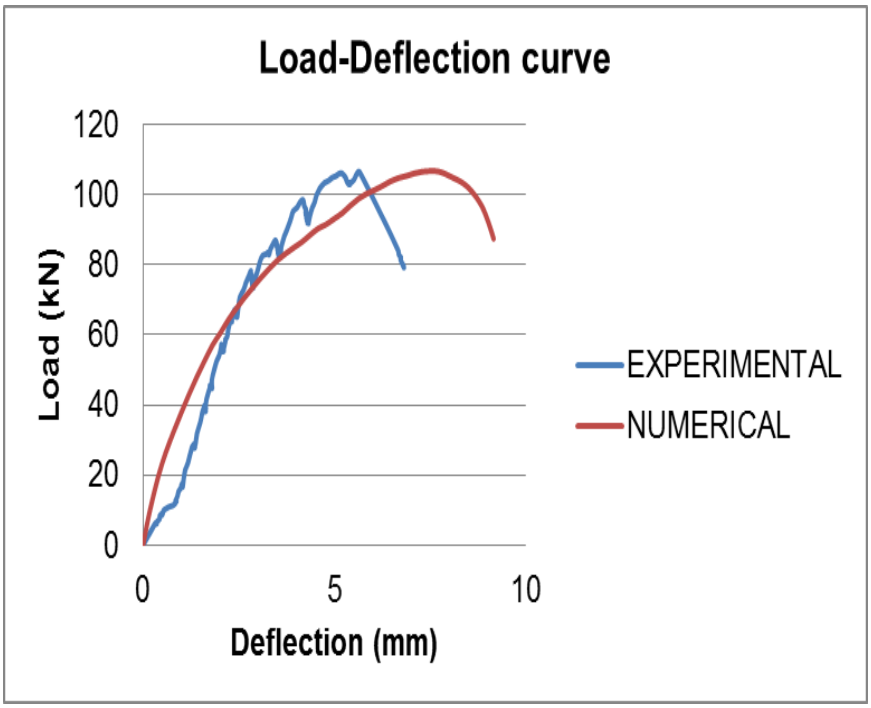

Fig.8.1 Load-displacement curve for experimental and numerical for Slab 1 (at slab-column connection.

And also the variation in displacements between the measured and numerical is caused by the loading rate and the effective in-situ concrete tensile strength, which was affected by curing and restrained shrinkage.

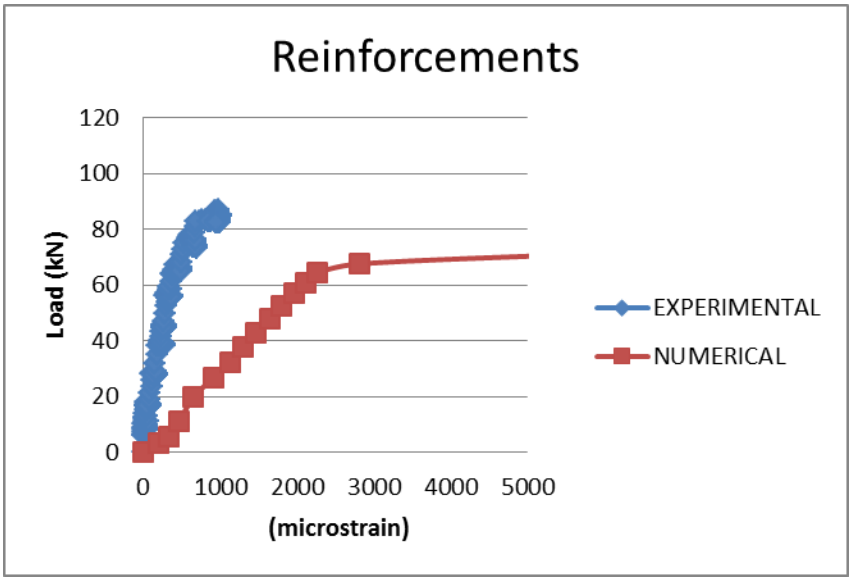

Fig.8.2: Load- strain curve for tensile reinforcements for slab 1 (within the vicinity of the slab-column connection)

Fig.8.2 shows the strain measurements on the tensile reinforcement at the bottom of the slab. The appearance of the first incipient hair width crack occurred at a load of 60kN, which was visually inspected. The result shows that flexural yielding of reinforcement occurred with a load of 80kN in the experiment. At this load, the cracks widened which indicates that concrete has been severely damage by tensile cracking, whereas in the numerical, 64.38kN was obtained.

8.20 Discussion on Experimental and Numerical results for Slab 2.

The experimental failure load gives .111.35kN while the numerical failure load gives 117.76kN as shown in fig 8.3. The numerical failure load deviated from the experimental failure load by 5.76%. A deviation of 12.98% was observed for displacement at failure load. These deviations may be attributed to the initial micro cracking induced in the concrete as a result of restrained shrinkage during curing could reduce the elastic modulus which reduces the stiffness of the concrete.

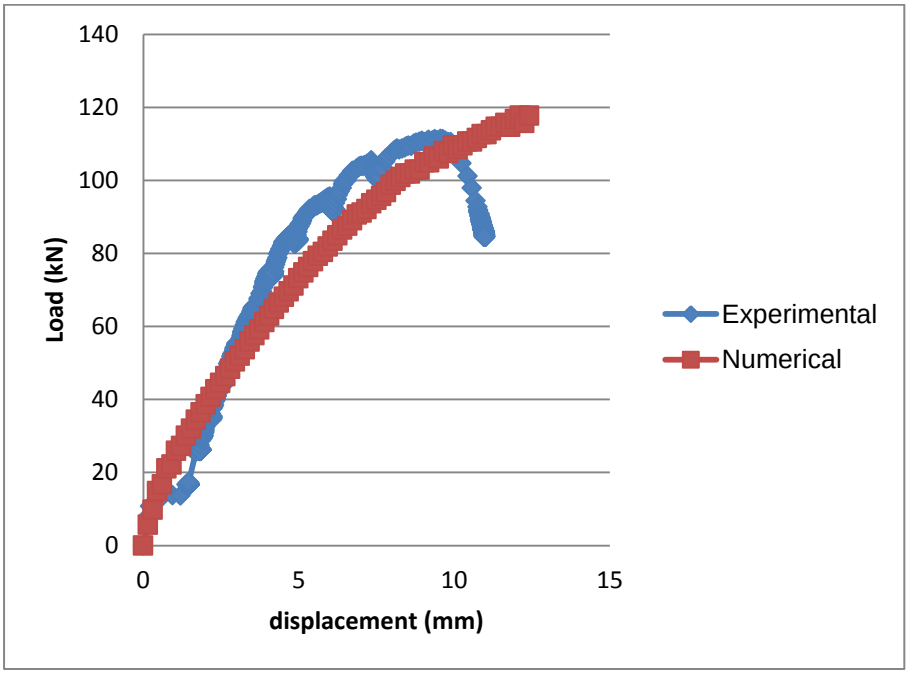

Fig.8.3: Load displacement curve for experimental and numerical models.

Initial yielding of reinforcement occurred at a load of 90.62kN, in the numerical model as shown in fig 8.4. Reinforcement yielded in the vicinity of the column and

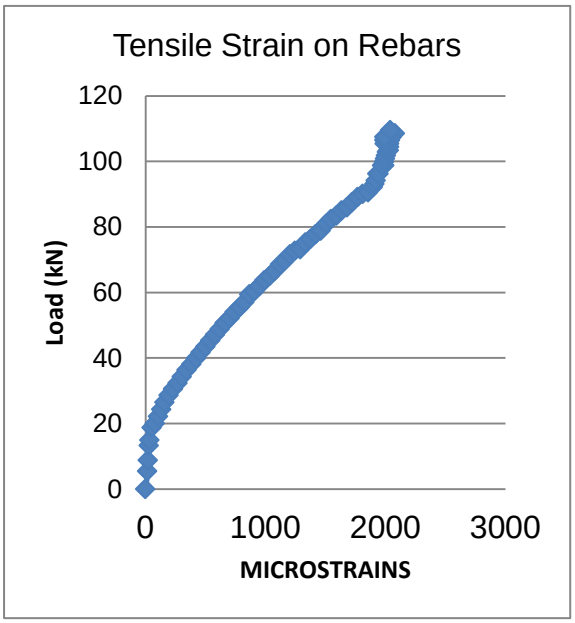

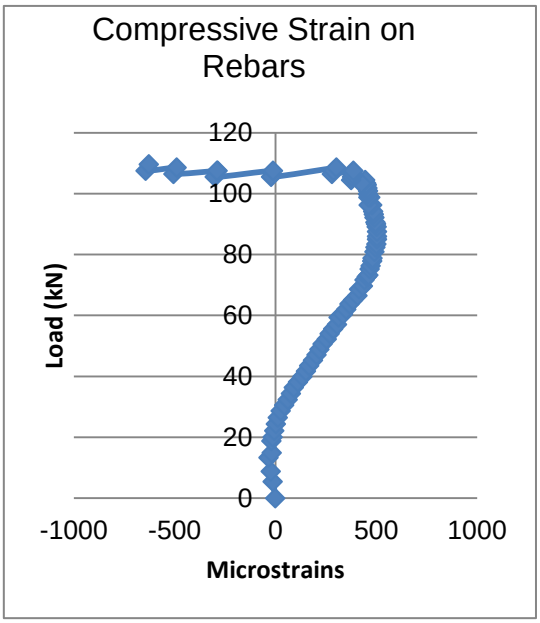

Fig.8.4a: strain on tensile reinforcement Fig 8.4b strain on compression rebars.

no other yielding zone was observed; which shows that structural deformations are concentrated within the vicinity of the column. This is consistent with experimental observation.

8.2.1 Strains on Shear arms

Based on the yield strength and elastic modulus of steel assumed for the shearhead, an axial yield strain of -0.0017 was calculated; and compared the axial compressive strain on the compressive flange of shear arms for both measured and numerical models. The measured and numerical axial compressive strain gives approximately -0.003 which is slightly above the calculated yield strain. This reveals that plastic deformation of the shearhead occurred prior to punching shear failure which is desirable. The measured tensile strain was very haphazard and was discarded.

It could be observed that a similar evolution of compressive strain occurred under incremental loading for both experimental and numerical. The strain increases linearly between a load value of zero to 20kN and becomes approximately steady until punching shear failure occurred. The graph also shows that considerable bond was maintained between the shearhead and the concrete since there was no divergence. Moreover, perfect bond was assumed between the embedded shearhead and the concrete.

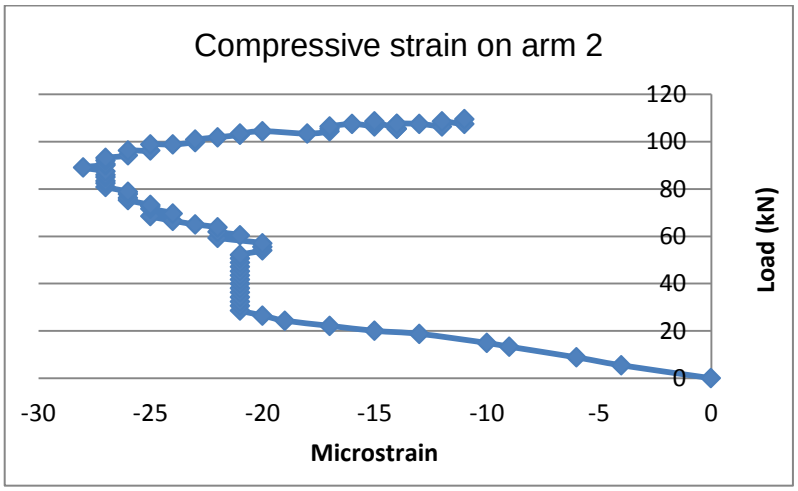

Fig.8.5: strain on compressive flange of shear arm 2

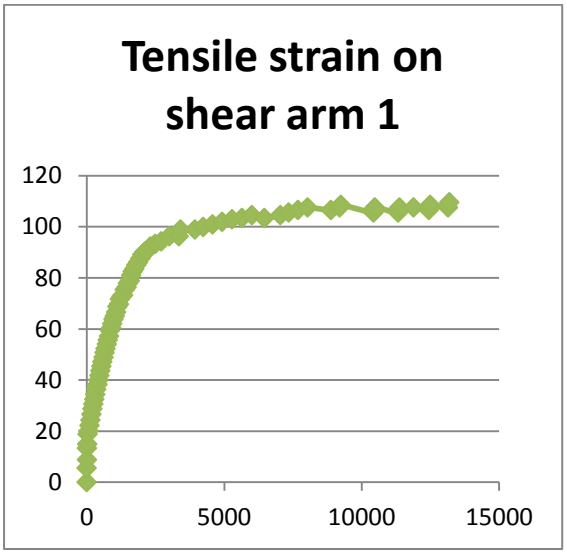

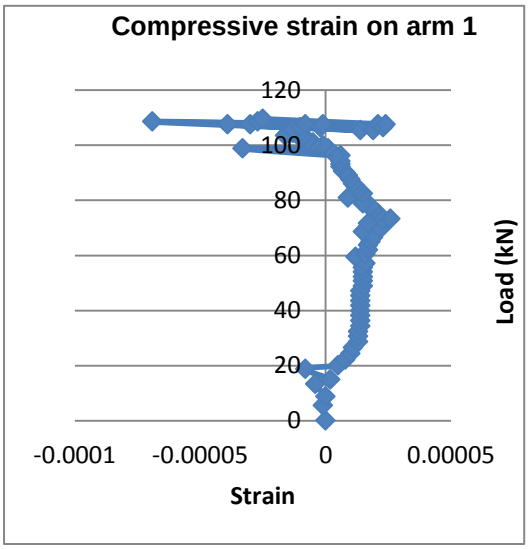

Fig.8.6a: strain on tensile flange of shear arm 1 Fig.8.6b: compressive strain (arm 1).

8.2.2 Effect of Bending Stiffness ratio between shearhead and concrete

ACI 318-05 recommended that a bending stiffness ratio of $\alpha \geq 0.15$ should be maintained for shearhead design. Therefore, α was varied between 0.075 and 0.3 to investigate its influence on the punching shear strength of the connection. Results revealed that $\alpha = 0.075$ slightly reduces the failure load. Mechanically, this means that the stiffness of the shearhead is reduced to half of its original value. However, the failure load increases significantly for $\alpha = 0.3$.This indicates that the stiffness of sheadhead is double while that of the concrete is constant. This means that higher value of α may exaggerate the punching shear capacity of the connection.

8.2.3 Effect of Shear arm Length

Three values of shear arm length were investigated which are: $l_v = 60$ $l_v = 120$, and $l_v = 185$. The failure load increase as the shear arm length increases but there was no significant increase in displacement.

8.2.4 Effect of Shearhead Cross section

The **I**-section shear arm was increased to an overall depth of 80mm. The thickness of its flanges and web were doubled to 6mm and that of the plate was increased to 10mm. This resulted to a significant increase in the failure load as depicted in fig 8.7. This indicates that increase in shearheads increases the punching shear capacity.

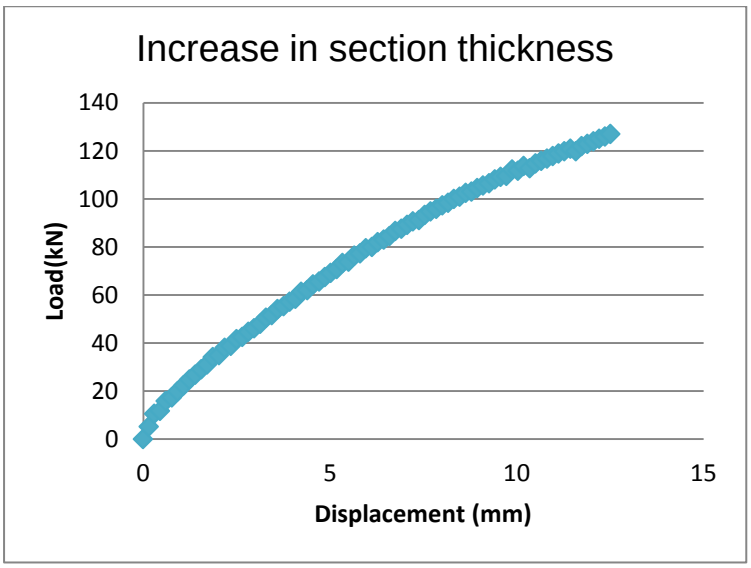

Fig.8.7: increase in shearhead section thickness

8.2.5 Shear Force on Shearheads

The axial forces, shear forces and bending moments were determined by numerical integration as thus:

$N = \int_A \sigma \, dA$ where A represent the shear arm cross sectional area.

As shown in fig 8.8, it implies that the shear arms resisted the vertical load but not completely uniform in distribution along the arm. The shear arms ideally acts like a cantilever beam in which the bending moment becomes maximum at the column.

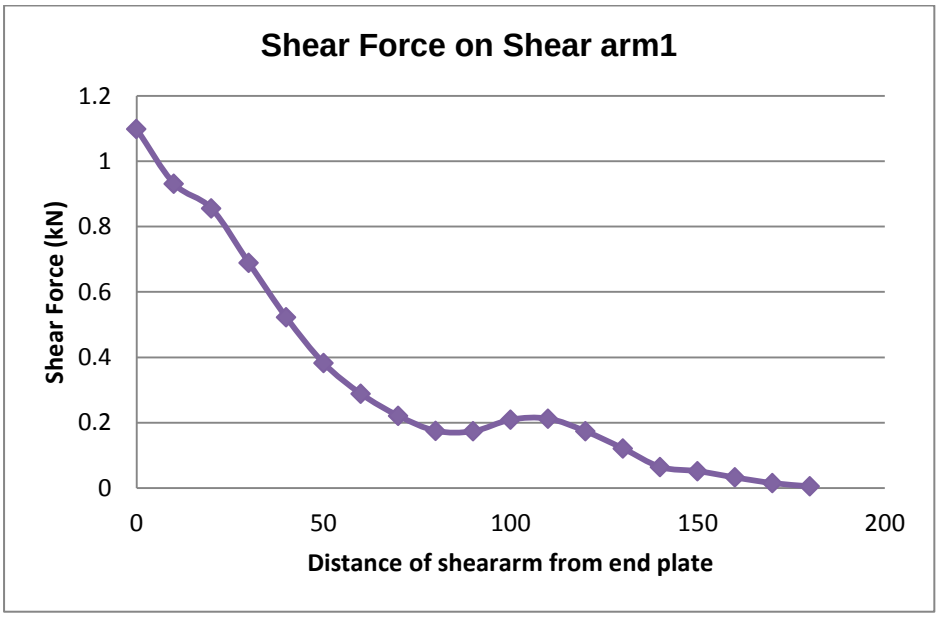

Fig.8.8: shear Force along shear arm 1

8.2.6 The Effect of Concrete Elastic Modulus on slab 2

The model on slab 2 was investigated for its sensitivity to Elastic Modulus which is related to concrete ultimate strain as depicted in equation 3.13.The elastic modulus of obtained from control specimen was substituted into equation 3.13 gives an ultimate strain of -0.00145.The Elastic modulus was reduced to its corresponding value of ultimate compressive strain when the concrete completely softened in compression. This occurs when a compressive strain of - 0.0035 is reached. The graph in fig 8.9 shows that the failure load was reduced slightly for the reduced value of elastic modulus. This reveals that the ultimate compressive strain has considerable effects on failure load as opposed to the earlier observation of Eder et.al (2010) that variation in compressive strains does not have any significant effect on the failure load. Variation in Elastic modulus directly affects the stiffness of the concrete.

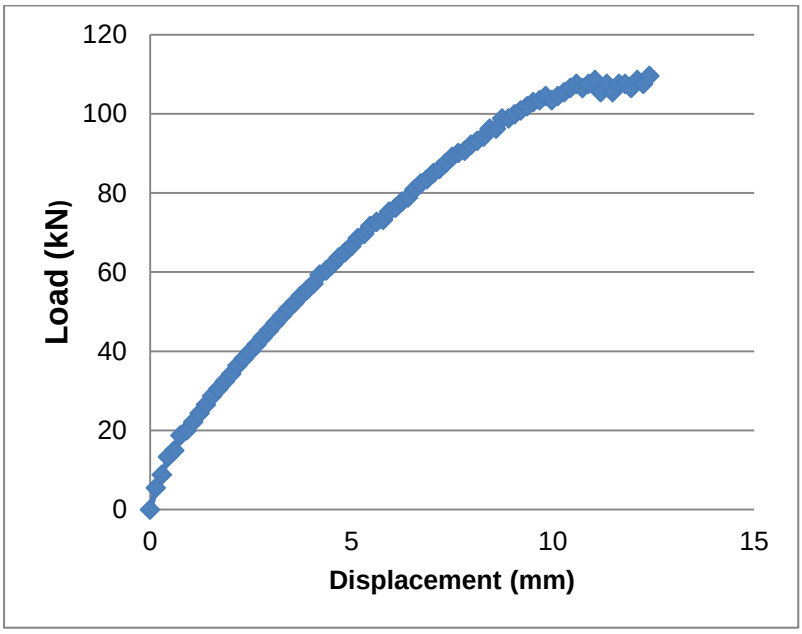

Fig.8.9: Variation of Elastic of Elastic Modulus of concrete on slab 2

The deflection obtained from numerical model is slightly higher than that of the measured. This could be attributed to the reduction in concrete elastic modulus in the slab which is caused by the effect of creep and loss of tension stiffening under incremental loading. In addition to the fluctuation in the loading rate due to manual hydraulic jack.

The value of shear retention (β) was varied to examine its influence on the connection punching shear capacity. It was observed that increased in(β) increases the failure load as previously observed in Slab 1. It was also observed that higher values of β overestimates the punching shear strength of the connection.

8.2.7 Effect of Geometric Nonlinearity

As shown in fig 8.10, when geometric non-linearity was activated in the model, there was a slight increase in failure load; which overestimated the measured failure load. This increase may be attributed to the tensile membrane action developed by the shearheads

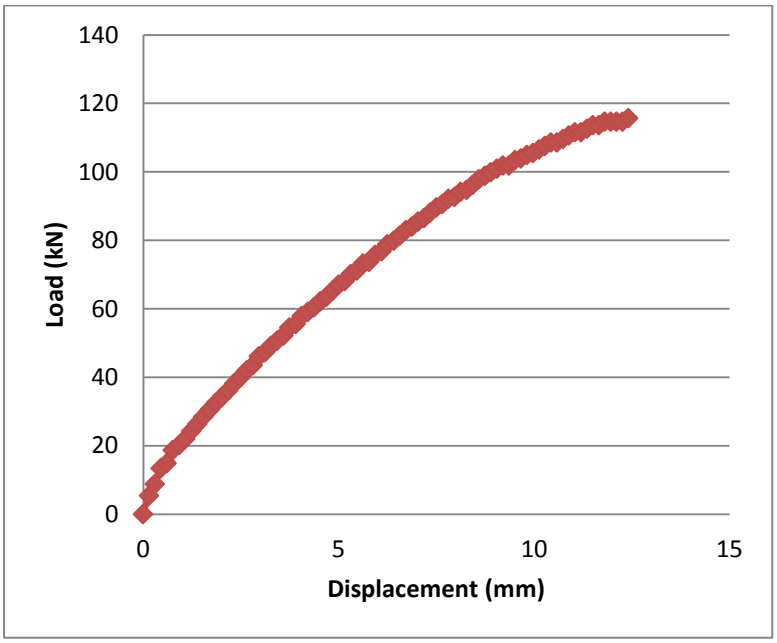

Fig.8.10: Effect of Geometric nonlinearity

8.3.0 Comparison between Experimental and Code Equations for slab 1

This section compares the experimental results with code predictions. Most codes were formulated based on the mean values of the material properties such as: the compressive and tensile strength. And ignore the partial safety coefficients.

8.3.1 ACI 318-05 Code Prediction

The ACI code ignores the significant contribution of reinforcement to punching shear capacity of the connection. The punching shear capacity of the edge connection is calculated as thus;

$$V_{c,ACI} = 0.33\sqrt{f'_c}\ b_o\ d \quad \text{..... (8.1)}$$

Where b_o= control perimeter as shown in fig 8.11 f'_c is the cylinder compressive strength.

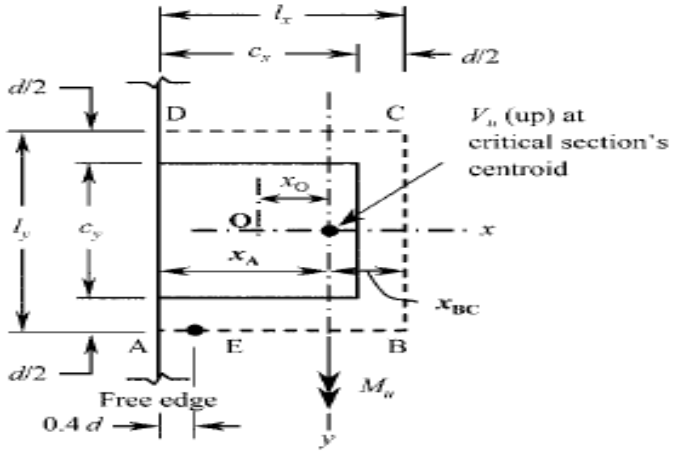

Fig 8.11 ACI 318-05 control perimeter around edge column (Park and Choi 2007)

The punching capacity is calculated as thus,

$b_o = 2\,(C_1 + \ 0.5d) + C_2 + \ d$

$d \ = \ h - c - \emptyset/2$ For square column $C_1 = C_2$

$d \ = \ 130 - 20 - 8/2 = 106mm$.

$b_o = 2\,(100 + \ 0.5 \ \times 106) + 100 + 106 = 512\ mm$

$V_{c,ACI} = 0.33\sqrt{27.86} \times 512 \times 106 \quad = \quad 94.01kN$

So far, this experimental investigation shows that ACI 318-05 equation underestimated the punching shear capacity of the edge connection. Punching shear capacity predicted by ACI 318-05 equation gives 94.01kN while the measured gives 104.98kN. A significant deviation of 10.37% is obtained. Based on this deviation, it could be suggested that the critical section for flexure provided by ACI 318-05 should be increased. Youm, Kim and Moo (2014) also observed that ACI punching shear model significantly underestimated punching shear capacity of the slab especially when the flexural ratio is high. This is attributed to the negligence of the significant effect of reinforcement ratio in ACI equation. This inadequacy observed in the ACI 318-05 has indirectly affected the unbalanced moment induced at the edge connection due to the interaction between unbalanced gravity and lateral load, although this aspect is not dealt with in this investigation.

8.3.2 Eurocode 2 Code Prediction

The punching resistance of slabs was computed to EC2 using equation 8 .2

$$V_R = 0.18 . k . (100 . \rho . f_c)^{1/3} . u . d \quad \text{..... (8.2)}$$

Where ρ represents the reinforcement ratio. And d represents the effective depth of the slab. f_c is the cylinder strength in MPa.

k is a factor accounting for size effect whose value can be obtained by equation 8.

$$k = \left(1 + \sqrt{\frac{200}{d}}\right) \leq 2 \qquad d \text{ in } mm \qquad (8.3)$$

According to reduced control perimeter for edge column depicted in fig 8.12

Fig 8.12.control perimeter for edge column (Eurocode 2).

$$V_{R,EC} = 0.18 . 2 . (100 . 0.06 . 27.86)^{1/3} \times 533.052 \times 106 = 112.03 kN$$

8.4 Design Recommendation for shearhead connection

The punching shear strength of flat slab supported on edge column can be expressed as

$$V_u = \beta \boldsymbol{\nu_{R,DC}} + V_{sh} \qquad (8.4)$$

β represents a reduction factor. β was introduced because EC2 prediction slightly overestimates the strength of the edge connection Therefore, β should vary between 0 and 1 . The punching shear capacity of concrete ($V_{R,dc}$) to EC2 is same as in equation 8.2. EC2 equation was adopted because it provides the best prediction when compared with experimental results.

$V_{R,dc}$ is the shear resistance provided by concrete without shear head.

V_{sh} is the contribution of the shearhead.

$$V_{sh} = \phi \frac{M_p}{L} \quad \text{..... (8.5)}$$

Therefore, equation 8 can be written as thus,

$$V_c = \beta V_{R,dc} + n\,\phi \frac{M_p}{L} \quad \text{..... (8.6)}$$

M_P represents the plastic moment of resistance of shearheads

n is the number of shear arms. Other parameters have been defined in chapter 7.

Equ 8.6 is the analytical equation formulated for punching shear capacity for edge connection reinforced with shearheads.

Chapter 9: Conclusion and Recommendation

9.1 Conclusion

Flat slabs construction is gaining more popularity than the normal frame structure due to its economical and construction merit. From available literature, the use of steel column as alternative to reinforced concrete is relatively scarce. This research focuses on edge connection because punching shear failure is aggravated by the presence of unbalanced moments. Due to significant dearth of data on edge connection, the data interior connection were used to calibrate the punching shear capacity of edge connection; which significantly underestimates its punching shear capacity. This becomes one of the hypotheses of this research.

Steel column was used to replace the conventional reinforced concrete column in the slab-column connection. These dissimilar materials (steel column and concrete slab) were connected using shearhead assembly. Therefore, this research work focused on the design of a novel shearhead system for the edge connection.

Punching shear failure of edge connection without shear reinforcement was investigated experimentally and numerically and compared to design codes equations. Comparison revealed that ACI318-05 code significantly underestimates punching shear capacity of edge connection, whereas Eurocode 2 equation shows a very good correlation with experimental and numerical results. Therefore, it was adopted in the formulation of the proposed analytical equation.

ACI 318-05 and New Zealand are design codes that provide design principles for shearhead connection. But the principles were proposed for RC column supporting flat slab. Therefore, the codes recommendation was modified for applicability to steel column system as provided in the design guidance.

In order to apply the most appropriate methodologies for punching shear failure at edge connection, various theoretical, experimental and numerical models were reviewed. It was revealed that most theoretical and empirical models ignore the residual tensile strength of cracked concrete, which lead to poor prediction of punching shear capacity of slab-column connection. Therefore, most theoretical and empirical models were ignored.

Whereas, the TS-model which account for the residual tensile strength of cracked concrete was adopted.

Various material constitutive models implemented in Midas FEA were compared which revealed that the TS -model was the most appropriate for punching shear analysis; because it accounts for the residual tensile strength of cracked concrete and also provides explicit account of how crack initiation and propagation can be captured using smeared crack approach. T.S model materialises the tension softening behaviour of concrete in terms of fracture energy. Concrete fracturing is associated with complex mechanism such as: aggregate interlocks, crack branching and crack face friction; these mechanisms were adequately captured using energy approach.

Prior to implementation, the adopted modelling scheme was validated using analytical solution of plate and previous experimental work .Comparison shows a good correlation therefore, it was adopted.

Elastic analysis was conducted to investigate the boundary conditions that provide the closest solitude between the prototype and the laboratory specimen. The prescribed boundary conditions were implemented in the numerical simulations of both slabs. NLFEA was conducted on both slabs which were validated by the experimental results.

Results of both numerical and experimental investigations reveal the following:

- Increase in tensile strength of concrete increases the punching shear capacity of the connection.
- Results obtained from both experimental and numerical revealed that ACI318-05 significantly underestimate the punching shear capacity of edge connection. Whereas Euro code 2 equation provides a better prediction, therefore, it was adopted in the formulation of the analytical equation for edge connection reinforced with shearhead.
- Both experimental and numerical results obtained for slab 2 indicates that the sheadhead contributes about 5% to the punching shear capacity of the connection when compared to ACI 318-05 equation. Whereas, no significant deviation was observed when compared to Eurocode 2 equation.
- Based on these results, it can be deduced that punching shear failure of the connection depends largely on concrete shear strength. The contribution of shearhead is not too significant as suggested by previous researchers. Punching

shear would likely occur when concrete shear strength is reached, despite the robustness of the shearhead connection.

- Bending stiffness ratio between the shearhead and cracked concrete significantly influences punching shear capacity of the connection.
- The shearhead acts like a cantilever beam by transferring shear force from the tip into the connection.
- Increase in concrete mechanical properties such as: tensile strength, fracture energy, elastic modulus increase punching shear capacity of the connection.
- Yielding of reinforcement occurs prior to punching shear failure in both slabs investigated experimentally and numerically.

9.2 Findings

The following are the useful findings:

- The adopted modelling scheme based on TS-model implemented in Midas FEA is capable and reliable for predicting punching shear failure of RC flat slabs. It could be seen in the Load-displacement diagrams that the post-crack regime of concrete was adequately captured prior to failure.
- The degradation of shear stiffness due to the progressive damage of concrete of concrete was modelled with shear retention factor (β). Various values of β were examined; it was revealed that $\beta = 0.3$ correlated very well with the experimental results. Therefore, $\beta = 0.3$ is recommended.
- Parametric study revealed that shear retention factor (β) and concrete tensile strength are the most influential factors for punching shear.
- The experimental and numerical investigations confirmed that ACI318-05 significantly underestimate the punching shear strength at edge connection.
- In course of this research, the author has proposed a method for creating a similitude between a continuous structure (prototype) and a representative slab using linear elastic finite element analysis.
- Proposed comprehensive design guidance for design of shearheard connection for edge connection. This design guidance can also be adopted for design of interior connection.

- Because of the significant dearth of information on shearhead assembly, previous investigators have not complied strictly some in any regard to ACI318-05 recommendation; which is attributed to the insufficient design guidance provided by ACI 318-05 code. To overcome this, the author combines both design guidance. ACI 318-05 and New Zealand codes to proposed detail design guidance for shearhead assembly. This study has provided sufficient design recommendation for the shearhead connection. By following the detail procedure provided in chapter 7 and equation 8.6, it will be quite easy for designers to construct shearhead assembly and predict the punching shear capacity adequately.

9.3 Contribution to Knowledge

- A new analytical equation for punching shear capacity reinforced with novel shearhead has been proposed.
- A detail procedure for the design of shearhead assembly embedded in concrete slab has been proposed by combining, the design codes of ACI318-05 and New Zealand codes.
- The influence of bending stiffness ratio between the structural steel section and the cracked concrete was investigated.
- Results obtained from parametric study reaffirmed and clarified some contradictions on the influence of various governing parameters on punching shear strength.

9.4 Recommendations

This section provides both recommendations for the design of shearhead assembly for edge connection and future work.

9.4.1 Design Recommendations

For the purpose of achieving an effective shear head assembly for edge connection, a sequential and logical design procedure is presented as thus:

1. For effective composite action with concrete, I- section should used for shearhead
2. The maximum shear force at the slab-column connection should be calculated, using theoretical shear strength equation of ACI 318-05 and should be factorised by 1.15.
3. Compute the basic shearhead perimeter
    a. calculate concrete shear strength

b. calculate shear perimeter required.

4. Compute the minimum length of the shearhead.

5. Compute the flexural stiffness ratio α_v between the shearhead and the cracked concrete. It should be assumed that the concrete is partially cracked. The stiffness ratio must not be less than 0.15 as recommended by ACI 318-05.

6. If the ratio is less than 0.15 increase the shearhead section.

7. Calculate shearhead moment required.

8. Calculate shearhead moment capacity. If the moment capacity of the shearhead is greater than the moment due to applied load then, the section used is satisfactory.

9.4.2 Recommendations for future work

The followings are recommended for future work

- Experimental model should be carried out to apply lateral load on the connection, to investigate punching shear capacity of the connection under cyclic loading.
- Numerical model of the shearhead connection subject to lateral load should be simulated.
- Other concrete constitutive model such as damage plasticity model (DPM) should be used to model the structural response of the edge connection.
- A scenario where service hole is located in the vicinity of the slab-column connection should be investigated.

9.5 Limitation of Research

The proposed shearhead assembly is not applicable to region vulnerable to significant seismicity, especially if a shear wall is not used to resist lateral loading. Furthermore, the effect of lateral load was not considered. This may require a special type of connection, in which a hole is opened in the vicinity of the column; to enhance amble ductility of the shearhead. Due to the significant dearth of research works on steel column supporting flat slabs, the results were compared to ACI 318-05 and EC2 design codes. There was a need for wider comparison.

List of References

ACI Committee 318 (2008).*Building code requirements for structural concrete* (ACI 318-08) and commentary (ACI 318R-08). USA

ACI318. (1995) 'Building Code Requirements for Structural Concrete and Commentary'. (ACI 318-95 and ACI 318R-89), ACI, Detroit.

Adel,A. and Ghali,A. (1996*) 'Moment transfer by shear in slab-column connections*

Alexander S. D. B., and Simmonds, S. H. (1986). "*Shear-Moment Transfer in Column-Slab Connections," Structural Engineering Report*, No. 141, Department of Civil Engineering, University of Alberta, 95 pp

Almeida et al. (2016) '*Punching behaviour of RC flat slabs under reversed horizontal cyclic loading.* Engineering Structures. 117, 204-217

Bazant,Z.P. and Cao,Z. (1987) '*Size effect in punching shear failure of slabs*, ACI Structural Journal 84,44-53.

Belletti ,B. Walraven, J.C. and Trapan, F. (2015) '*Evaluation of compressive membrane action effects on punching shear resistance of reinforced concrete slabs* Engineering Structures, , 95, 25-39.

Bortolotti, L. (1990), *Punching Shear Strength in Concrete Slabs*. ACI Structural Journal, Vol.87, No.2, pp. 208-219.

Belytschko T , Liu W.K and Moran B .(2000) *'Nonlinear Finite Elements for Continua and Structures'*. John Wiley and Sons Ltd, Chichester, England.

Bresler B, Scordelis A. (1963). '*Shear strength of reinforced concrete beams*. Journal American Concrete Institute; 60(1):51–72.

British Standards Institution. European standard EN-1992-1-1:2004. Eurocode 2: design of concrete structures. Part 1, general rules and rules for buildings. BSI. London; 2004. [25] British Standards Institution.

BS 8110 (1997).Structural use of concrete, part 1, code of practice for design and construction.London: British Standards Institution.

Carneiro, F.L.L.B. and Barcellos, A. (1953) 'Resistance a La Traction Des Betons. Bulletin RILEM, 13, 97-108.

CEB,C.E.I.D.B. (1990), 'CEB-FIB Model Code 1990:Design Code, Thomas Telford.

CEN (2002), Euro code 2: Design of concrete structures — Part 1-1: General rules and rules for buildings. British Standards Institute, London.

Chana ,BS and Desai ,SB (1992) *'Membrane Action, and Design Against Punching Shear*.'. Structural Engineering United Kingdom 70 (19), 339-343

Cheo-Ho,L., Jin-Won,K. and Jin-Gyu,S. (2008) '*Punching shear strength and post-punching behaviour of cft column to rc flat plate connections'* Journal of Constructional Steel Research 64,11.

Cheol-Ho. L, Jin-Won .K and Song.J. (2008). *'Punching shear strength and postpunching behavior of CFT column to RC flat plate connections.*Journal of Constructional Steel Research. 64 , 418-428.

Choi JW and Kim J-H (2012) *'Experimental Investigations on Moment Redistribution and Punching Shear of Flat Plates'*. ACI Structural Journal 109 (3), 329-338

Corley,G. and Hawkins,N.(1968) '*Shearhead reinforcement for slabs*, ACI Structural Journal October 1968,811-824.

Davison.B,and Owens,.G. (2012) *'steel designers Manual*, steel construction institute 7th edition Wiley-Blackwell Publishers.

De Borst, R and Nauta, P. (1985).'*Non-orthogonal cracks in a smeared finite element model*. Engineering computation, 2:35-46

Duarte M.V. Valter J.G, Ramos A.P. (2012). '*Post-punching behaviour of flat slabs strengthened with a new technique.* Engineering structures ELSEVIER. 40 (1), 383-397

Eder, M. A., Vollum, R. L., Elghazouli, A. Y., and Abdel-Fattah, T. (2010) *'Modelling and Experimental Assessment of Punching Shear in Flat Slabs with Shearheads'. Engineering Structures 32 (12), 3911-3924.*

Einpaul J, Miguel F.R and Muttoni A (2015) *'Influence of Moment Redistribution and Compressive Membrane Action on Punching Strength of Flat Slabs'*. Engineering Structures 86, 43-57

Elgabry ,A. and Ghali.(1988) *'Moment Transfer by Shear in Slab-Column Connection*. ACI Structural Journal 93(17), 187-196.

Elstner, R.C,and Hognestad ,E.(1956) '*Shearing strength of reinforced concrete slabs*. ACI J;28(1):29-58

Erdogen, H.,Binici, B and Ozcebe, G (2011) '*Effect of column rectangularity on CFRP-strengthened RC flat plates*. Magazine of concrete research 63(7), 511-527.

Euro code 2. (2002) Design of concrete structures part 1: general rules and rules for buildings European Committee for Standardization Brussels.

Feenstra, P.H. (1993) '*Computational Aspects of Biaxial stress in plain and reinforced concrete*, PhD thesis, Delft University of Technology.

CEB-FIP (2001) Bulletin 12, Technical report, Punching of Structural Concrete. Federal Institute of Technology Laussane, Switzerland.

Genikomsou A.S and Polak M.A 'Finite element analysis of punching shear of concrete slabs using damage plasticity model in ABAQUS. Journal of Engineering structures. 2015. vol 98 pg 38-48

Ghali, A.; Elmasri, M.Z.; Dilger, W. (1976). '*Punching of flat plates under static and dynamic horizontal forces*, ACI Structural Journal, Vol. 73, No. 10, pp. 566-572.

Gomes, R. And Regan, P.E. (1999), '*Punching strength of slabs reinforced for shear with off cuts of rolled steel I-section beams',* Magazine of Concrete Research 51 (2),121-129.

Gomes, R. And Regan, P.E. (1999), '*Punching strength of slabs reinforced for shear with off cuts of rolled steel I-section beams*', Magazine of Concrete Research 51 (2),121-129.

Hallgren, M. (1996) *'Punching shear capacity of reinforced high strength concrete slabs*. Doctoral Thesis, KTH Stockholm, TRITA-BKN. Bull.9,1996, Royal Institute of Technology, Stockholm, 206 pp.

Hillerborg . A and Petersson P.E (1976) *Analysis of crack formation and crack growth in concrete by means of fracture mechanics and finite elements*. Cemen Concr Res :6:773-82.

Hinton, E. and Owen, D.R.J. (1984) 'Finite element Software for plates and shells,

Hordijk (1991), D.A, *Local approach to fatique of concrete*, PhD thesis, Delft University of Technology.

Kinnunen, S., and Nylander,H. (1960) '*Punching of concrete slabs without shear reinforcement*. Transactions No.158. Stockholm;Royal Institute of Technology

Koppitz .R , Kenel .A and Keller. T. (2008). *'Effect of punching shear on load–deformation behavior of flat slabs. Engineering Structures*. 80 (1), 444-457.

Krueger, G., Burdet, O.and Favre, R.(1998) *'Punching tests on rc flat slabs with eccentric loading*.

Kupfer H.B., Hildorf, H.K, and Rusch H. (1969) '*Behaviour of concrete under biaxial stresses*, ACI Journal 66(4); 656-666

Lee, S.K., Woo,S.K and Song, Y.C.2008), 'Softening response properties of plain concrete by large scale direct tests', Magazine of Concrete Research 60 (1),60.

Lee, S.K., Woo,S.K and Song, Y.C.2008), 'Softening response properties of plain concrete by large scale direct tests', Magazine of Concrete Research 60 (1),60.

M.A. Eder, R.L. Vollum, and A.Y. Elghazouli (2011) '*inelastic behaviour of tubular column-to-flat slab connections*

Marinkovic S.B, and Alendar V.H (2008) '*Punching failure mechanism at edge columns of post-tensioned lift slabs'.* Engineering Structures 30 ,2752-2761.

Menetrey, P. (2002), '*Synthesis of punching failure in reinforced concrete'*, Cement and Concrete Composites 24, 497-507.

Midas FEA (1989) Advanced Nonlinear and Detail Program. Analysis and Algorithm.

Moehle, J. (1988) *'Shear Strength of Column edge connections*. ACI Structural Journal 85 (11), 89-98.

Moehle, J.P., Kreger, M.E., Leon, R., "*Background to Recommendations for Design of Reinforced Concrete Slab-Column Connections*," ACI Structural Journal. Vol. 85, No. 6, 1988, 636-644

Muttoni A. (2008) *Punching shear of reinforced concrete slabs without transverse Reinforcement*. ACI Struct J ; 105(4):440–50

Ockleston, A. (1955) 'Load Tests on a Three Storey Reinforced Concrete Building in Johannesburg'. Structural Engineering United Kingdom 33 (10), 304-22

Oyenuga, V (2001). Simplified Reinforced Concrete Design. Lagos Nigeria: ASROS LIMITED. 83-100.

Ozbolt ,J., Bazant, Z.P. (1996). '*Numerical smeared fracture analysis*: Nonlocal micro crack interaction approach, International Journal for Numerical Methods in Engineering,Jg. 39,Nr.4:635-661

Ozbolt, J.; Vocke, H.; Eligehausen, R.(2000*) 'Three-Dimensional Numerical Analysis of Punching Failure, Proceedings of the International Workshop on Punching Shear Capacity of RC Slabs*, Royal Institute of Technology, Department of Structural Engineering, Stockholm, , p. 65-74

Pan, A.D. and Moehle, J.P. (1992). *An experimental study of slab-column connections*. ACI Structural Journal 89:6, 626-638.

Park, H. And Choi,K. (2006), '*Improved strength model for interior flat plate-column connections subject to unbalanced moment*', Journal of Structural Engineering ASCE 132(5), 694-704

Piel, W.and Hanswille.G. (2006) '*Composite Shear Head Systems for improved Punching Shear Resistance of Flat Slabs*. Composite Construction in Steel and Concrete V. pp. 226-235.

Polak, M.A. (1998) *'Modelling Punching Shear of Reinforced Concrete Slabs Using Layered Finite Elements* .ACI Structural Journal 95(8)

Potts, D.M and Zdravkovic,L. (1999),*' Finite element analysis in geotechnical engineering/ Theory*, Vol.1,Thomas Telford, London.

Rocco,C.,Guinea ,V.,Planas,J., and Elices,M. (1999) *Size effect and boundary conditions in the brazilian test*: theoretical analysis Material and structures 32, 437-444

Rodrigues (2007). 'Shear strength of reinforced concrete bridge deck slabs.

Rots JG. (1988) 'Computational modelling of concrete fracture. Doctoral thesis,Technical University of Delft; 1988. p.132.

Sagaseta. J Tassinari. L , Fernández M ,R, Muttoni.A. (2014). 'Punching of flat slab supported on rectangular columns'. Engineering Structures. 77 (1), 17-33.

Selby, R.G and Vecchio, F.J. (1993) 3D Constitutive Relations for Reinforced Concrete, Tech, Rep.93-02 ,Department of Civil Engineering, Toronto, Canada.

Staller, D. (2000).'*Analytical studies and Numerical Analysis of Punching Shear Failure in Reinforced Concrete Slabs*. FIB Bulletin 2001.

Standards of New Zealand, concrete structures standards Draft no DZ 3101

Surendra, P.S, Stuart, E. and Chengsheng. (1995) '*Fracture Mechanics of concrete Applications of Fracture Mechanics to concrete, Rock and other Quasi-Brittle materials.*

Theodorakopoulos,D.,and Swamy,R.N. (2002) '*Ultimate punching shear strength analysis of slab-column connections*

Timoshenko and Krieger (1970) '*Theory of plate and shell.* 2nd ed. London: Mcgraw-Hill book company. 85-90.

Tsang.T (1994) *'Effects of Load-Distributed width on slit Tension of unnotched and notched cylindrical specimens' Journal of Testing and Evaluation*. 10.1520/JTE12656J 401 online publication.

Vanderbilt,M.D.(1972) '*Shear strength of continuous plates'* J Structural Div ASCE;98 (ST5): 961-973

Vecchio FJ, Shim W.(2004) *'Experimental and analytical re-examination of classic concrete beam* tests. J Struct Eng; 130(3):460–9.

Vecchio, F.J., and Collins, M.P (1986) *'The Modified compression field theory for reinforced concrete elements subjected to shear* ACI Journal 83, 22, 219-231.

Vollum, R.,Abdel-Fattah, T.,Eder,M. And Elghazouli,A. (2009) ‘Efficiency of ACI type punching shear reinforcement’

Wood ,J.M. (2003). Pipers Row Car Park, Wolverhampton Quantitative Study of the Causes of the Partial Collapse on 20th March 1997. Available: http://www.hse.gov.uk/research/misc/pipersrowpt1.pdf. Last accessed 24th April 2013

Yankelevsky,D . and Leibowitz, o. (1995). *Punching shear in concrete slabs*. International Jornal of mechanical sciences 21:1, 1-15

Youm .K, Kim.J, and Moon.J (2014). 'Punching shear failure of slab with lightweight aggregate concrete (LWAC) and low reinforcement ratio.Construction and Building Materials. 65 (1), 92-102.

APPENDIX

APPENDIX 1: Equivalent Frame analysis on prototype structure.

5.2.1 Extraction of Specimen from Prototype structure

The test specimen was obtained from a prototype edge panel of a flat slab building scaled down to 50 percent. The prototype slab was designed based on its spans of 5m in both directions with a superimposed dead load of $6kN/m^2$ and live load of $1.5kN/m^2$.

By considering this loading on the prototype, structural analysis was carried out to obtain points of contra flexure and maximum bending moment. In the direction where lateral load was assumed to predominate, the free edge was assumed. At the intermediate edge column B, points of zero bending moment (contra flexure) on both sides were calculated. Considering Along edge (AD) where maximum bending moment occurs perpendicular to the free edge in the prototype was calculated and the slab was extracted along these lines.

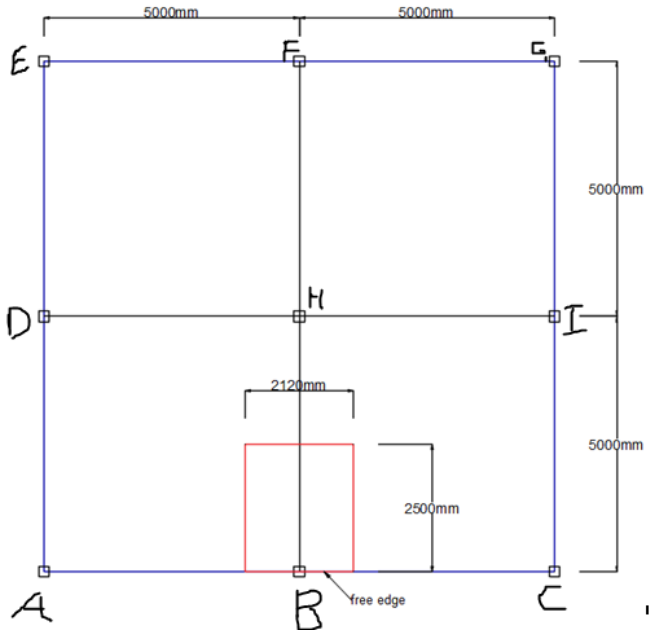

Fig 5.1a Prototype structural Layout

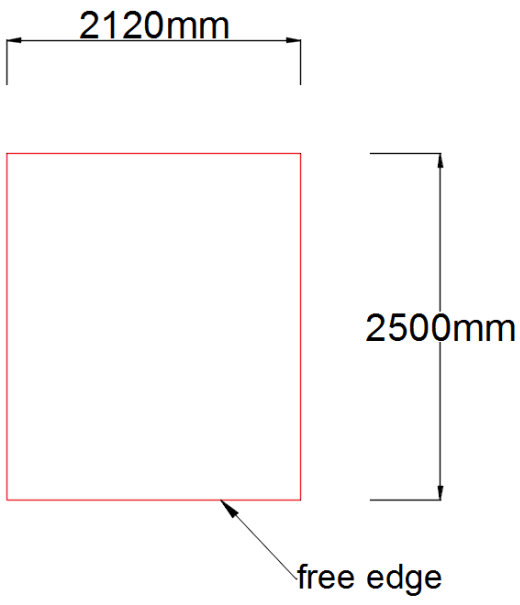

Fig 5.1b: Extracted specimen

The design load on the slab is computed as thus.

Unit weight of concrete = $24kN/m^3$

Overall thickness of slab =250mm

Slab own weight = $24kN/m^3$ × 0.250m = $6kN/m^2$

Live load on slab = $1.5kN/m^2$

Design Load on slab (F) = 1.4 G_k+ 1.6 Q_k

$$1.4 \times 6 + 1.6 \times 1.5 = 10.8\ kN/m^2$$

$$10.80 \times 2.5 = 27kN/m$$

The slab is analysed as a continuous beam as thus

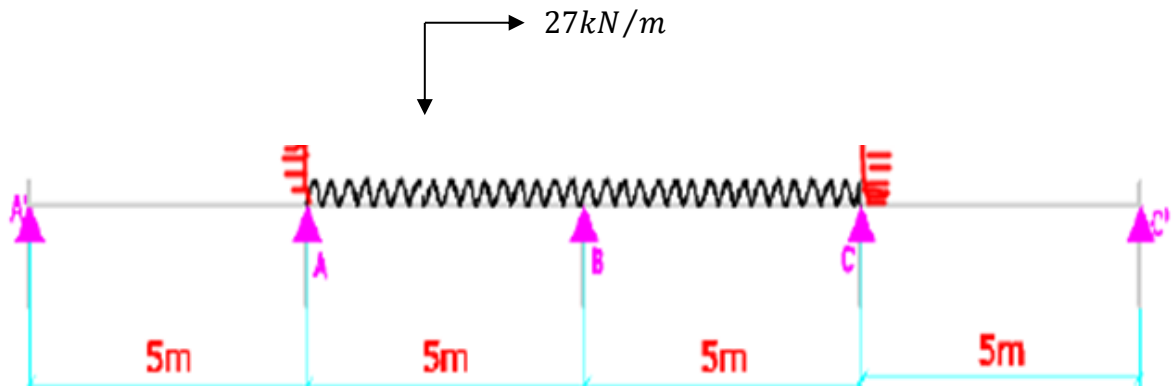

Fig 5.2: continuous beam

The Claypeyon's theorem is used to determine the fixed end moments as thus,

$M_A \times L_1 + 2M_B\ (L_1 + L_2) + M_C \times L_2 = \frac{wl^3}{4}$ ..... (6.1)

Considering span A'AB

10 M_A + 5M_B = 843.75..... (6.2)

Considering span ABC

5M_A + 20 M_B + 5M_C = 1687.5..... (6.3)

Considering span BCC'

5M_B+ 10 M_C = 843.75 ..... (6.3)

By solving the equations

M_A = 56.25 kNm, $M_B = 56.25\,\text{kNm}$,

Shearing Force

$V_{AB} = \frac{wl}{2} + \left[\frac{M_A - M_B}{L}\right]$ But $M_A = M_B$

$V_{AB} = \frac{27 \times 5}{2}$ = 67.5 kN. m

$M = V_A x - \frac{27x^2}{2}$ - 56.25

At Max bending moment $\frac{dm}{dx}$ = V = 0

$$x = 2.5m$$

The points of zero bending moment along the slab is

$$V_A x - \frac{27x^2}{2} - 56.2 = 0$$

Solving the quadratic equation gives $x = 3.94m \; or \; x = 1.060m$

Span moments = $\frac{wl^2}{8} = \frac{27 \times 25}{8}$ = 84.375kN.m

The Bending moment diagram is depicted as thus

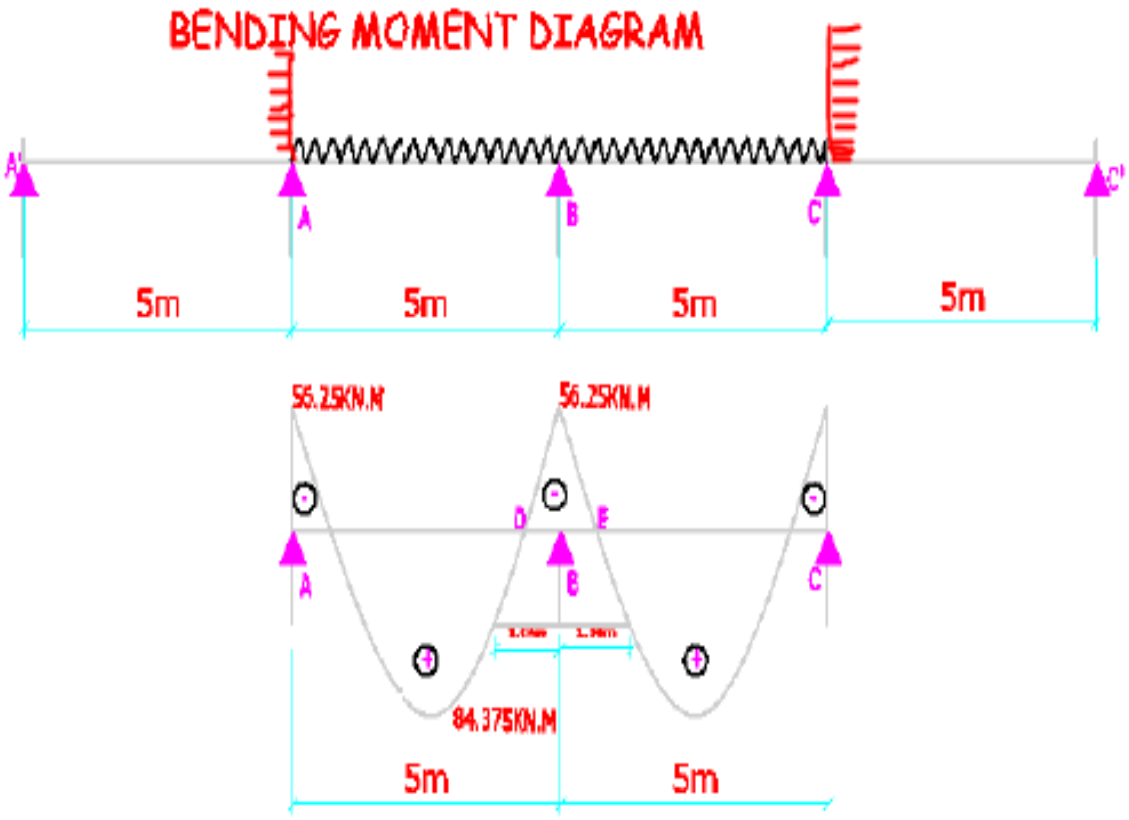

Fig 5.3: Bending moment diagram

The contraflexure bound slab was extracted and prepared in the laboratory. The specimen was scaled down to 50 percent resulting to the following dimension (1250 × 1060 × 130mm)

APPENDIX 2: Concrete mix design

Mix design calculation for water/Cement ratio = 0.52

REF	CALCULATION	OUTPUT
Lydon F.D	1. Target strength = $50/mm^2$ 2.For a maximum aggregate size of 20mm, the water content could $170kg/m^3$ 3. The cement content = $\frac{170}{0.52} = 327kg/m^3$	

	4. The average density relative density of 2.65, the fresh concrete density is taken as $2420kg/m^3$ 5. The aggregate content = 2420-327-170 = $1923kg/m^3$ 6. Aggregate/Cement ratio = $\frac{1923}{327} = 5.88$ 7.With 35% sand the mix proportions are 1:2.06:3.82, 0.52 For a trial batch of $0.2m^3$ the weights of the ingredient are: $Cement = 65.4kg$ $sand = 134.72kg$ $granite = 249.83kg$ $Water = 34.02kg$	

APPENDIX 3: COMPUTATION OF CONCRETE TENSILE STRENGTH

Failure load of specimens from the tensile test are presented as thus

S/N	Failure load (P) in kN	Tensile stress (σ_t) in N/mm^2
1	91.27	2.91
2	87.10	2.77
3	81.99	2.61

S/N	Failure load (P) in kN	Tensile stress (σ_t) in N/mm^2	Corrected value
1	91.27	2.91	2.62
2	87.10	2.77	2.49
3	81.99	2.61	2.39

Average Tensile strength = $2.49N/mm^2$

The tensile stress is calculated using equation 3 as thus

$$\sigma_{t1} = \frac{2P}{\pi dl} = \frac{2\times91.27}{3.142\times0.1\times0.2} = 2.91$$

$$\sigma_{t2} = \frac{2\times87.10}{3.142\times0.1\times0.2} = 2.77$$

$$\sigma_{t3} = \frac{2\times81.10}{3.142\times0.1\times0.2} = 2.61$$

Because of the effect of strip, the tensile strength is reduce as thus

$\boldsymbol{\beta} = \frac{b}{D} = \frac{26}{100} =$ 0.26

$\boldsymbol{\sigma}^{c}_{max}(P,\boldsymbol{\beta}) = \frac{2P}{\pi BD}\left[1-\boldsymbol{\beta}^2\right]^{3/2} = 0.9$

By substitution $\boldsymbol{\sigma}^{c}_{max}(P,\boldsymbol{\beta}) =$ 0.9

APPENDIX 4: COMPUTATION OF CONCRETE FRACTURE PARAMETER

REF	CALCULATION	OUTPUT
CEB-FIP 90	1.The elastic modulus is calculated as thus $E_c = E_{c0}\left(\frac{f_{cm}}{f_{cm0}}\right)^{1/3}$ $E_{c0} = 2.15\times10^4\ \ (^{N}/_{mm^2})$ $E_c = 2.15\times10^4\left(\frac{35.82}{10}\right)^{1/3}$ $E_c = 32882(^{N}/_{mm^2})$ **2.** Fracture Energy The fracture energy is calculated based on aggregate size as	

	$G_{f0} = 0.024 + \frac{0.0053\ 20^{0.95}}{8}$ = 0.0354 Fracture energy in Tension = $$G_f = G_{f0}\left[\frac{f_{cm}}{f_{cm0}}\right]^{0.7}$$ $$G_f = 0.0354\left[\frac{35.82}{10}\right]^{0.7}$$ G_f = 0.086 Fracture energy in compression = 8.6	